

CHAPTER 5 – Impedance Spectroscopy Results

This chapter discusses the transport properties of NASICON compounds $\text{Li}_{1.3}\text{Al}_{0.3-x}\text{M}_x\text{Ti}_{1.7}(\text{PO}_4)_3$ system using various formalisms of the impedance spectroscopy.

5.1 Introduction

Impedance Spectroscopy (IS) is a tool to study the impedance behavior of ion conducting solid material. As the material is subjected to AC frequencies (in increasing order), the ions within the solid get polarized. Their tendency to get polarized and accordingly their motion within the solid can help us understand the ion conducting behavior and consequently determine if the material can be used in electrochemical applications. This study can be performed from room temperature to increasing temperatures. The impedance data can also be expressed in various formalisms like dielectric, modulus and conductivity as per the need. The data (impedance, dielectric etc) can be expressed on a Nyquist plot (real versus imaginary axes). From impedance measurements, the AC and DC conductivities of the Li^+ can also be deduced for a ceramic solid material. Based on frequency behavior the transport of ions can be bifurcated in terms of conduction in grain and grain boundary regions in case of ceramic solids. In the below sections, the results of impedance and conduction formalisms are described first for samples of the reference system i.e., $\text{LiTi}_2(\text{PO}_4)_3$ (LTP) and $\text{Li}_{1.3}\text{Al}_{0.3}\text{Ti}_{1.7}(\text{PO}_4)_3$ (LATP). Subsequently, the reference system LATP was doped with trivalent cations like Y^{3+} , Ga^{3+} , Sc^{3+} to study their effect on Li^+ conductivity studies.

5.2 Conductivity Studies

5.2.1 Reference LTP and LATP systems

$\text{LiTi}_2(\text{PO}_4)_3$ (LTP) and aluminum doped LTP system with general formula $\text{Li}_{1+x}\text{Al}_x\text{Ti}_{2-x}(\text{PO}_4)_3$ (LATP) (where $x = 0.1$ to 0.7) are titanium based phosphate NASICON ceramic compounds which are widely studied for their Li^+ conducting properties and have application as electrolytes and electrodes in Li-ion conducting batteries. The structure of both $\text{LiTi}_2(\text{PO}_4)_3$ (LTP) and $\text{Li}_{1+x}\text{Al}_x\text{Ti}_{2-x}(\text{PO}_4)_3$ (LATP) is rhombohedral ($R\bar{3}c$) [1, 2, 3] in which Li^+ can diffuse and intercalate in the cation vacancies within the 3D cage structure. These vacancies are called M1 and M2 sites. In order to study the effect of doping of trivalent cations of increasing ionic radii (Ga^{3+} , Sc^{3+} , Y^{3+}) in LATP system to replace Al^{3+} , it is mandatory to first study the LTP and LATP samples as reference system. Therefore in the below sections the

electrical properties of $\text{LiTi}_2(\text{PO}_4)_3$ (LTP) and $\text{Li}_{1.3}\text{Al}_{0.3}\text{Ti}_{1.7}(\text{PO}_4)_3$ (LATP) samples are presented.

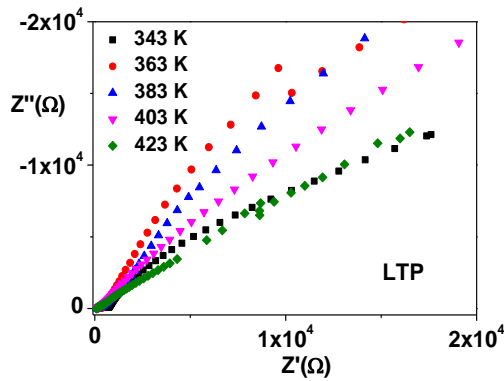


Fig. 5.1 Nyquist plot of $\text{LiTi}_2(\text{PO}_4)_3$ (LTP) sample at different temperatures.

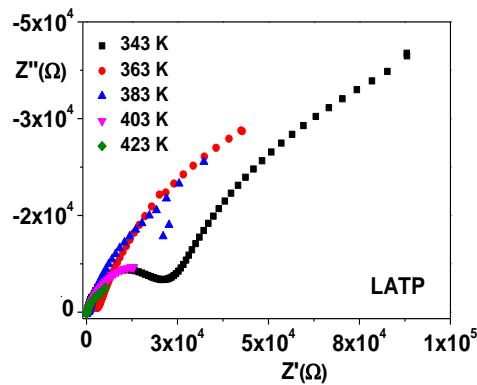


Fig. 5.2 Nyquist plot of $\text{Li}_{1.3}\text{Al}_{0.3}\text{Ti}_{1.7}(\text{PO}_4)_3$ (LATP) sample at different Temperatures.

The real and imaginary values of impedance of LTP and LATP systems are plotted for different temperatures in Figs.5.1 and 5.2 respectively. The bulk resistance of the sample is obtained by the intercept of semi circle on (real) impedance axis (Z') [5, 9, 28]. Two semicircles are the main features of the given spectra in LTP and LATP systems. The first semi circle formed at high frequency is relatively small, depressed and is only partially formed while the other semi circular arc which is formed at lower frequencies is large. The first depressed semi circle intercept on real impedance axis gives impedance of the bulk material while the second semi circular arc provides high impedance value. The Li^+ ion generally travels in the grain region where the periodic arrangement of the lattice sites and vacancies enables an easy motion, hence it experiences low impedance. The second larger semi circular arc corresponds to grain boundary region. It can be seen that the intercept of the semi circular arc shifts towards the origin as the temperature increases. It means the value of impedance decreases with increasing temperature. The insets in Figures 5.1 and 5.2 show the high frequency arcs.

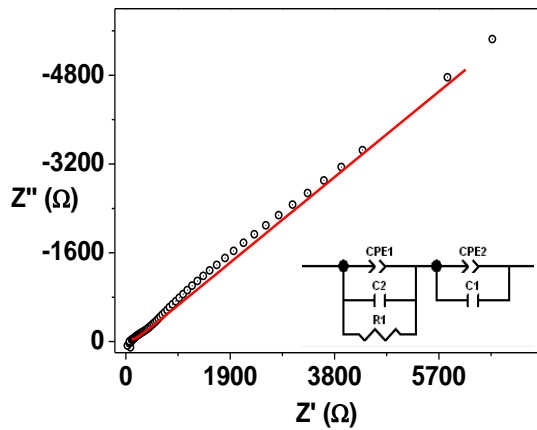


Fig. 5.3. Nyquist plot at 413 K for $\text{LiTi}_2(\text{PO}_4)_3$ (LTP) sample with equivalent circuit

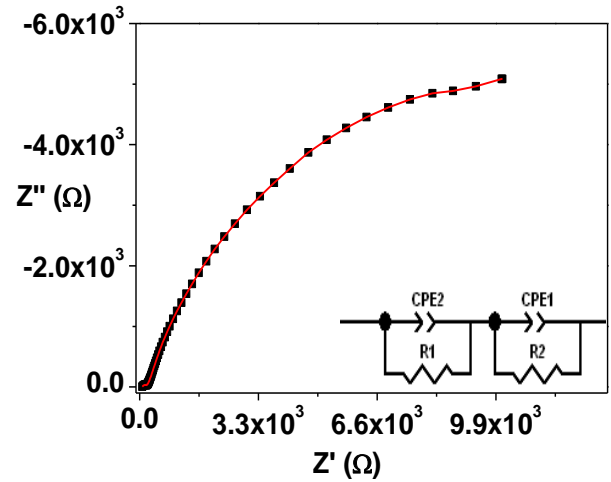


Fig. 5.4 Nyquist plot for $\text{Li}_{1.3}\text{Al}_{0.3}\text{Ti}_{1.7}(\text{PO}_4)_3$ (LATP) sample with equivalent circuit.

Figs.5.3 and 5.4 depict the fitted values in the Nyquist plot of LTP and LATP samples, respectively at 140 °C (413 K). The fitting is done using a combination of R, C and CPE for grain and grain boundary regions. In the inset the equivalent circuits are pictured.

In Figs. 5.5 and 5.6, Arrhenius plots of reference systems: $\text{LiTi}_2(\text{PO}_4)_3$ (LTP) and aluminum doped $\text{Li}_{1.3}\text{Al}_{0.3}\text{Ti}_{1.7}(\text{PO}_4)_3$ (LATP) are given for grain and grain boundary regions respectively. It is clear from the plots that the conductivity increases with temperature for both regions of the ceramic NASICON material. It is also observed that the grain conductivity is higher than grain boundary conductivity for LTP and LATP samples.

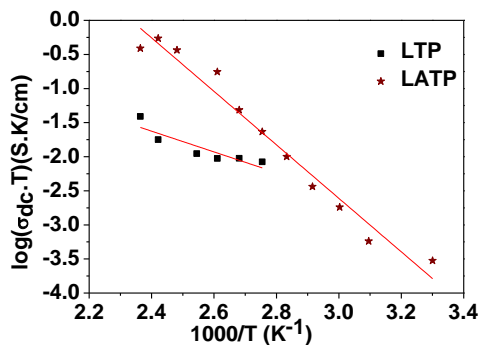


Fig. 5.5 Arrhenius plot of $\text{LiTi}_2(\text{PO}_4)_3$ and $\text{Li}_{1.3}\text{Al}_{0.3}\text{Ti}_{1.7}(\text{PO}_4)_3$ samples for Grain (Bulk) region

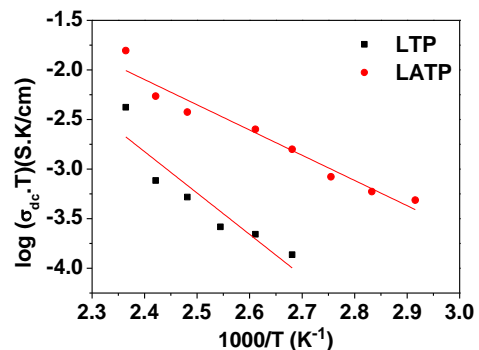


Fig. 5.6 Arrhenius plot of $\text{LiTi}_2(\text{PO}_4)_3$ and $\text{Li}_{1.3}\text{Al}_{0.3}\text{Ti}_{1.7}(\text{PO}_4)_3$ samples for Grain Boundary region

The DC conductivity indicates the long range (translational) diffusive motion that the Li^+ ion makes under the influence of electrochemical potential difference on account of defect sites. The Li^+ is not bounded with any molecule in this state. As temperature increases, the number of defects increase leading to higher values of DC conductivity.

In the below subsection, frequency dependent conductivity of LTP and LATP samples at increasing temperatures is presented. Post this, the reasons of the superior Li^+ conductivity in LATP parent system compared to LTP are discussed. Figures 5.7 and 5.8 show the conductivity isotherms of LTP and LATP samples, respectively at different temperatures. The isotherms exhibit a dispersive relaxation (shown by red dashed arrow in the Figure). The relaxation shifts towards higher frequencies as temperature increases. Besides, the LTP sample also exhibits a change in the pattern of relaxation at higher temperatures and intermediate frequencies which is indicated by black solid arrows in Fig. 5.7. This indicates a change in the local microstructure at grain boundary. This kind of change is also seen in the fitted equivalent circuit plot of LTP in Fig. 5.3 in which the grain boundary impedance values are fitted using a capacitance C. The capacitance indicates presence of space charge region which points to the presence of gaps in the microstructure at grain boundary. LATP has a superior Li^+ conductivity compared to LTP which is noticeable in all the above Figures.

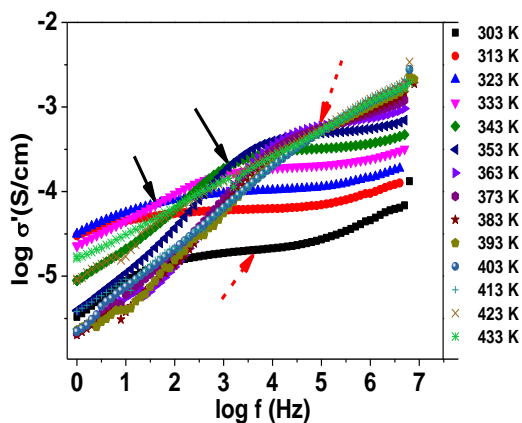


Fig. 5.7 Conductivity isotherms of $\text{LiTi}_2(\text{PO}_4)_3$ (LTP) sample at different temperatures

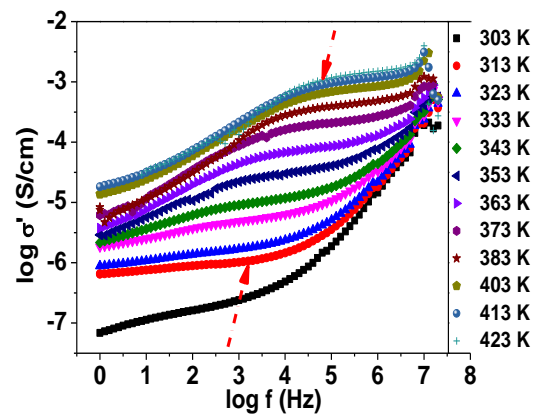


Fig. 5.8 Conductivity isotherms of $\text{Li}_{1.3}\text{Al}_{0.3}\text{Ti}_{1.7}(\text{PO}_4)_3$ (LATP) sample at different temperatures.

Highest Li^+ conductivity for LATP is 2×10^{-3} S/cm, at 423 K (150 °C), was noted in the present study which is similar to the results (Li^+ conductivity of $\sim 10^{-3}$ S/cm) reported by other workers [3, 6, 7, 10] for Al concentration $x = 0.3$ in $\text{Li}_{1.3}\text{Al}_{0.3}\text{Ti}_{1.7}(\text{PO}_4)_3$ (LATP) system for Al concentration $x = 0.3$. In the Fig. 5.9 (below), a comparison of grain and grain boundary conductivities is shown. The Li^+ conductivity for grain boundary is 1-2 order lesser than grain conductivity. This is explained as follows: Due to segregation of insulating phases like AlPO_4 , TiO_2 , TiP_2O_7 , LiTiPO_5 and LiP_2O_5 at grain boundary, the motion of Li^+ also gets blocked and the pathways become constricted [4]. Very small peaks in the XRD patterns are observed, which indicates very small amounts of insulating phases.

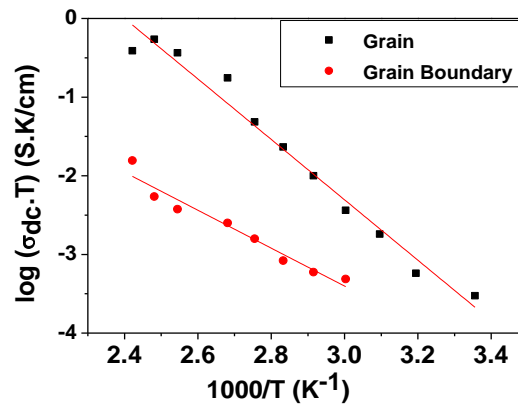


Fig. 5.9 Arrhenius plots of grain and grain boundary regions of $\text{Li}_{1.3}\text{Al}_{0.3}\text{Ti}_{1.7}(\text{PO}_4)_3$ sample

At low frequencies, due to diffusion (DC conductivity) the Li^+ ions migrate longer distances upto grain boundaries where they encounter space charge regions. These accumulated charges exert a repulsive influence on other incoming Li^+ and prohibit their smooth motion. This space charge barrier is characterized by reactive capacitance in equivalent circuit fitting [17, 18, 20, 21]. Mariappan *et al.* have reported that the Mott Schottky type of space charge potential barrier cannot explain the space charge barrier potential in an LATP system [21, 44].

Hence the overall (bulk) conductivity is the reference system LATP system is $\sim 10^{-3}$ S/cm [10, 11] and that of LTP system is $\sim 10^{-4}$ S/cm at room temperature which are comparable to the reported values [3, 14, 16, 34]. In the below sections we report results of the Li^+ conductivity when optimized system LATP is doped by trivalent cations like Y, Ga and Sc.

5.2.2 $\text{Li}_{1.3}\text{Al}_{0.3-x}\text{Y}_x\text{Ti}_{1.7}(\text{PO}_4)_3$ LAYTP system

In this study, yttrium, a trivalent cation is doped in the $\text{Li}_{1.3}\text{Al}_{0.3}\text{Ti}_{1.7}(\text{PO}_4)_3$ (LATP) system. The concentration of yttrium (x) in the system is varied to study the effect of Y^{3+} doping on the Li^+ conductivity. The study can help understand the effect of yttrium on LATP structure and also on the Li^+ conductivity. It is known that Al in LATP system is located at tetrahedral and octahedral sites [48, 49, 50]. Replacing Al^{3+} (0.53 \AA) by a large trivalent cation Y^{3+} (0.93 \AA) at tetrahedral and octahedral sites of Al in the rhombohedral structure ($\text{R}\bar{3}\text{c}$) can result in electropositive repulsive influence on other members of the LATP lattice and can affect the Li^+ conductivity in the LATP compound. However if the concentration of dopant is optimized, the resulting material can be of interest as electrolyte in Li^+ ion batteries [23, 24, 25, 26] due to its Li^+ conduction properties. Y^{3+} is a rare earth element with $3d^{10}$ electrons in valence shells. The hybrid bonds created by Y^{3+} with phosphates $(\text{PO}_4)^{3-}$ also affect the local configuration which may alter the NASICON structure. Hence it would also be interesting to know effect of compounds with yttrium as a dopant. Taking these objectives into consideration, the Y^{3+} was doped in the LATP system and subsequently electrical properties were studied. There are only a few studies [24-26] related to Y^{3+} doped in a parent system $\text{Li}_{1.3}\text{Al}_{0.3}\text{Ti}_{1.7}(\text{PO}_4)_3$ (LATP). These studies have addressed the formation of secondary phases using NMR studies, the formation of different types of oxygen vacancies through XPS studies and types of conduction executed by ^6Li and ^7Li in the M1 and M2 vacancy sites.

In Fig. 5.10, the Nyquist plot at different temperatures for $x = 0.01$ of yttrium is presented. A smaller depressed semi circle is formed at higher frequencies (shown in inset for 423 K temperature) which corresponds to the bulk Li^+ conductivity. Following this, there is a

larger semi circular arc in low frequency regions, and a steep rise in the impedance at very low frequency region (at the right most side) of the $Z'-Z''$ plot. The spike corresponds to high value of capacitance which arises due to double layer of Li^+ formed at electrode–electrolyte interface [27].

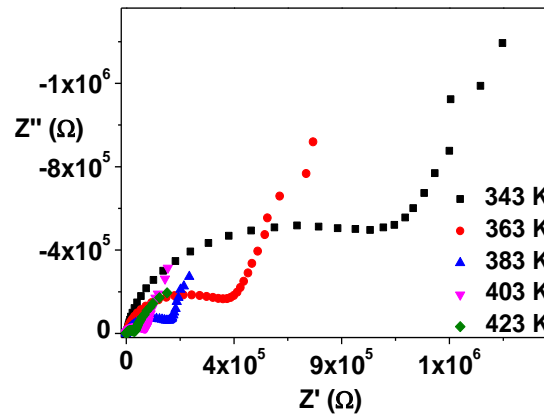


Fig. 5.10 Nyquist plot of $\text{Li}_{1.3}\text{Al}_{0.29}\text{Y}_{0.01}\text{Ti}_{1.7}(\text{PO}_4)_3$ sample of LAYTP series at different temperatures.

This double layer capacitance is generally denoted as C_{dl} . This capacitive layer is formed as a result of space charges and prevents the conduction of Li^+ across. The same scenario is seen in below Figure 5.11 where the Nyquist plot of concentration ($x = 0.15$) of yttrium. In the grain boundary region along with electrode effects (C_{dl}) are not very clearly manifested in the low frequency regions. The yttrium accumulated at grain boundaries in form of YPO_4 phase due to its insulating nature, is instrumental in compromised conductivity of Li^+ ions. YPO_4 is detected in the XRD patterns as mentioned in earlier chapter. YPO_4 phase prevents regular motion of Li^+ ions by constricting the pathways at the grain boundaries [24, 26].

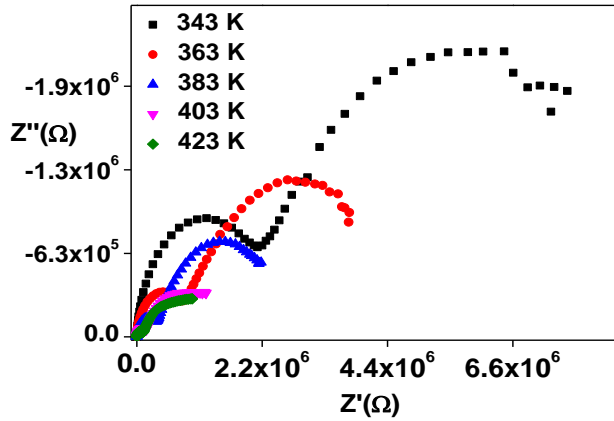


Fig. 5.11 Nyquist plot of $\text{Li}_{1.3}\text{Al}_{0.15}\text{Y}_{0.15}\text{Ti}_{1.7}(\text{PO}_4)_3$ (LAYTP) sample at different temperatures

Pinus *et al.* [29] have suggested that the presence of a very large cation like Nb^{5+} (1.03 \AA) or Y^{3+} (0.93 \AA) as dopant in the LTP structure causes the accumulation of such large cations near the M1-M2 bottlenecks which constricts the Li^+ motion and thereby compromises the Li^+ conductivity. Impurity phases like YPO_4 and LiTiPO_5 are segregated towards grain boundary and change their structure with temperature. They alter the structure the bottlenecks due to large size and narrow the pathways through which Li^+ are conducted. The structure of bottlenecks alters and increases the Li^+ conductivity, as the temperature increases. As seen in the Figs. 5.10 and 5.11, as temperature increases, the intercept of smaller (corresponding to grain region) and bigger semi circular arcs (corresponding to grain boundary region) shifts towards the origin (left side) on the real (Z) axis. Hence the bulk impedance of the LAYTP system decreases with temperature.

In Fig. 5.12 and 5.13 the fitted Nyquist plots of samples S1 ($x = 0.01$) and S6 ($x = 0.15$) for two different temperatures 403 K and 423 K are shown. The fitting is done using a combination of equivalent circuit elements R and CPE for sample S1, but capacitance was needed in fitting the grain and grain boundary region impedance plots for sample S6, (which contains more amount of yttrium compared to S1) in the frequency range of $2 \times 10^7 \text{ Hz}$ to 10 Hz).

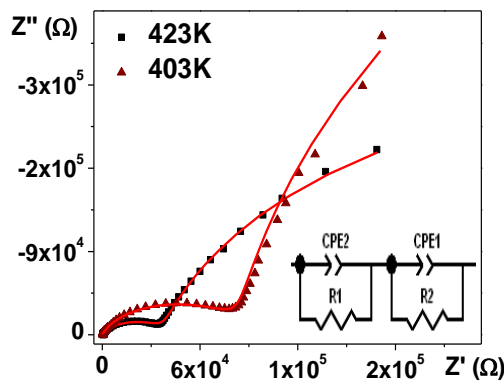


Fig. 5.12 Nyquist plots for $\text{Li}_{1.3}\text{Al}_{0.29}\text{Y}_{0.01}\text{Ti}_{1.7}(\text{PO}_4)_3$ sample with equivalent circuit

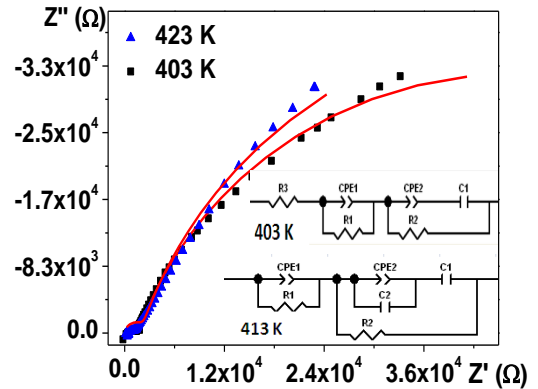


Fig. 5.13 Nyquist plots for sample $\text{Li}_{1.3}\text{Al}_{0.15}\text{Y}_{0.15}\text{Ti}_{1.7}(\text{PO}_4)_3$ with equivalent circuit

The inset contains the equivalent circuit used to fit the impedance data for both the samples. The presence of capacitance for low frequency data indicates accumulation of space charge within these regions. The space charge zones arise due to presence of blocking phases, 2-D defects or discontinuities like cracks [30]. It can be noticed that with increasing temperature, the intercept of the arc shifts towards origin. That is, the impedance values decrease. The blocking phases and grain boundary structure get modified with increasing temperature resulting in decrease of impedance.

In Figs. 5.14 and 5.15, the temperature activated behavior of grain and grain boundary regions are given as Arrhenius plots. The DC conductivity increases with temperature for both regions of the ceramic NASICON material. It can be observed that the grain conductivity is higher than grain boundary conductivity for all the samples of LAYTP series. The DC conductivity of sample S1 ($x = 0.01$) is higher than any other samples both – for grain and grain boundary regions. The highest Li^+ conductivity is $5 \times 10^{-4} \text{ S/cm}$ for S1 ($x = 0.01$) in grain (bulk) region at 423 K. As the amount of yttrium in the samples increases, the long range (translational) diffusive motion of the Li^+ is impeded by the impurity phases and the presence of large sized cations Y^{3+} within the LATP lattice. This has been discussed in the later part of this section.

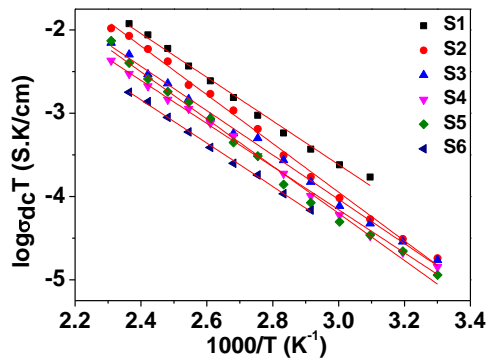


Fig. 5.14 Arrhenius Plots of $\text{Li}_{1.3}\text{Al}_{0.3-x}\text{Y}_x\text{Ti}_{1.7}(\text{PO}_4)_3$ samples for grain (bulk) region

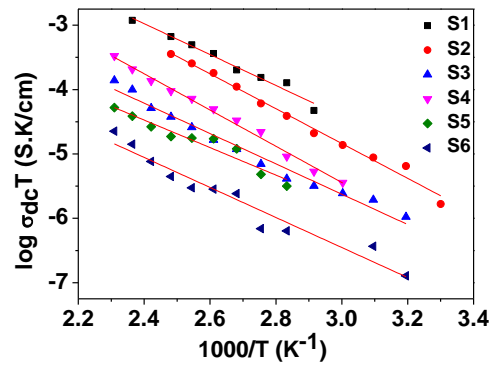


Fig. 5.15 Arrhenius Plots of $\text{Li}_{1.3}\text{Al}_{0.3-x}\text{Y}_x\text{Ti}_{1.7}(\text{PO}_4)_3$ samples for grain boundary region

In Figs. 5.16 below, the conductivity isotherms for different temperatures for each of the samples S1 to S6 are given at 413 K wherein the sample S1 ($x=0.01$) has the highest conductivity at higher frequencies which corresponds to grain region in the solid.

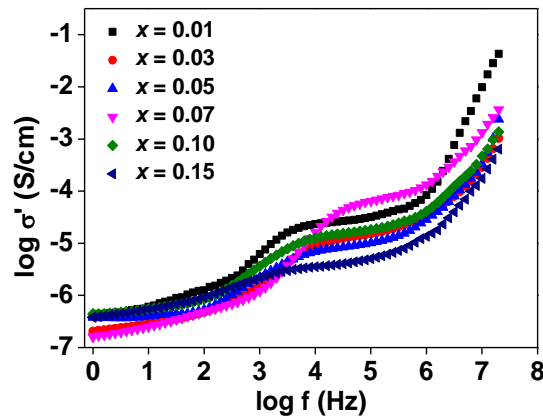


Fig. 5.16 Conductivity isotherms of $\text{Li}_{1.3}\text{Al}_{0.3-x}\text{Y}_x\text{Ti}_{1.7}(\text{PO}_4)_3$ (LAYTP) samples at 413 K

In Fig. 5.17 (below) the temperature activated Li^+ conductivity behavior as a function of frequency can be seen for temperatures ranging from 343 K to 423 K for samples of all concentrations of the LAYTP series. The conductivity plots at different temperatures (also called conductivity isotherms) exhibit a dispersive relaxation behavior. The relaxation shifts towards higher frequencies as the temperature increases. It can be noticed that the dispersion in the relaxation is high for sample S1 across temperatures. But as yttrium increases in the system, the dispersion progressively decreases upto sample S4 (yttrium concentration $x =$

0.07) and again increases for samples S5 and S6 with temperature. It can also be noticed that for sample S6, the conductivity isotherms corresponding to different temperatures, do not overlap (as in case of other samples) except at very high (10^5 Hz) frequencies. It indicates that the local microstructure in grain and grain boundary regions for sample S6 is slightly different than other samples. It can also be noticed, that sample S6 has the lowest bulk conductivity compared to other samples. This change can also be correlated to the fitted equivalent circuit plots of S1 and S6 at two different temperatures in Figs. 5.12 and 5.13, where extra capacitance C had to be used for fitting impedance in grain and grain boundary regions. The capacitance in the equivalent circuit indicates space charge region which points to the presence of gaps or ion blocking (and insulating) phases (which also constricts the pathways of Li^+) in the microstructure [19, 31, 39]. The dispersion in low and intermediate frequency region is caused by a distribution of barrier potentials seen by Li^+ ions as temperature increases [28]. The motion of Li^+ is not localized at low and intermediate frequencies hence they diffuse over large distances (unto several nanometers and upto grain boundary).

Hence the Li^+ ions experience a host of barrier potentials, distributed across the system as they diffuse over distances [9, 33]. The barriers are caused by presence of parasite phases like AlO_4 , AlPO_4 , YPO_4 , TiO_2 , TiP_2O_7 and LiTiPO_5 – which are formed in grain and grain boundary regions. The peaks of these phases have been detected in the XRD patterns which are described in earlier section. Of these, rutile phases: TiO_2 , TiP_2O_7 and alumina phases: AlO_4 , AlPO_4 are known to be of insulating in nature [4, 11, 34].

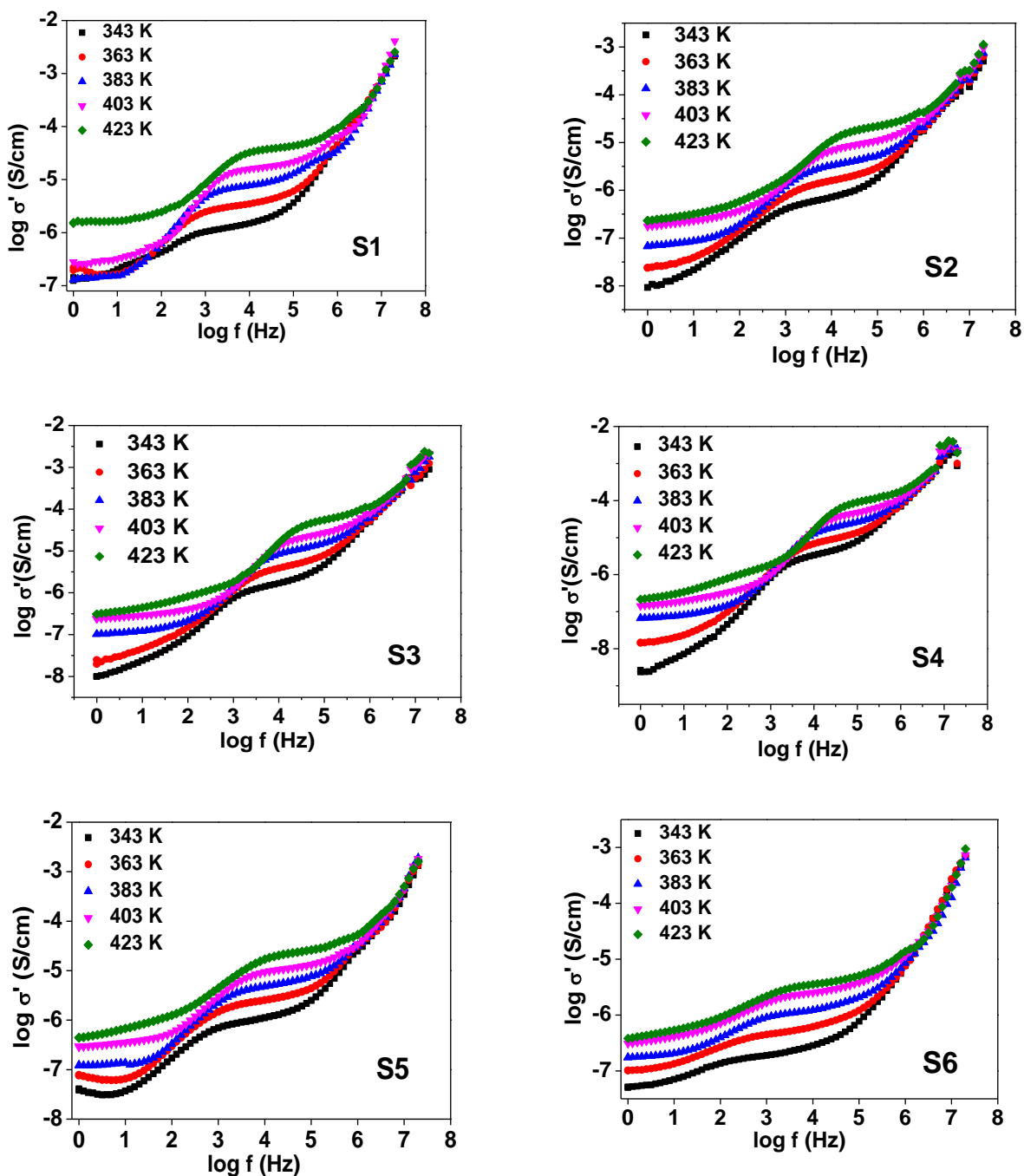


Fig. 5.17 Conductivity isotherms of $\text{Li}_{1.3}\text{Al}_{0.3-x}\text{Y}_x\text{Ti}_{1.7}(\text{PO}_4)_3$ (LAYTP) system at different temperatures

It is also observed that the dispersive relaxation shifts towards higher frequencies as the temperature increases. This is because, as the temperature increases, the mobility of Li^+ increases in the system. Due to this thermal energy gain (and agitations), the Li^+ are able to diffuse even at somewhat higher frequencies (10^5 Hz). Hence the dispersion shifts (extends) to higher frequencies at higher temperatures in all the samples [27, 33]. At high frequencies

the Li^+ does not get enough time to traverse longer distance because the electric field direction changes rapidly. Hence its motion is largely localized and Li^+ is more likely to fall back into the same or nearby vacancy. That is, its motion (hopping) is localized as against the non localized motion at lower and intermediate frequencies. Thus at higher frequencies, the conductivity isotherms exhibit least dispersive behavior [36, 37] this is explained in terms of Jump relaxation model proposed by Funke and co-workers. It should also be noted that, the hopping frequency is related to the conductivity as $\sigma' = \sigma_{dc}[1 + (\frac{\omega}{\omega_p})^n]$ (5.1)

according to Almond West formalism, it is also temperature dependent as below

$$\omega_p = \omega_0 \exp\left(\frac{-E}{kT}\right) \dots\dots\dots(5.2)$$

where ω_0 is the attempt frequency and E is the activation energy barrier. In our case of ternary system, the value of E is ~ 0.45 eV which is higher than the reported values [25]. Hence the probability to attempt a jump and enter a vacancy site also depends on temperature. This is more prominent at lower and intermediate frequencies. At higher frequencies, the Li^+ ions do not get enough time to delocalize themselves. Hence there is little or no dispersion at higher frequencies.

It is also observed from the figures above that as the amount of yttrium increases in the system, the dispersive relaxation becomes more prominent. That is, for sample S6 ($x = 0.15$), the dispersion is much wider especially at lower and intermediate frequencies. This indicates the presence of parasitic phases (especially at grain boundary) due to which Li^+ experience a wide variation of barriers and also sites to relax. At higher frequencies (more than 10^5 Hz) and all temperatures obey the Jonscher's power law [38, 89] given as:

$$\sigma' = \sigma_{dc} + A\omega^n \dots\dots\dots (5.3)$$

behavior as they overlap into an almost single curve. This indicates that the relaxation mechanism in grain region for all Li^+ at all temperatures is same [38, 43]. The low and intermediate frequency regions also show dispersion. It shows a variation with temperature, within same sample. It indicates a different relaxation behavior and a changed environment

for the Li^+ to relax. This will be further discussed in the modulus and dielectric spectroscopy sections. It is also clear that Y^{3+} due to its large size cannot replace Al^{3+} in the LATP system. Instead it tries to replace Ti^{4+} (0.60 \AA) which have comparable ionic radii.

At grain boundary core, oxygen vacancies are formed as V_{O}^{\bullet} , \dot{h} , etc. leave out the core. This leaves the grain boundary core positively charged. Hence negatively charged defects like Y'_{Ti} get segregated towards grain boundary [39, 41, 44] under the influence of electrostatic attractive forces. Heavy dopant – yttrium segregates towards grain boundary where it forms YPO_4 and YAlO_4 type of impurity phases. This effect is further explained in detail in the next section about segregation of dopants towards grain boundary due to heat treatment. These compounds help enhance the density of material at grain contacts. This is the reason of increase in the density values with increasing yttrium content (Ch.4).

5.2.3 Heat Treated $\text{Li}_{1.3}\text{Al}_{0.3-x}\text{Y}_x\text{Ti}_{1.7}(\text{PO}_4)_3$ system

Heat treatment (sintering) of the two samples of the $\text{Li}_{1.3}\text{Al}_{0.3-x}\text{Y}_x\text{Ti}_{1.7}(\text{PO}_4)_3$ (LAYTP) system for two concentrations ($x = 0.01$ and $x = 0.15$) are given below. The heat treatment was performed for 2 hours and 3 hours durations of two samples ($x = 0.01$ and 0.15) of the same batch to understand the changes in microstructure. Yttrium is a rare earth element which is relatively stable even at higher temperatures ($> 800^\circ \text{C}$). It imparts physical strength and durability, ruggedness and stability to withstand chemical attack of lithium in a lithium ion battery. This is necessary physical conduction for stable performance of lithium based electrolytes. By varying the time of heat treatment and studying its effect on density and Li^+ conductivity is important. Besides, yttrium is widely accepted as a good sintering aid in inorganic compounds. Its properties to get segregated at grain boundary are widely accepted and studied [61]. Subjecting yttrium doped NASICON ceramic compound to heat treatment can reveal some interesting characteristics of the grain boundary behavior and thereby Li^+ conductivity. To our best knowledge nobody has attempted to study the Li^+ conduction in LAYTP system as a function of sintering duration.

The impedance behavior of sample S1 at different temperatures for 2hr and 3 hr sintering duration is given in the Fig.5.18 and 5.19. In the impedance plots the small depressed semi circle corresponding to grain region is not visible. It can be seen that the impedance values for both – 2 and 3 hours heat-treated samples comes out to be almost the same for grain boundary regions. This is followed by a spike corresponding to the electrolyte-electrode interfacial capacitance (known as double layer capacitance). This indicates that space charge region is created at the interface between the electrolyte and electrode interface which prevents an easy passage of Li^+ . The values of grain boundary impedance are than those of grain.

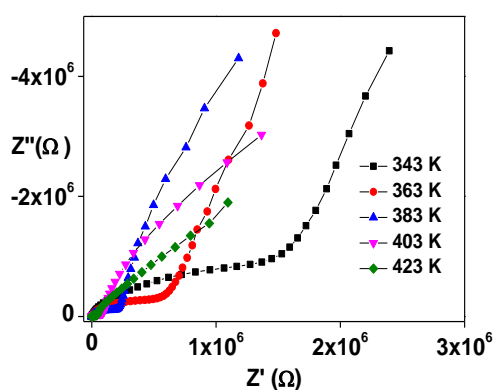


Fig. 5.18 Nyquist plot for S1-H2 samples of $\text{Li}_{1.3}\text{Al}_{0.3-x}\text{Y}_x\text{Ti}_{1.7}(\text{PO}_4)_3$ system at different temperatures

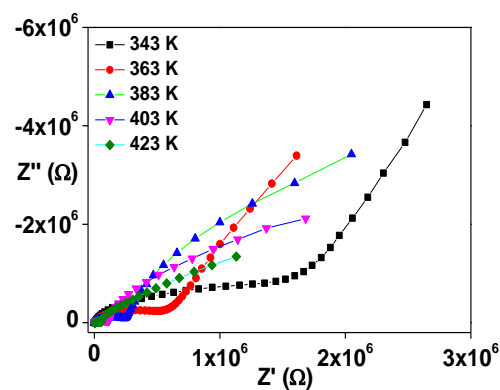


Fig. 5.19 Nyquist plot for S1-H3 samples of $\text{Li}_{1.3}\text{Al}_{0.3-x}\text{Y}_x\text{Ti}_{1.7}(\text{PO}_4)_3$ system at different temperatures

It is clear from Figs. 5.18 and 5.19, that there is no significant and noticeable change in the impedance behavior of the 2 and 3 hour heat treated samples and that the structure of grain is not modified much. The fitted impedance plots for 413 K temperature are given in the following Figs. 5.20 and 5.21 for the sample with $\text{Li}_{1.3}\text{Al}_{0.3-x}\text{Y}_x\text{Ti}_{1.7}(\text{PO}_4)_3$ sample with $x = 0.01$ composition which is prepared by normal procedure. Notice that an extra capacitor C is used for low frequency region which corresponds to electrode-electrolyte interface. The fitting was performed using a set of R and CPE values for both grain and grain boundary regions.

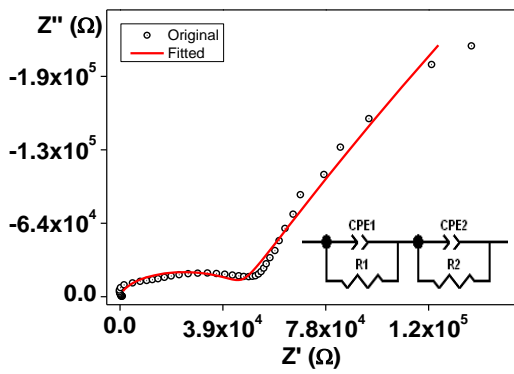


Fig. 5.20 Nyquist plot for $x = 0.01$ sample of $\text{Li}_{1.3}\text{Al}_{0.3-x}\text{Y}_x\text{Ti}_{1.7}(\text{PO}_4)_3$ system with equivalent circuit at 413 K

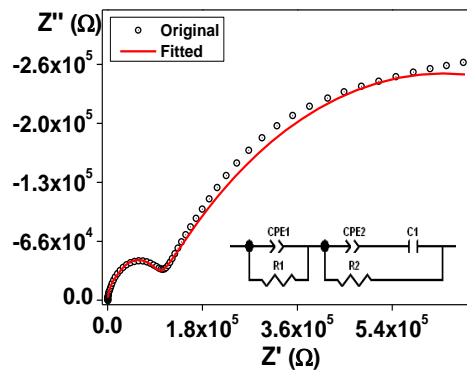


Fig. 5.21 Nyquist plot for $x=0.15$ sample of $\text{Li}_{1.3}\text{Al}_{0.3-x}\text{Y}_x\text{Ti}_{1.7}(\text{PO}_4)_3$ system with equivalent circuit at 413 K

In Figs. 5.22 and 5.23, is the representation of fitted values of S1 and S6 samples (yttrium concentration $x = 0.01$ and 0.15) sintered for 2 hours while Figs. 5.24 and 5.25 show the fitted Nyquist plots for samples of same concentration sintered for 3 hours duration.

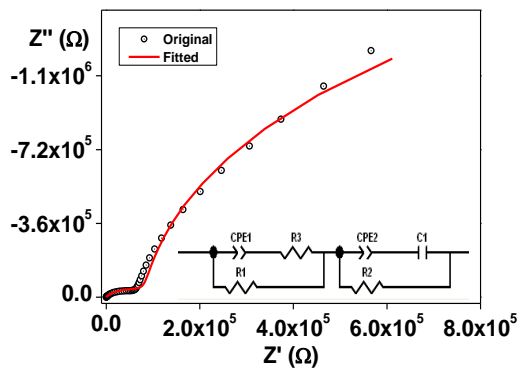


Fig. 5.22 Nyquist plot 413 K for S1-H2 sample of $\text{Li}_{1.3}\text{Al}_{0.3-x}\text{Y}_x\text{Ti}_{1.7}(\text{PO}_4)_3$ system with equivalent circuit.

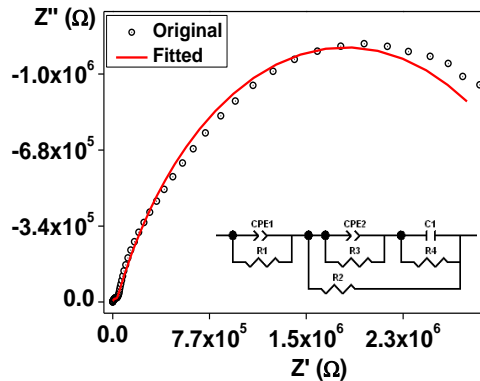


Fig. 5.23 Nyquist plot 413 K for S6-H2 sample of $\text{Li}_{1.3}\text{Al}_{0.3-x}\text{Y}_x\text{Ti}_{1.7}(\text{PO}_4)_3$ system with equivalent circuit.

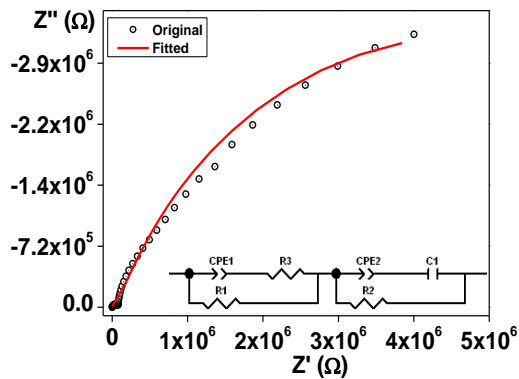


Fig. 5.24 Nyquist plot 413 K for S1-H3 sample of $\text{Li}_{1.3}\text{Al}_{0.3-x}\text{Y}_x\text{Ti}_{1.7}(\text{PO}_4)_3$ system with equivalent circuit.

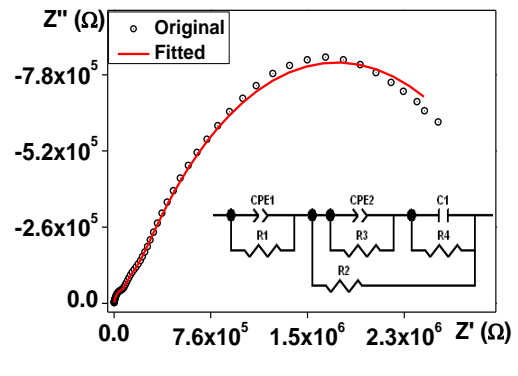


Fig. 5.25 Nyquist plot 413 K for S6-H3 samples of $\text{Li}_{1.3}\text{Al}_{0.3-x}\text{Y}_x\text{Ti}_{1.7}(\text{PO}_4)_3$ system with equivalent circuit

The above figures represent the fitted values of S1 sample which are subjected to heat treatment for 2 and 3 hrs at temperature of 413 K. The impedance values fall in almost the same range ($\text{M}\Omega$) although some points are missing in the low frequency region for S1_2H sample. The inset also contains the equivalent circuit which is used to fit grain and grain boundary data. In the below Figures 5.26 and 5.27, the DC conductivities are presented for samples of heat treated series.

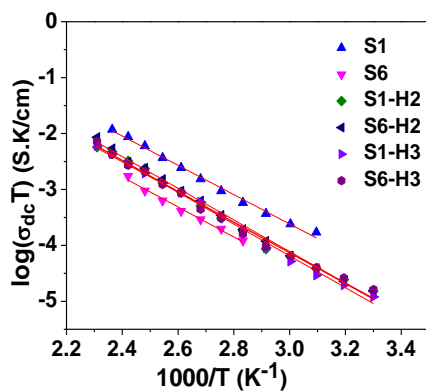


Fig. 5.26 Arrhenius plots for $\text{Li}_{1.3}\text{Al}_{0.3-x}\text{Y}_x\text{Ti}_{1.7}(\text{PO}_4)_3$ system for grain region for normal and heat treated samples

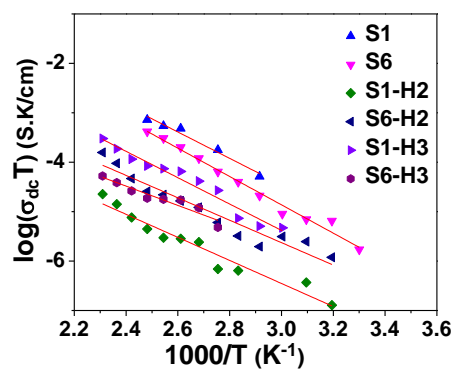


Fig. 5.27 Arrhenius plots for $\text{Li}_{1.3}\text{Al}_{0.3-x}\text{Y}_x\text{Ti}_{1.7}(\text{PO}_4)_3$ system for grain boundary region for normal and heat treated samples.

The temperature activated behavior of the Li⁺ conductivity in all the four samples gives an idea of number of defects created in due to increase in temperature according to the following relation:

$$n = n_o \exp (-E/kT) \quad \dots\dots\dots (5.4)$$

Therefore from the above it is clear that S1-H1 has the maximum number of defects. It is clear that due to large size of Y³⁺ the blocking phases are created which block the M1 and M2 sites. Hence the number of defects is less. The corresponding Li⁺ conductivity also is less in these samples. The yttrium phases like YPO₄ at higher temperatures become mobile and segregated towards grain boundary [39, 40]. This is explained as follows: The grain boundary core is positively charged due to migration of defects like V_O^{••} away from the grain boundary. The positively charged defects like Y'_{Ti} are formed in grain region. They are formed when trivalent yttrium cations try to replace tetravalent titanium cations. Thus a deficiency of positive charge is created. This aggregate of negative charge is attracted towards positively charge grain boundary core (which is deficient of negative charges like V_O^{••}). Hence the gaps in the structure of oxygen vacancies are filled in by Y'_{Ti}. These defects migrate towards the grain boundary core at higher temperatures where they fill in the gaps in the microstructure at core [41]. Due to this, the grain boundary conductivity increases with temperature. An indirect evidence of presence of space charge region at grain boundary for our system is explained below from the fitted impedance plots. The fitting is possible only by the usage of capacitance in the grain and grain boundary regions. Mariappan *et al.* [44] have tried using the Mott Schottky barrier potential.

The presence of charges inside the grain boundary core attracts the opposite charges from the grain. But due to gap between the grain and grain boundary core, a capacitance develops. This is seen also in the fitting of heat treated samples. As mentioned above, when the defects due to heat treatment migrate towards grain boundary core, fill in the microstructural gaps in the grain boundary region and enhance the grain boundary conductivity. This is seen prominently in samples which contain larger quantity of yttrium

(S6 where concentration of yttrium, $x = 0.15$). Due to this reason, the yttrium rich heat treated samples benefit better and Li^+ conductivity at grain boundary increases in such samples. This behavior is also seen for frequency dependent conductivity in the following plots:

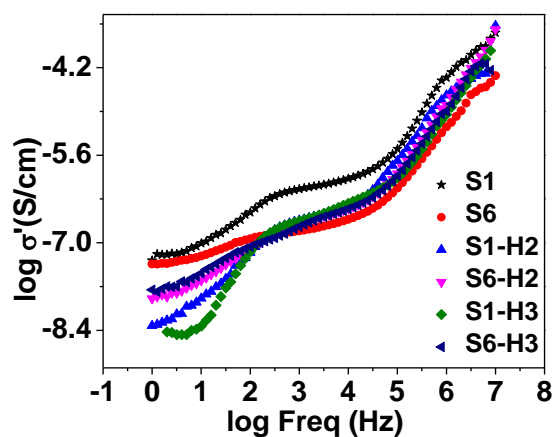


Fig. 5.28 Frequency dependent conductivity for $\text{Li}_{1.3}\text{Al}_{0.3-x}\text{Y}_x\text{Ti}_{1.7}(\text{PO}_4)_3$ system at 333 K for $x=0.01$ and 0.15 concentrations prepared by normal procedure and heat treated for 2 and 3 hrs.

In the Fig. 5.28, the conductivity isotherms are presented. The lower frequencies ($< 10^4$ Hz) corresponds to grain boundary region while that above it corresponds to grain region. The conductivity corresponding to S1 sample for 1 hr is highest while that for S6 for 1 hr is the lowest in the frequency range 10^4 to 10^7 Hz. The conductivity in low frequency region for heat treated samples for yttrium rich sample S6 is higher. Hence, it can be inferred that the solid is not electrically neutral at the grain boundaries and presence of charges at the interfacial regions and subsequent heat treatment promotes the migration of dopants like yttrium towards grain boundary and the space charge regions therein, which increases the Li^+ conductivity. If the samples are rich in yttrium content then they yield better Li^+ conductivity if heat treated.

5.2.4 $\text{Li}_{1.3}\text{Al}_{0.3-x}\text{Ga}_x\text{Ti}_{1.7}(\text{PO}_4)_3$ (LAGTP) System

To replace Al^{3+} , Ga^{3+} – a trivalent cation is doped in the LATP system at the aluminum site to prepare $\text{Li}_{1.3}\text{Al}_{0.3-x}\text{Ga}_x\text{Ti}_{1.7}(\text{PO}_4)_3$ (LAGTP) ($x = 0.01, 0.03, 0.05, 0.07$) system where x is varied in steps of 0.02. The Nyquist plots of LAGTP system for each of the concentration of x are shown in Figs. 5.29 and 5.30. The presence of a spike and absence of a

semi circular arc at low frequencies for samples G1 and G4 indicates that the formation of polarization zone near the grain boundary region. The fitted plots in Figs. 5.31 and 5.32 for samples G1 and G4 consist of small semi circular arc corresponding to the grain region while, a larger semi circular arc corresponding to grain boundary region. For the sample G1, in which the gallium is small in quantity, only a single depressed semi circular arc is formed followed by a spike. It means that the contribution of grain boundary region is negligible or not observable and easily described by combination of R and CPE. While grain boundary dominates in case of samples with higher amount of gallium (Fig. 5.32) After fitting of data, it shows the contribution of R, CPE and C. Apart from the main phase, $\text{Li}_{1.3}\text{Al}_{0.3-x}\text{Ga}_x\text{Ti}_{1.7}(\text{PO}_4)_3$ (LAGTP), secondary phases like $\text{LiGa}_2(\text{PO}_4)_3$ (LGP), $\text{Li}_{1.3}\text{Ga}_{0.3}\text{Ti}_{1.7}(\text{PO}_4)_3$ (LGTP), etc are also present. According to Aono et al. [3, 51] GaPO_4 , LiTiPO_5 phase are also formed, however in the present study we observe only GaPO_4 peaks in the XRD patterns (mentioned in Ch.4) and is generally situated at the grain boundaries as discussed by Yan et al. [40]. The presence of this phase constricts the pathways and has irregular structures. This is identified by the presence of extra resistance R in the equivalent circuit shown by blue circle in Fig 5.32, which hinders the conduction of Li^+ at grain boundary. Therefore, conductivity of Li^+ ions at grain boundary is less than that of grain by at least 2 orders. The increase in Gallium content creates more GaPO_4 and AlPO_4 phases at the grain boundary. Since the Ga^{3+} ionic radii are comparable to Al^{3+} and that of Ti^{4+} also, the gallium is easily able to replace both these cations. Hence, the size of bottlenecks becomes large and thus, favorable for Li^+ conduction through channels. Due to this, the Li^+ conductivity increases for G2 ($x=0.03$) compared to parent system LATP. The fitting of these plots for low gallium content is done using a combination of R and CPE while, for higher content of gallium, the fitting is possible using a combination of R, C, CPE for grain boundary region. The presence of insulating secondary phases at grain boundary is represented by R.

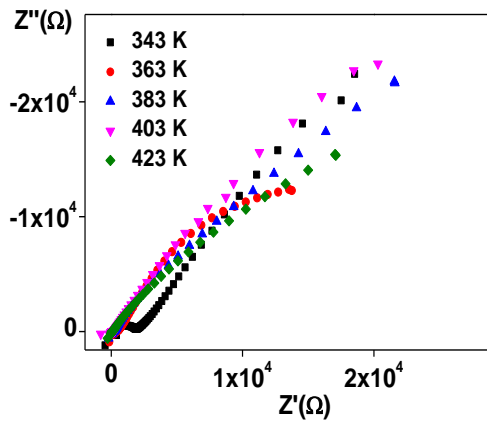


Fig. 5.29 Z' vs Z'' plot for $\text{Li}_{1.3}\text{Al}_{0.3-x}\text{Ga}_x\text{Ti}_{1.7}(\text{PO}_4)_3$ system for $x=0.01$ sample at different temperatures.

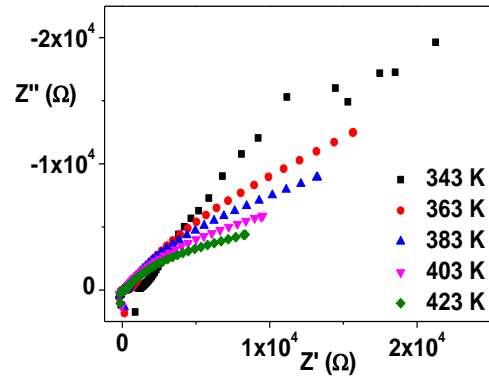


Fig. 5.30 Z' vs Z'' plot for $\text{Li}_{1.3}\text{Al}_{0.3-x}\text{Ga}_x\text{Ti}_{1.7}(\text{PO}_4)_3$ system for $x=0.07$ sample at different temperatures.

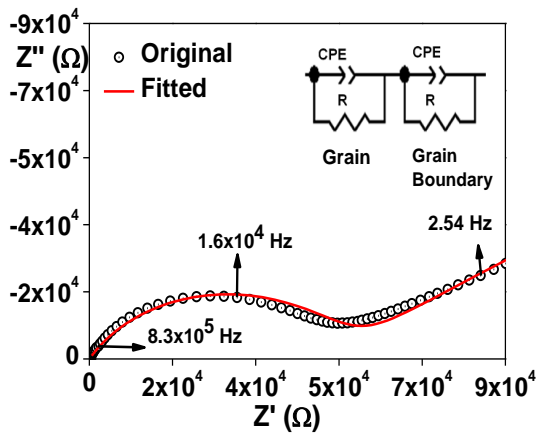


Fig. 5.31 Nyquist plot for $\text{Li}_{1.3}\text{Al}_{0.3-x}\text{Ga}_x\text{Ti}_{1.7}(\text{PO}_4)_3$ system for $x = 0.01$ sample at 303 K with equivalent circuit.

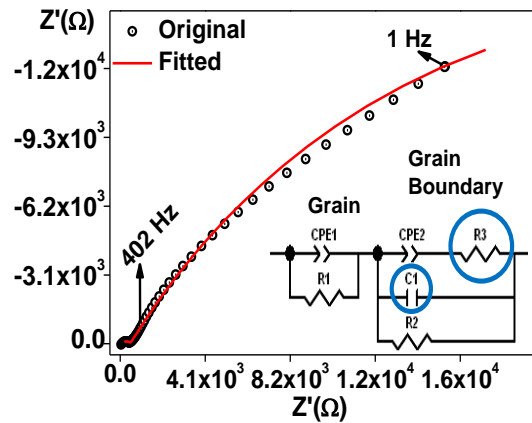


Fig. 5.32 Nyquist plot for $\text{Li}_{1.3}\text{Al}_{0.3-x}\text{Ga}_x\text{Ti}_{1.7}(\text{PO}_4)_3$ system for $x = 0.07$ sample at 363 K with equivalent circuit

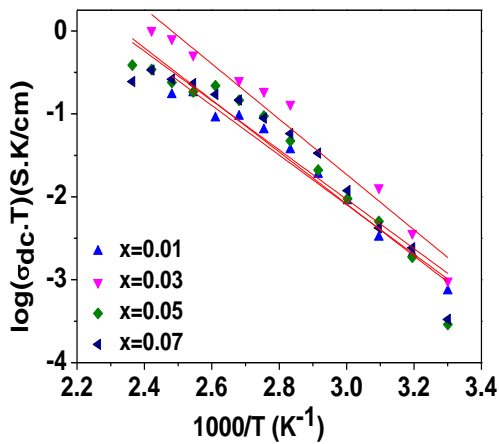


Fig. 5.33 Arrhenius plots for grain region of $\text{Li}_{1.3}\text{Al}_{0.3-x}\text{Ga}_x\text{Ti}_{1.7}(\text{PO}_4)_3$ system

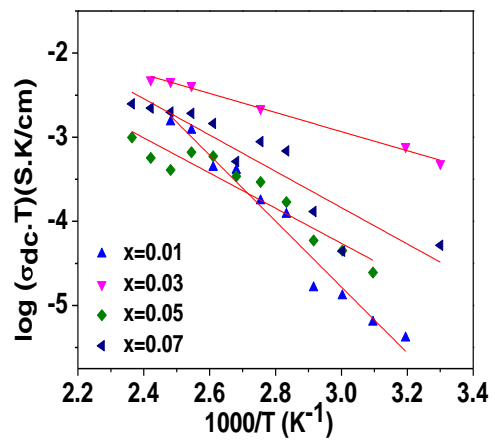


Fig. 5.34 Arrhenius plots for grain boundary region of $\text{Li}_{1.3}\text{Al}_{0.3-x}\text{Ga}_x\text{Ti}_{1.7}(\text{PO}_4)_3$ system

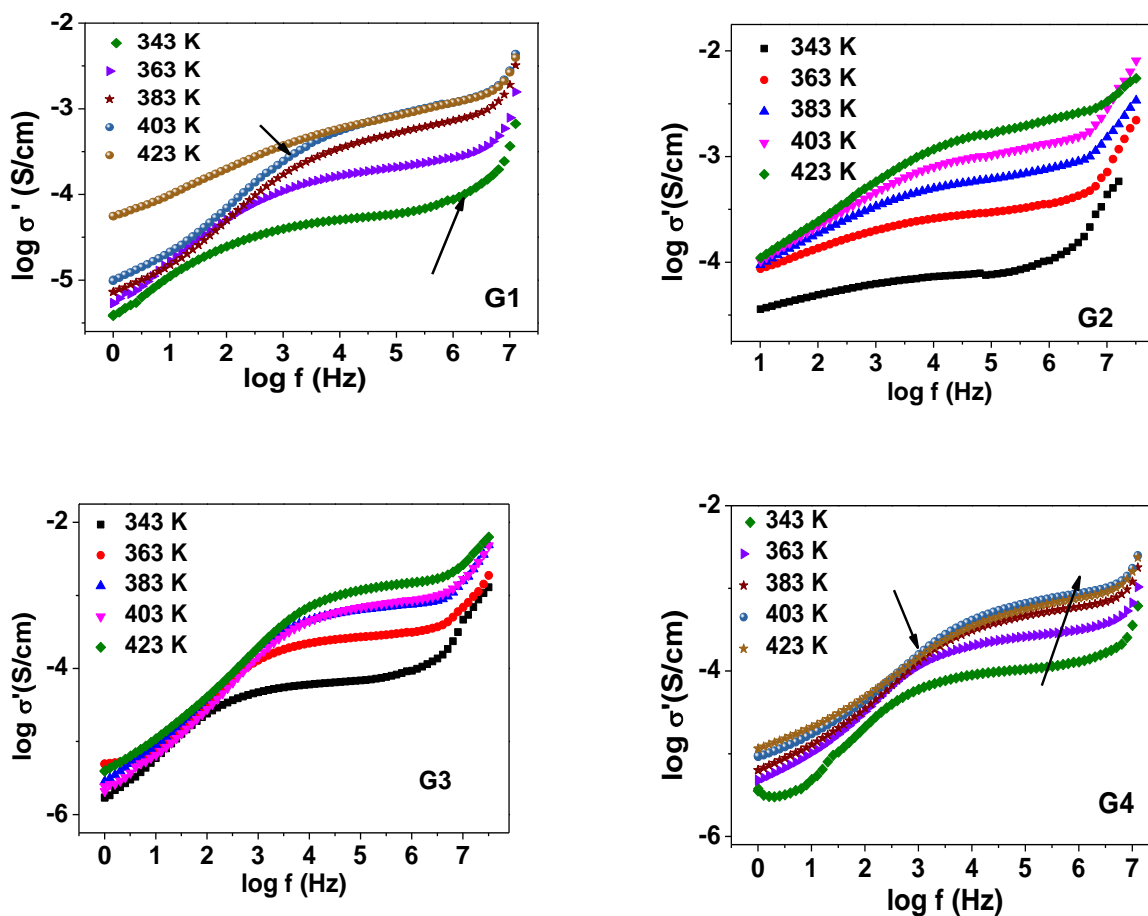


Fig. 5.35 Frequency dependent conductivity plots for $\text{Li}_{1.3}\text{Al}_{0.3-x}\text{Ga}_x\text{Ti}_{1.7}(\text{PO}_4)_3$ series at different temperature

Presence of reactive capacitor in grain boundary which indicates the space charge region has been discussed by [39, 44].

The temperature activated behavior of all samples of LAGTP series for grain and grain boundary regions are given in Fig.5.33 and 5.34 respectively. In Fig. 5.34, the Arrhenius plot of the grain boundary shows a wider variation amongst the samples. This behavior indicates that the local structure experienced by the Li^+ ion is changed with temperature of LAGTP compound. The sample G2 ($x=0.03$) has the highest DC conductivity for grain and grain boundary regions as seen in the Fig. 5.33 and 5.34.

Plots in Fig. 5.35 represent the frequency dependent behavior of conductivity for different temperatures for all compositions of LAGTP series. The conductivity isotherms show a steep rise in conductivity after 10^3 Hz. From the changing patterns of impedance plots

near the intermediate and lower frequency regions, it is clear that microstructure of grain boundary changes due to the formation of secondary phase GaPO_4 at grain boundaries with increase of temperature of higher gallium amount. For G1 sample (Fig.5.35) the isotherm for 423 K is relatively flat while those isotherms corresponding to temperatures lower than 423 K seem to overlap at lower frequencies. For G2 sample, conductivity spectra are well defined and represent uniform dispersive relaxation behavior. This indicates the main (LAGTP) and secondary (LGTP, GaPO_4) phases are uniformly distributed in the sample. Hence the Li^+ exhibit uniformity in relaxation pattern. The samples G3 has an overlap of all isotherms at lower frequencies. There is also a drop in conductivity of these isotherms. This indicates presence of blocking phases at grain boundary. For sample G4 in Fig. 5.35, the dispersive relaxation is somewhat uniform across temperatures which indicate that the secondary phases are more or less uniformly distributed in the grain and grain boundary regions.

At low frequencies, a steep drop in conductivity values in all four samples which points to the electrode-electrolyte capacitance and the presence of space charge region in this interfacial region which does not allow the diffusion of Li^+ through the grain boundaries. It points to the polarization effect due to the double layer capacitance created by Li^+ when they are trapped near the blocking phases at grain boundary. The conductivity behavior in terms of microstructure / defects is discussed as follows: due to comparable ionic radii of Ga^{3+} (0.62 Å) with Ti^{4+} (0.68 Å), Ga^{3+} cations can go near to M1 and M2 sites in the $\text{LiTi}_2(\text{PO}_4)_3$ lattice. The presence of Ga^{3+} and Ti^{4+} cations near the M1 and M2 vacancy sites increases the mobility of Li^+ ion at these sites. Hence there is an increase in the bulk conductivity. Due to presence of Ga^{3+} near the LTP sites, the bottleneck size is likely to increase and is conducive for Li^+ migration. Due to partial replacement of Ti^{4+} by Ga^{3+} at these sites, some Ti^{4+} is freed and likely forms rutile phase like TiO_2 or TiP_2O_7 . These rutile phases are present inside the grain and are insulating by nature. They are seen as small peaks in samples like G4 where Gallium content is more compared to other samples. Hence they act as impurities and block the Li^+ ion motion in G3 and G4 samples. The insulating effect of such impurity phases is

seen clearly wherein the resistance (circled blue) is used in the fitting of the grain region in Fig. 5.34

Ga^{3+} cations also replace Al^{3+} the series $\text{Li}_{1.3}\text{Al}_{0.3-x}\text{Ga}_x\text{Ti}_{1.7}(\text{PO}_4)_3$, in NASICON system [48, 49, 50] at Al_T tetrahedral sites and those at octahedral sites denoted by Al_O . At tetrahedral sites where Al_T coordinates with PO_4 tetrahedra, the GaPO_4 phases are formed. They are segregated when the quantity of Gallium in the system increases as more Ga^{3+} replaces Al_T . These GaPO_4 phases are seen as peaks in the XRD patterns [52]. When Ga^{3+} replaces Al_O , a likely phase formed is Li-Ga-Ti-P (LGTP) which also has a NASICON rhombohedral structure and contributes to the Li^+ ion conductivity at M1 and M2 sites [11, 12, 13]. Formation of such secondary phases like LGTP has been studied extensively by Aono [3, 51]. At the sites where Ga^{3+} has not been able to replace either Al^{3+} or Ti^{4+} , the Li-Al-Ti-P (LATP) phases – remain. Thus a likely reason for lower Li^+ ion conductivity of G3 and G4 samples compared to G1 and G2 could be presence of phases like GaPO_4 (when Ga^{3+} content is increased), the presence of rutile phases and change of crystalline structure from rhombohedral to monoclinic. Other workers [26] have also concluded that the segregated glassy phases at grain boundaries do contribute to impedance in the ionic motion along with density. This is also evident from density measurements where the increasing concentration of gallium also enhances the density of samples.

5.2.5 $\text{Li}_{1.3}\text{Al}_{0.3-x}\text{Sc}_x\text{Ti}_{1.7}(\text{PO}_4)_3$ (LASTP) system

The effect of doping of Scandium in the $\text{Li}_{1.3}\text{Al}_{0.3}\text{Ti}_{1.7}(\text{PO}_4)_3$ (LATP) system were studied according to the formula $\text{Li}_{1.3}\text{Al}_{0.3-x}\text{Sc}_x\text{Ti}_{1.7}(\text{PO}_4)_3$ where $x = 0.01, 0.03, 0.05$ and 0.07 . Scandium, a trivalent cation (Sc^{3+}) can replace another trivalent cation Al^{3+} in this system. Many studies concerning the scandium doped Lithium titanium phosphate system have been conducted [29, 51]. In general such studies conclude that the doping of scandium a main group element as a trivalent cation beyond a certain limit ($x > 0.8$) and its replacement in the NASICON lattice cell expands it. Due to this expansion of the unit cell, phase of the

synthesized NASICON compound changes from rhombohedral to monoclinic and on doping further ($x > 1.4$) even to triclinic [52, 53]. The latter two phases are relatively broad and occupy much more volume than the rhombohedral phase. The outer valence shell of scandium is spherical [50] like aluminum. Due to this it is easy for scandium to replace aluminum in a NASICON structure although the difference of ionic radii of Sc^{3+} (0.74 \AA) compared to Al^{3+} (0.53 \AA) is higher.

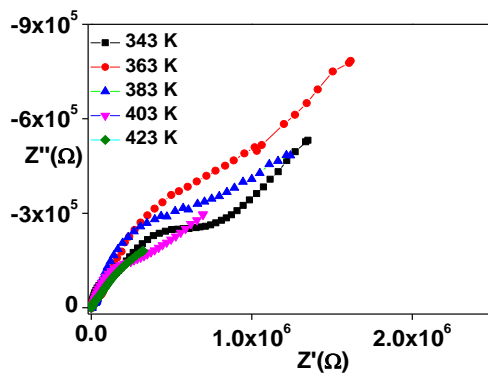


Fig. 5.36 Z' vs Z'' plot of $\text{Li}_{1.3}\text{Al}_{0.3-x}\text{Sc}_x\text{Ti}_{1.7}(\text{PO}_4)_3$ System for $x=0.01$ sample at different temperatures.

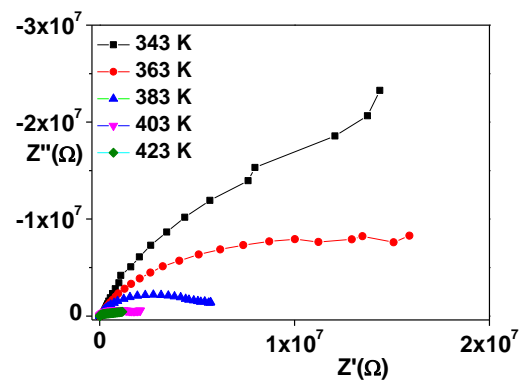


Fig. 5.37 Z' vs Z'' plot of $\text{Li}_{1.3}\text{Al}_{0.3-x}\text{Sc}_x\text{Ti}_{1.7}(\text{PO}_4)_3$ System for $x=0.07$ sample at different temperatures.

Fig. 5.36 and 5.37 represent the Nyquist plots for samples N1 ($x=0.01$) and N4 ($x=0.07$). The intercept on the Z' axis shifts towards the origin as the temperature increases. It can be noticed that the impedance of N1 sample is lesser than N4 sample for all temperatures. It can be seen from Fig. 5.37 that a following spike is formed after the second semi circular arc while for sample N4, the spike is not seen clearly. The presence of a spike in the low frequency region indicates polarization due to electrode-electrolyte interface. Fig. 5.38 shows the fitted plot for sample N1 at 363 K. It can be noticed that the fitting is done using the R and CPE circuit elements only (for both grain and grain boundary regions). Fig.5.39 and 5.40 depict the fitting for sample N4 ($x = 0.07$) at two different temperatures. At 373 K the fitting is done using an extra C and CPE element for low frequency (grain boundary) region. When the temperature is increased to 413 K, the fitting for grain boundary region is done using a capacitor only. It is known that C (pure reactance) is used when there is space charge between

the grain boundary layers in the system and CPE can be used in fitting only when impurities are present near the space charge regions [9, 45, 53]. It can be seen from the fitted impedance values in these plots that the grain is represented by R and CPE while separate C and CPE have to be used to fit the grain boundary region of scandium rich sample N4. This indicates that such secondary phases of scandium are segregated towards grain boundary and form space charge. The segregation of these secondary phases at grain boundary is explained below: when Sc^{3+} (0.72 \AA) tries to replace Al^{3+} (0.53 \AA) and Ti^{4+} (0.68 \AA), it succeeds in replacing only Ti^{4+} due to its comparable ionic radii. Thus a negatively charged defect Sc'_{Ti} is formed due to charge deficiency in the replacement. Similarly the grain boundary core loses oxygen and forms a positive charge at its core.

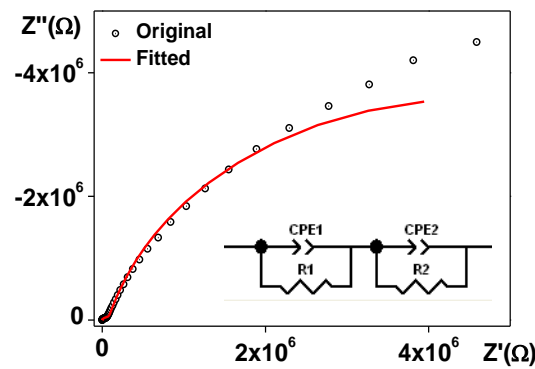


Fig. 5.38 Z' vs Z'' plot for $\text{Li}_{1.3}\text{Al}_{0.3-x}\text{Sc}_x\text{Ti}_{1.7}(\text{PO}_4)_3$ system for ($x=0.01$) at 363 K with equivalent circuit.

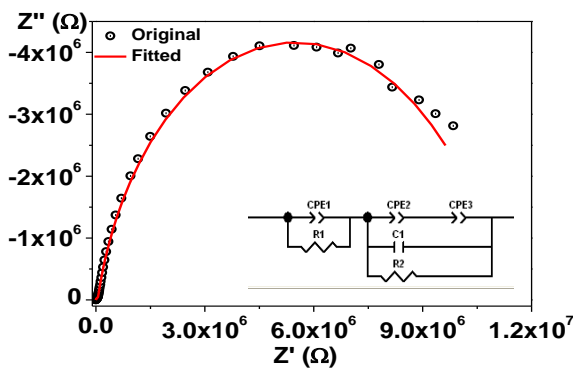


Fig. 5.39 Z' vs Z'' plot for $\text{Li}_{1.3}\text{Al}_{0.3-x}\text{Sc}_x\text{Ti}_{1.7}(\text{PO}_4)_3$ system for $x=0.07$ at 373 K with equivalent circuit.

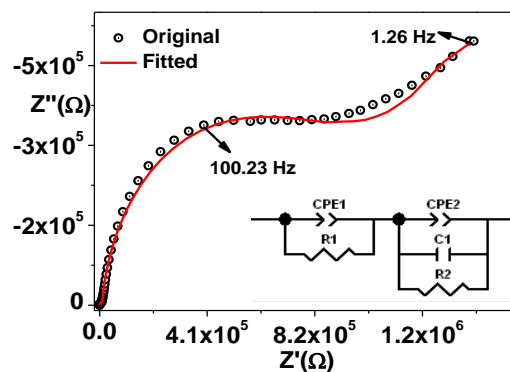


Fig. 5.40 Fitted Z' vs Z'' plot for $\text{Li}_{1.3}\text{Al}_{0.3-x}\text{Sc}_x\text{Ti}_{1.7}(\text{PO}_4)_3$ for $x=0.07$ sample at 413 K with equivalent circuit.

These negatively charged defects are electrostatically attracted towards the positively charged grain boundary core. A space charge is formed near grain boundary when negatively charged defects like Sc_{Ti}' travel towards positively charged grain boundary core (which is deficient in $V_{\dot{O}}$ (oxygen vacancies). The increased temperature (more than 1000° C during the third heat treatment during the synthesis of the samples) helps these defects to move across distances [39]. Hence when these negatively charged defects are attracted by electrostatic forces towards grain boundary they form $ScPO_4$ like phases at grain boundary. At low frequencies the Li^+ drift long distances and reach the electrode-electrolyte interface where they get accumulated at this interface. This causes the formation of a spike at low frequencies. The impedance values of the spike can be fitted using a capacitance. The segregated $ScPO_4$ phases at grain boundary increase with an increase in Sc-doping in the system. This is evident from the increasing height of $ScPO_4$ peak in the XRD patterns. These phases coexist with the main phase (which is $LiTi_2(PO_4)_3$ in our case) as mixed phases [51, 55]. An extensive study was carried out by Tran Qui *et al.* [56, 57, 58] for indium doped LTP system in which the existence of mixed phases and the conversion of rhombohedral phases to monoclinic and triclinic phases were reported.

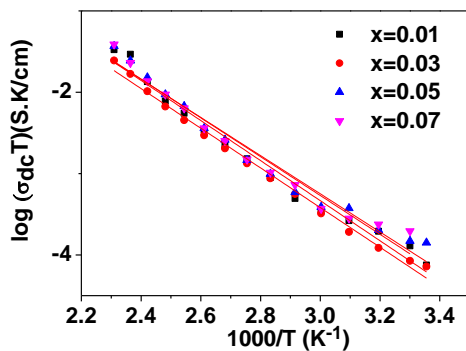


Fig. 5.41 Arrhenius plots for grain region of $Li_{1.3}Al_{0.3-x}Sc_xTi_{1.7}(PO_4)_3$ series

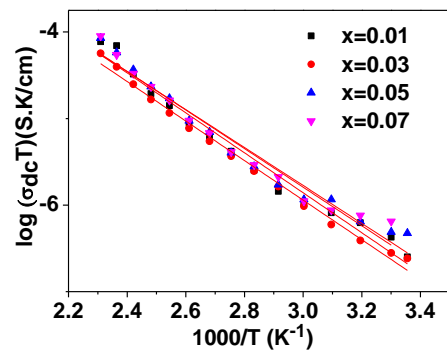


Fig. 5.42 Arrhenius plots for grain boundary region of $Li_{1.3}Al_{0.3-x}Sc_xTi_{1.7}(PO_4)_3$ series

Figs.5.41 & 5.42 give the Arrhenius plots for all four samples of $Li_{1.3}Al_{0.3-x}Sc_xTi_{1.7}(PO_4)_3$ (LASTP) series. It is clear from these figures that all four samples behave almost the same. That is, slopes of the lines of the linear fitted points for all four samples are

almost the same. The DC conductivity values are temperature activated. This is because, the population of Li^+ ions increases with temperature as they are able to overcome the activation energy barriers. These free Li^+ ions tend to drift along and diffuse along the conduction pathways over large distances in the 3-D network, which enhances the DC conductivity. The Fig. 5.43 shows the frequency dependent Li^+ ion conductivity in all the four samples of LASTP series. From Fig. 5.43, it is clear that there are two dispersive relaxation regions – one corresponding to intermediate frequencies for grain boundary and the other for higher frequencies for grain region. The dispersion in the frequencies shifts towards higher frequencies as temperature increases for each sample.

At frequencies higher than 10^6 Hz, overlap of the conductivity isotherms indicates that the Li^+ ions do not have enough relaxation time as their motion becomes localized and the effect of temperature on the hopping frequency is less. The dispersive region and the shift towards higher frequencies for all the samples is almost the same.

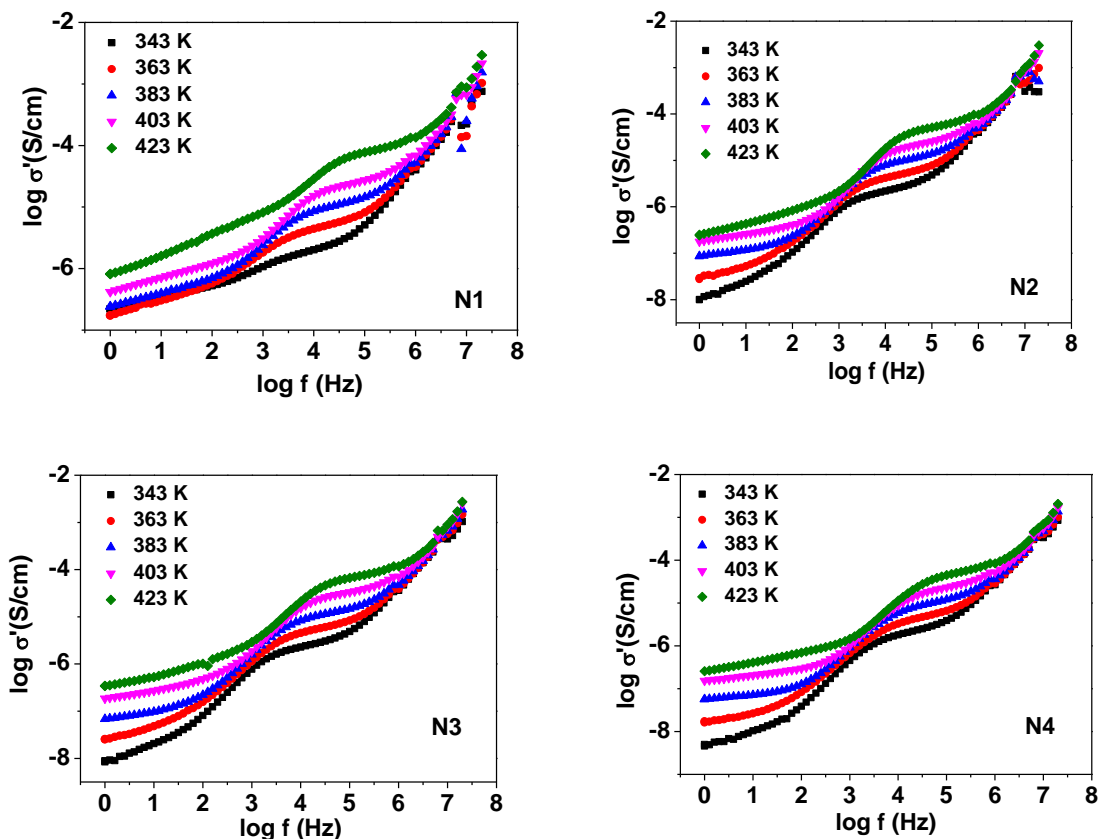


Fig. 5.43 Frequency dependent conductivity plots for samples of $\text{Li}_{1.3}\text{Al}_{0.3-x}\text{Sc}_x\text{Ti}_{1.7}(\text{PO}_4)_3$ series at different temperatures

The Li^+ conductivity in LASTP system can be explained as follows: the Sc^{3+} (0.72 \AA) tries to replace Al^{3+} (0.53 \AA) at tetrahedral and octahedral sites, while it replaces Ti^{4+} (0.60 \AA) at octahedral sites in the LASTP system. It is successful in replacing Ti^{4+} due to lesser difference in ionic radii [28, 39]. But it is not able to replace Al^{3+} due to larger difference in ionic radii. It gets segregated towards grain boundary where Sc forms secondary phases like ScPO_4 [24-26]. At grain boundary the uniform distribution of such phases which are insulating in nature is seen across all samples. The highest conductivity is seen for N1 sample whose composition closely resembles (parent) LATP system (which has the highest Li^+ conductivity).

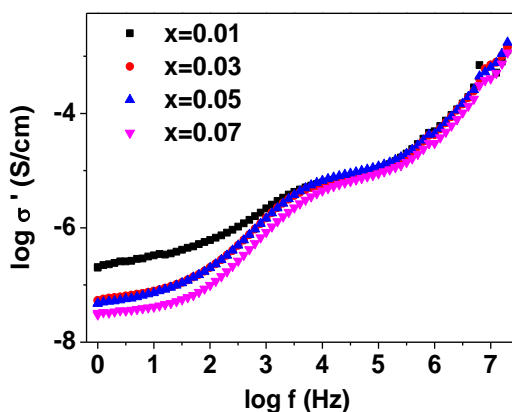


Fig. 5.44 Comparison of frequency dept. conductivity plots of $\text{Li}_{1.3}\text{Al}_{0.3-x}\text{Sc}_x\text{Ti}_{1.7}(\text{PO}_4)_3$ series at 373 K

Fig. 5.44 (above) gives a comparison of the conductivity at 373 K for all samples. It is clear that the behavior of conductivity isotherms is almost the same at high frequency region (which as discussed in Nyquist plots corresponds to grain region) for all samples but that for grain boundary conductivity is better for N1 sample. Hence it can be concluded that the presence of increased amount of scandium produces secondary phases which inhibit the Li^+ at grain boundary. This is also seen in case of fitted plots of Figs. 5.39 and 5.40 of sample N4 (where concentration of scandium $x = 0.07$) in which capacitance C and resistance R are used, apart from the CPE element that was used in fitting the data of sample N1 ($x = 0.01$) (Fig. 5.38) for grain boundary region and interfacial region between electrode and electrolyte.

Figs. 5.45 & 5.46 (below) show the ionic conductivity behavior in frequency range of 20 MHz to 1 Hz for samples of all three dopants at one temperature 343 K. A comparison with parent systems LTP and LATP shows that these samples have a superior conductivity compared to the doped samples. This shows that the dopants induce impurity phases in the parent system. In fact, there is a difference of an order of magnitude in the conductivity between the parent and doped systems. In Fig. 5.45 it can be seen that at high frequencies, amongst the doped samples the conductivity of gallium, yttrium and scandium containing systems is comparable but at low the conductivity for gallium containing sample is better than others.

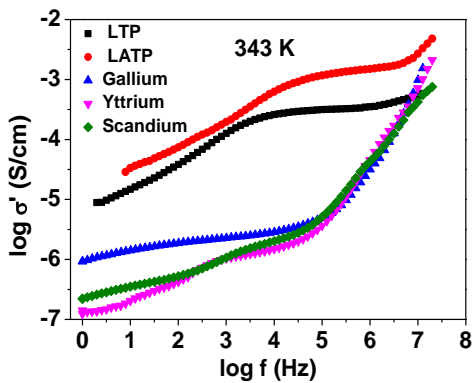


Fig. 5.45 Conductivity behaviour of different dopants for $x = 0.01$ concentration at 343 K.

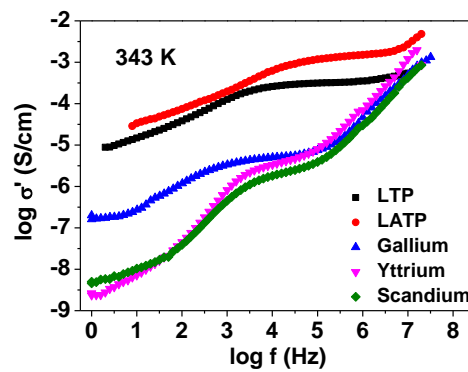


Fig. 5.46 Conductivity behaviour of different dopants for $x = 0.07$ concentration at 343 K.

At low concentration ($x = 0.01$) of the dopants, small amounts of impurity phases are not segregated completely towards grain boundary. But gallium has a low melting point and segregates better and faster towards grain boundary than heavy yttrium and scandium. Besides, Ga^{3+} (0.64 \AA) has smaller ionic radii compared to Y^{3+} (0.93 \AA) and scandium (0.74 \AA). Due to this, Ga^{3+} is able to better replace both Al^{3+} (0.53 \AA) and Ti^{4+} (0.60 \AA) at the tetrahedral and octahedral sites in the LATP lattice. Due to their larger volume, the Y and Sc atoms may block the conduction pathways (bottlenecks) and hinder the passage of Li^+ . This may be a primary reason of decreased conductivity of the yttrium and scandium doped samples compared to the parent system LATP in the grain region.

In Fig. 5.46, the conductivity isotherms at same temperature 343 K but for higher concentration ($x = 0.07$) of dopant are plotted. The parent systems LTP and LATP have better conductivity compared to heavily doped samples. It is seen clearly that at low frequencies, corresponding to the grain boundary region, the gallium has better conductivity than yttrium and scandium doped counterparts. At higher frequencies, the conductivity corresponding to grain region is comparable for all three dopants. At higher concentrations the dopants tend to form (secondary) phosphate phases (like YPO_4 , GaPO_4 and ScPO_4) which segregate more towards grain boundary. As mentioned earlier, in case of gallium – due to its low melting point, the gallium phases tend to segregate easily towards grain boundary while yttrium and scandium require exposure to higher temperature and longer times. Hence we performed sintering at 1000°C of yttrium doped samples. It was observed that grain boundary conductivity improved especially for samples with higher yttrium concentration.

5.3 Dielectric Studies

On applying an external time dependent electric field on the material electrons and ions get polarized within it. Different relaxation times corresponding to electronic, ionic, dipolar etc polarization within a material and at the electrode-electrolyte interfaces in a cell are observed. The dielectric property of a material associated with the polarization is studied using broadband dielectric spectroscopy and helps to identify the dominant relaxation mechanisms in the frequency range for the material. The material's resistive response to an electrostatic field is termed as dielectric behavior. Unlike metals, the dielectric materials contain no free electrons or charge carriers.

In ion conducting materials, the electrons are not the majority charge carriers. Hence it is important to understand the dielectric response of the material in ion conducting solids. When an electrostatic field is applied across a material, the electric field lines pass through it. Electrons under the influence of the applied electric field move. In dielectric material, by contrast, the electrons are tightly held by atoms. Hence a negligible number of electrons become mobile in the electric field. When a time varying (AC) electric field is applied across

an ion conducting material, the ions tend to become polarized in the medium. At lower frequencies the electric field cycle changes the polarity slowly hence the ions have enough time to travel a longer distance by diffusion. They travel a distance of several nanometers and sometimes upto grain boundary. At grain boundary and at electrode-electrolyte interface, they tend to pile up and build up a space charge region. At higher frequencies, however, the ions tend to execute hopping motion. However the ions have an electronic atmosphere around them. This electronic cloud cannot adjust to the rapidly varying electric field. Due to this the ions tend to develop a lag with respect to electric field. The ions cannot cope with the changing cycles of electric field. This lag in the ion's tendency to get polarized according to the electric field or orient with the external electric field is called the ionic or dielectric relaxation. During the relaxation time, the ions cannot accept the electrical field energy nor can accept the changed orientation of the electric field. Relaxation phenomenon points to the non linearity of stimuli (the changing electric field) and the ionic response (the lag in ionic motion). This deviation from the ideal behavior is also called the non Debye behavior of ions. The deviation from the ideal Debye behavior indicates the presence of local microstructural abnormalities that the ions experience when they relax. The net dipole moment leads to characteristic properties of the material (for example, the characteristic hopping frequency of the ion in a material system). Besides, the environments where ions tend to relax also have to undergo rapid change in the electrostatic configuration. That is, when an ion has to change the polarity according to the electric field, the delay (lag) is also caused by the electrostatic influence of the environment of the ion.

The capacitance between the parallel plates of a condenser is defined as the tendency to withstand the electric field created due to charges on the two plates as follows:

$$C = \frac{\epsilon A}{d} = \epsilon_0 \cdot k \frac{A}{d} \quad \dots\dots (5.5)$$

where $\epsilon_0 = 8.854 \times 10^{-12}$ F/m is the dielectric constant (permittivity) in vacuum, k is relative permittivity of the dielectric material between the plates, A is surface area of the plates and d is the separation between the plates.

When the dielectric material is exposed to the AC electric field, we define the complex dielectric function ϵ^* as follows: $\epsilon^* = \epsilon' - j \epsilon''$

here, ϵ^* indicates the molecular relaxation and transport properties of the charge carriers in the material. ϵ' which is the real part of the dielectric permittivity is termed as the tendency of material to store energy in each cycle of the electric field. Due to this elastic energy the ionic hopping motion and polarization takes place. Therefore, higher values of ϵ' indicate a better electrical response (and hence better electrical conductivity) of the material. ϵ'' is termed as loss of this electric field energy due to dissipation which is partly due to relaxation behavior of the ions. The ratio of ϵ'' to ϵ' is called the loss tangent (also defined in Ch.3)

When the temperature of the material is increased, the number of ions and vacancies in which they tend to diffuse into, also increase. But due to agitating motion due to thermal energy, the ions cannot relax completely. This causes a lag and increased tendency of the ions towards non Debye behavior of the ions. Thus the relaxation time (τ) also increases with temperature. Studying these characteristics helps us to understand not only the tendency of material to conduct but also present an indirect evidence of local inhomogeneities in microstructures where ions relax.

The dielectric studies are important to understand the reaction of the material under study to the electrical signal. The material's capacitive response to alternatively changing electrostatic field is termed as dielectric behavior. Unlike metals, the dielectric materials contain no free electrons or charge carriers. Hence the charge carriers in these materials are the conducting ions (Li^+) in our case. Hence it is important to understand the dielectric response of the material in ion conducting solids. In the below sections we have enumerated the dielectric response of different materials synthesized.

5.3.1 Reference LTP and LATP systems

LTP system has a rhombohedral NASICON structure which is not affected by doping (albeit in small concentration) by trivalent cations like Al^{3+} , Y^{3+} , Ga^{3+} , Sc^{3+} [51, 46]. From the

Reitveld studies it has been observed [11, 24, 25, 26, 82] that doping by elements of higher ionic radii (like replacing Al^{3+} (0.53 Å) by Y^{3+} (0.93 Å), Sc^{3+} (0.74 Å) and Ga^{3+} (0.64 Å) increases the lattice cell (of $\text{LiTi}_2(\text{PO}_4)_3$) size. Therefore the microstructure within grain and grain boundary regions are changed. Due to changed microstructure, the presence of various defects like cracks, gaps etc, space charge zones are formed. This gives rise to the capacitive response (double layer of ions (Li^+) and defects ($\text{Y}'_{\text{Ti}}, \text{V}''_{\text{O}}$) across the 2-D and 3-D structural defects like line defects, stack plane faults, chemical inhomogeneities and amorphous phases. The changing polarity of the electric field across such double layer capacitors affects the reactive (capacitive) element. Thus the dielectric properties of the material are altered and give an idea about the internal structure and arrangement within the Li^+ conducting material. In the below section, we have presented the results from dielectric studies for reference.

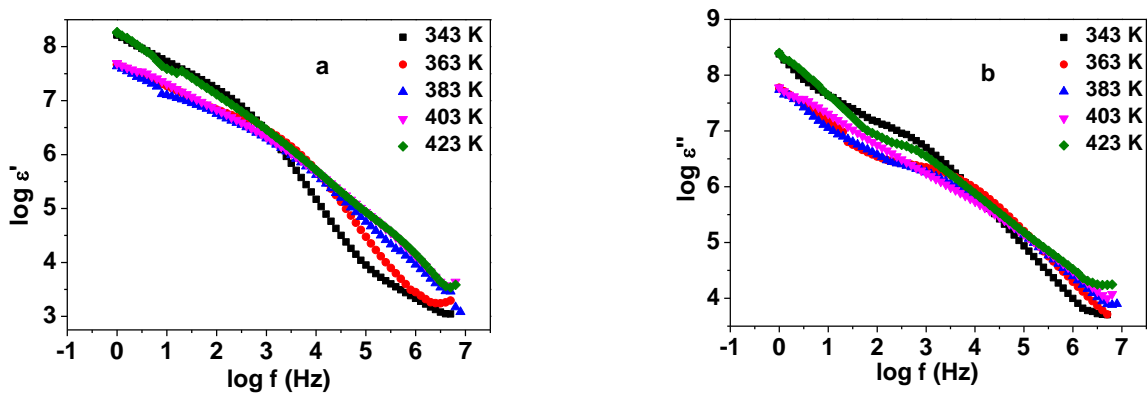


Fig. 5.47 Variation with respect to frequency for $\text{LiTi}_2(\text{PO}_4)_3$ sample of (a) real part of dielectric permittivity ϵ' (b) imaginary part of dielectric permittivity ϵ'' at different temperatures

Fig. 5.47 (a and b) give the variation of real and imaginary parts of dielectric permittivity for LTP sample. At low frequencies, a high value of permittivity is observed for LTP system. This is due to the polarization observed at electrode-electrolyte interface. That is all the energy from the electric field cycle is taken by the dipoles. The energy loss represented by imaginary part of dielectric permittivity also follows the same pattern of high values at low frequencies. At intermediate frequencies, the polarization disappears but there is very less dispersion observed. This is followed by a slight saturation at higher frequencies ($10^6 - 10^7$ Hz) which indicates the relaxation of Li^+ in their local area. The dispersion is not seen for

LTP system because of presence of insulating phases like TiO_2 in the grain region. These phases have been detected in XRD patterns. The saturation in values of ϵ' and ϵ'' values at high frequencies is due to that when the dipoles are exposed to very high frequencies, their motion becomes localized. They cannot jump and move to larger distance and hence are exposed to similar local environment. Hence the dielectric permittivity and the associated loss behavior is almost the same for every hop and jump motion that the Li^+ perform at their local sites [79, 80].

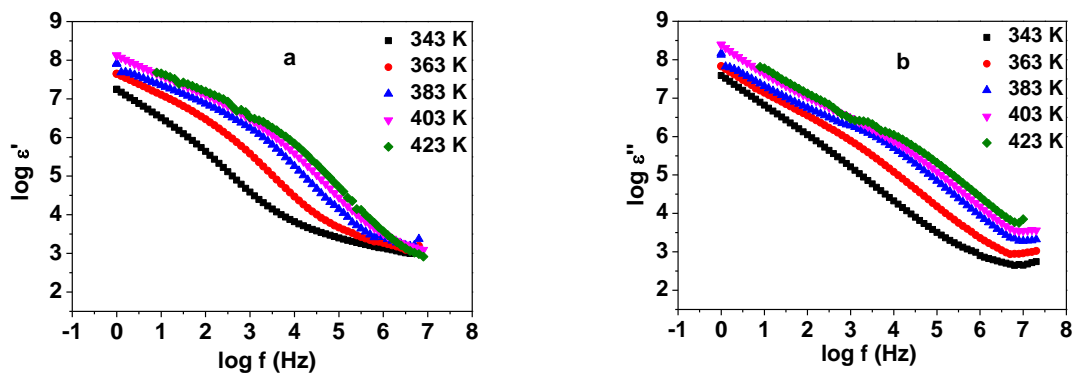


Fig. 5.48 Variation with respect to with frequency for $\text{Li}_{1.3}\text{A}_{0.3}\text{Ti}_{1.7}(\text{PO}_4)_3$ sample (a) of real part of dielectric permittivity ϵ' (b) of imaginary part of dielectric permittivity ϵ'' at different temperatures.

Fig. 5.48 (a and b) presents the behavior of real and imaginary part of permittivity for LTP sample. At low frequencies, the values of permittivity are high but in intermediate frequencies, there is a marked dispersion. It indicates that for LTP system in the grain boundary region, the Li^+ relaxes in different microstructural areas. This happens because the Li^+ have enough time to travel to different regions within grain and grain boundary before the next cycle of electric field. At high frequencies (10^6 Hz), there is saturation indicating that the Li^+ do not get enough time to travel larger distances and their motion is more or less localized. The relaxation is confined to local position (near the Li vacancies).

The same phenomenon is observed for all temperatures in LTP and LTP system indicating that dielectric permittivity behavior in this Li^+ ion conducting material is

independent of temperature (in the range in which the impedance measurements were performed).

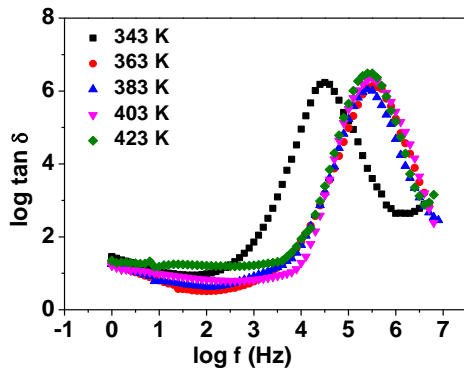


Fig. 5.49 Variation of loss tangent $\tan \delta$ with frequency for $\text{LiTi}_2(\text{PO}_4)_3$ sample at different temperatures.

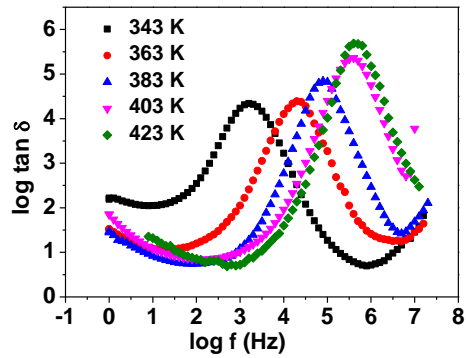


Fig. 5.50 Variation of loss tangent $\tan \delta$ with frequency for $\text{Li}_{1.3}\text{Al}_{0.3}\text{Ti}_{1.7}(\text{PO}_4)_3$ sample at different temperatures.

Fig.5.49 and 5.50 indicate the behavior of loss tangent of LTP and LATP respectively. The loss tangent is defined in previous chapters. The $\tan \delta$ values for LTP are superimposed for different temperatures, on a single curve, while that for LATP system is spread across for different temperatures. This indicates that the loss is constant for all temperatures in LTP system while it is not uniform for LATP system.

5.3.2 $\text{Li}_{1.3}\text{Al}_{0.3-x}\text{Y}_x\text{Ti}_{1.7}(\text{PO}_4)_3$ (LAYTP) system

The results of dielectric permittivity (real and imaginary parts) for yttrium doped LATP system are presented in Fig. 5.51. The doping is done for six concentrations from $x = 0.01, 0.03, 0.05, 0.07, 0.10$ and 0.15 . In the fig 5.51, the variation of real part of dielectric permittivity (ϵ') with respect to frequency are given. At intermediate frequencies, dispersion is observed across all temperatures and for all samples of the LAYTP series. The dispersion shifts towards higher frequencies, as temperature increases across all samples of the LAYTP series. It can also be noticed that the permittivity values increase with temperature for all samples. That is as temperature increases, the permittivity values are higher. At increasing frequencies, the values of permittivity decreases until they attain saturation across all temperatures.

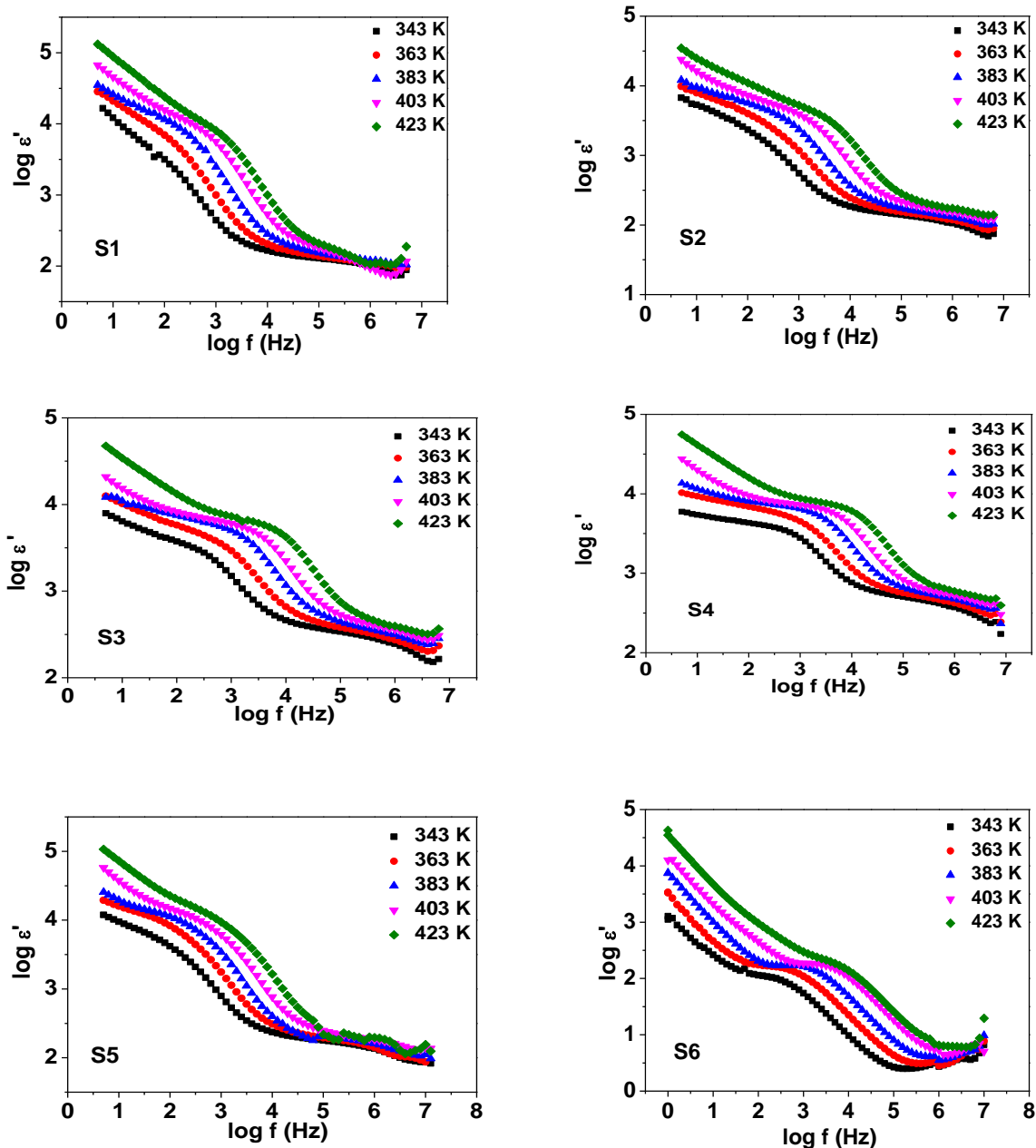


Fig. 5.51 Variation of dielectric permittivity ϵ' as a function of frequency for $\text{Li}_{1.3}\text{Al}_{0.3-x}\text{Y}_x\text{Ti}_{1.7}(\text{PO}_4)_3$ series at different temperatures.

This behavior can be explained as follows: At low frequencies, the electric field lines are permitted more through the medium. This causes an increase in the values of dielectric permittivity. Therefore at low frequencies, the dipoles formed by Li^+ ions experience long times before the polarity of the electric field changes. Dipole can easily adjust to the changing orientation of the electric field. Therefore the dielectric permittivity is also higher at low frequencies. In intermediate frequency range dispersion is observed because the Li^+ travels a

larger distances within grain and grain boundary regions before the next cycle of the electric field changes its orientation. Therefore dispersion is observed at intermediate frequencies. The amount of dispersion is seen more for the samples with lesser yttrium concentration – that is $x = 0.01$ and 0.03 compared to others. The Li^+ ions are easily able to travel across the grain and grain boundary regions in these samples with lesser amount of yttrium. This is because, as yttrium increases, the phases like YPO_4 and LiAlPO_5 also increases. This causes blocking effect of Li^+ in the system, due to which they tend to travel lesser distances in yttrium rich samples of LAYTP series than samples $x = 0.01$ and 0.03 .

The dispersion shifts towards higher frequencies as temperature increases, because, the dipoles at increased temperatures have high ro-vibrational energy. Hence these Li^+ ions (dipoles) are free easily at higher temperatures and can easily orient and adjust to changed electric field direction, compared to the dipoles at lower temperatures. Hence the time taken by the dipoles at higher temperatures is lesser. Hence as temperature increases, the dispersion shifts to higher frequency regimes for all samples. Also at higher temperatures, the number of available Li^+ will be higher. Hence the capacity of the material to accept, store the energy from electric field and finally orient itself according to its direction will also be more. Therefore it can be seen that the dielectric permittivity ϵ' increases with temperature. At higher frequencies, the tendency of the Li^+ , to accept the electric field energy and to orient according to it does not increase in the same proportion but tends to saturate for all temperatures. That is, the population of Li^+ at all temperatures, at higher frequencies is almost the same. Also, the dipoles (Li^+) have very less time to orient with the changed direction of electric field.

Hence, they neither orient completely nor do gain energy from the electric field before the next cycle of electric field appears. Besides, the Li^+ are confined to their local positions because of the rapidly changing field. Therefore, they appear to be in the same place which causes the dispersion to decrease. Due to these reasons, there is saturation in the higher frequency regime. In this series yttrium was doped in the LATP lattice. Due to presence of yttrium at grain and grain boundary, the following changes are formed in the structure. The

yttrium in grain tries to replace the Al^{3+} (0.53 Å) and Ti^{4+} (0.605 Å). But owing to its very large size Y^{3+} (0.93 Å) cannot be accommodated in the $\text{LiTi}_2(\text{PO}_4)_3$ (LTP) rhombohedral lattice. The yttrium forms compounds like YPO_4 [25, 51, 82] and gets segregated at the grain boundaries. Other compounds like $\text{Li}_3\text{Y}_2(\text{PO}_4)_3$ – called the mixed phases [62] are also likely formed in the system and due to inhomogeneities in the local structure. It can be seen from the (real) permittivity plots that with increasing quantity of yttrium the values of ϵ' does not seem to decrease. This indicates that with yttrium in the system, the local structure is adversely influenced and Li^+ conductivity decreases. With increasing yttrium concentration, the capacity to retain electric field energy and tendency of the dipole to orient with the externally applied field, decreases.

Similar behavior is exhibited by imaginary part of dielectric permittivity (see figures 5.52, 5.53 and 5.54 below). The losses at lower frequencies are significant compared to those at higher frequencies. The dielectric loss behavior shows a monotonic decrease with increasing frequencies. At mid (intermediate) frequencies, there is dispersion also. At higher frequencies, a saturation plateau after a cross over frequency is attained. The losses by the Li^+ dipoles due to charge accumulation decrease as the periodic reversing field frequency increases [84]. Thus the polarization losses associated with low frequencies decrease with increasing frequency. The losses are more significant with increasing temperature.

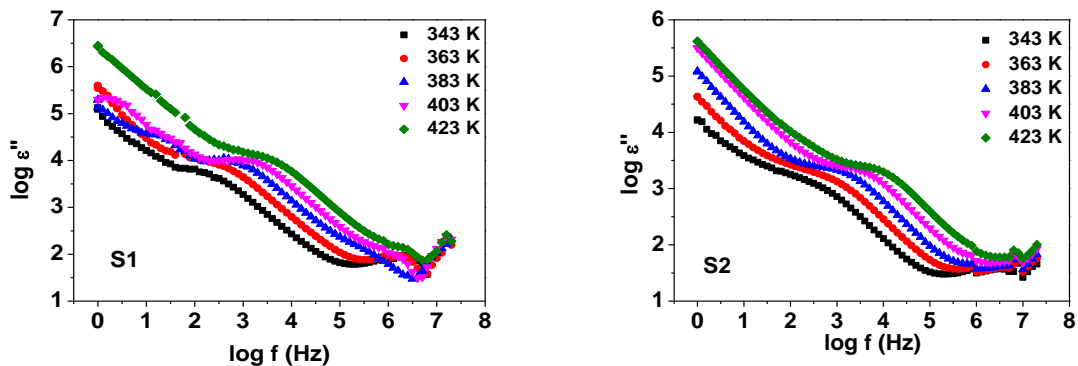


Fig. 5.52 The variation of dielectric permittivity ϵ'' with frequency for $\text{Li}_{1.3}\text{Al}_{0.3-x}\text{Y}_x\text{Ti}_{1.7}(\text{PO}_4)_3$ system for samples of $x=0.01$ and $x=0.03$ concentrations for different temperatures.

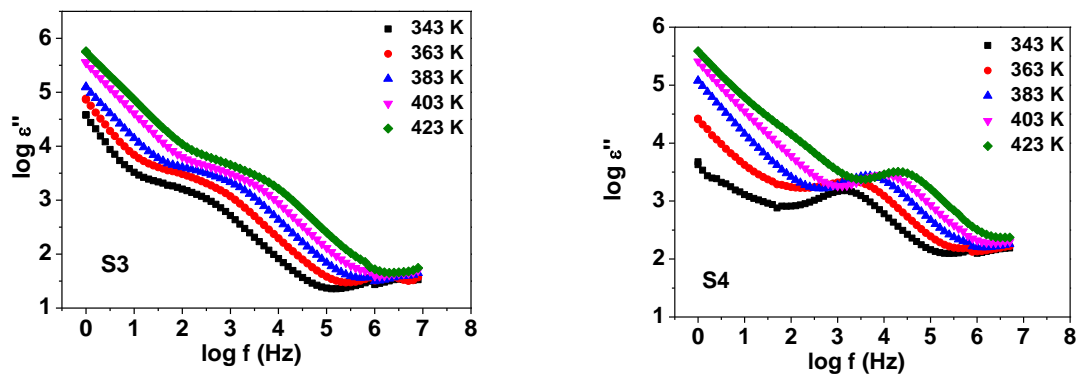


Fig. 5.53 The variation of dielectric permittivity ε'' with frequency for $\text{Li}_{1.3}\text{Al}_{0.3-x}\text{Y}_x\text{Ti}_{1.7}(\text{PO}_4)_3$ series for samples $x=0.05$ and $x=0.07$ for different temperatures.

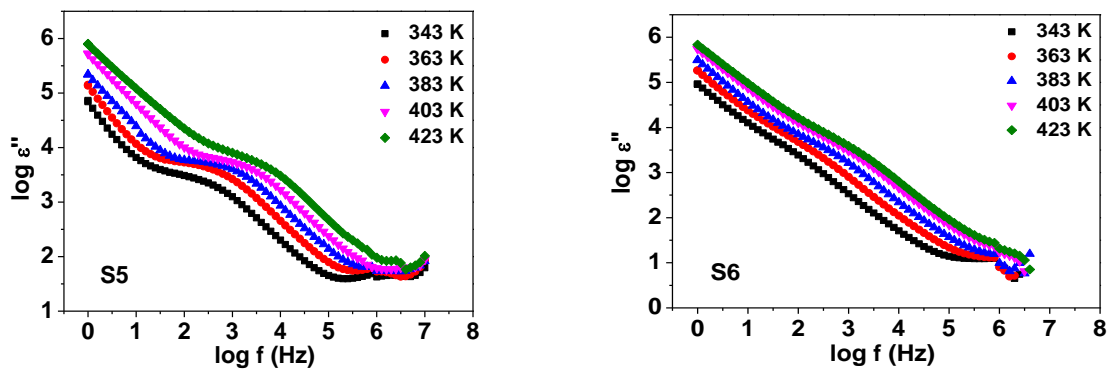


Fig. 5.54 The variation of dielectric permittivity ε'' with frequency for $\text{Li}_{1.3}\text{Al}_{0.3-x}\text{Y}_x\text{Ti}_{1.7}(\text{PO}_4)_3$ series for $x = 0.10$ and $x = 0.15$ samples for different temperatures.

This is, because random agitations of Li^+ ions increase with temperature. There are losses due to their random agitation due to higher thermal energy increases in the space charge region at the interface as well. Besides, with increased quantity of yttrium and temperature, there is a shift in the dispersion towards higher frequencies. The Li^+ which at higher temperatures has more thermal energy tend to attain the characteristic jump frequencies at higher frequencies only [85].

Figures 5.55, 5.56 and 5.57 below show the variation of $\tan\delta$ with frequency at increasing temperatures. It can be noticed that the loss in each sample increases with temperature. Also the peak shifts towards higher frequencies as temperature increases.

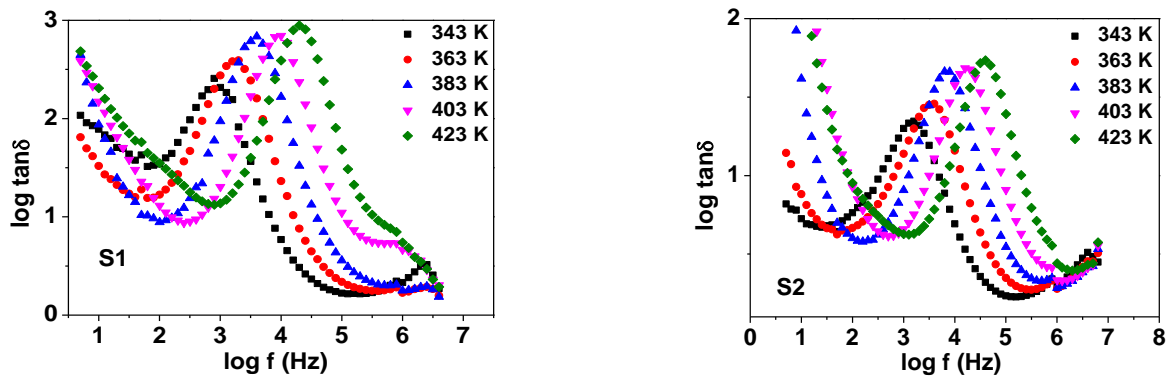


Fig. 5.55 The variation of loss tangent $\tan \delta$ with frequency for $\text{Li}_{1.3}\text{Al}_{0.3-x}\text{Y}_x\text{Ti}_{1.7}(\text{PO}_4)_3$ for $x = 0.01$ and $x=0.03$ concentrations at different temperatures.

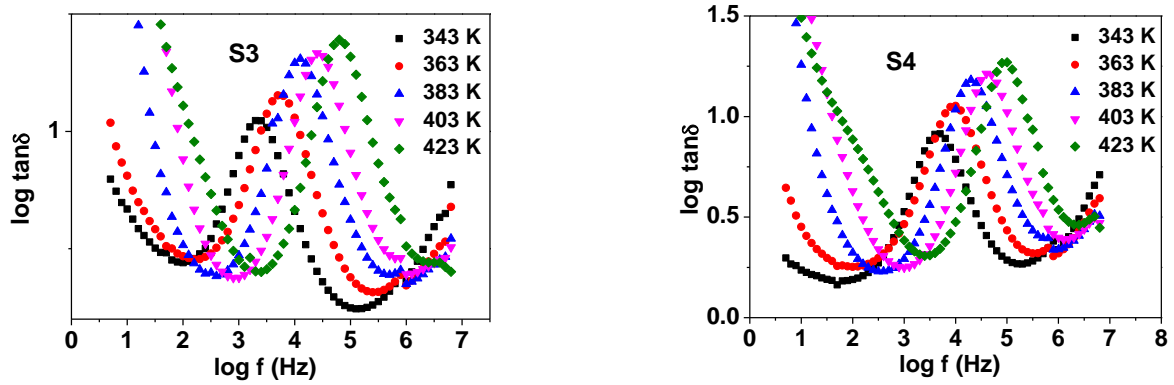


Fig. 5.56 The variation of loss tangent $\tan \delta$ with frequency for $\text{Li}_{1.3}\text{Al}_{0.3-x}\text{Y}_x\text{Ti}_{1.7}(\text{PO}_4)_3$ for $x=0.05$ and $x=0.07$ concentrations at different temperatures.

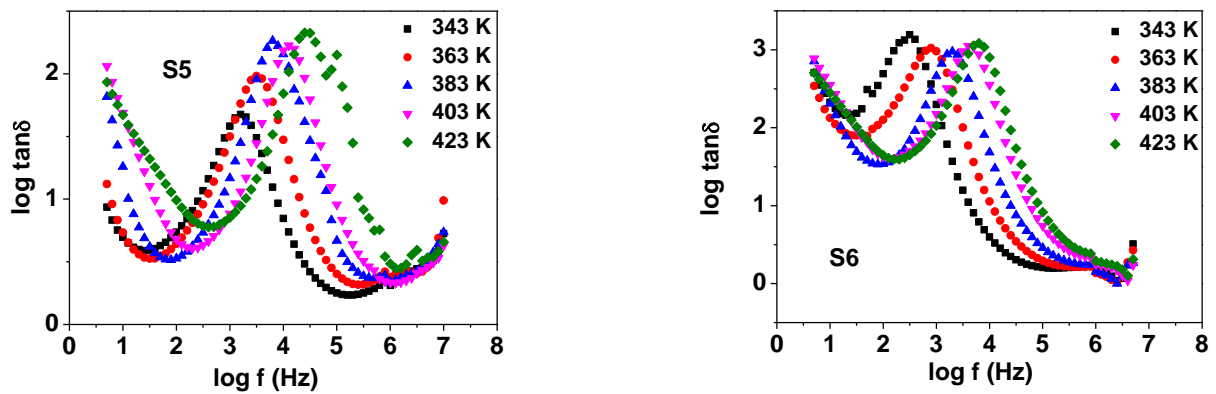


Fig. 5.57 The variation of $\tan \delta$ with frequency for $\text{Li}_{1.3}\text{Al}_{0.3-x}\text{Y}_x\text{Ti}_{1.7}(\text{PO}_4)_3$ for $x=0.10$ and $x=0.15$ concentrations at different temperatures.

The peaks correspond to the characteristic jump frequency of the Li^+ for that temperature. It can be noticed that loss peaks corresponding to the characteristic jump frequencies, shift towards higher frequencies, as temperature increases. Besides, the peaks also attain higher $\tan\delta$ values with increasing temperature. This can be explained as follows: as temperature increases, the random agitation of Li^+ also increases. Due to this, the Li^+ tends to lose the energy faster to its surroundings than it can gain energy. Hence under random thermal agitations, the dipoles tend to orient only at higher frequencies. Due to this the loss $\tan\delta$ peaks shift towards higher frequencies [86]. According to some authors the dispersion in $\tan\delta$ values in phosphate systems [87]. Some workers like Padmasree *et al.* [88] have found $\tan\delta$ values in phosphate glasses are independent of temperature at lower frequencies which they attribute to inverse dependence of $\tan\delta$ to some power of frequency. With increasing yttrium concentration, the $\tan\delta$ losses also tend to increase. Some authors attribute this to absorption by dopant impurity phases [89].

The losses at lower frequencies are significant compared to those at higher frequencies especially in the samples of higher dopant concentrations.

5.3.2 Heat Treated $\text{Li}_{1.3}\text{Al}_{0.3-x}\text{Y}_x\text{Ti}_{1.7}(\text{PO}_4)_3$ (LAYTP) system

When yttrium doped samples are heat treated for differing duration of time (2 hr and 3 hr) they exhibit almost similar behavior in terms of dielectric permittivity compared to that mentioned in the previous section for normal samples of LAYTP series. The results of LAYTP heat treated samples are presented below. In the below figures 5.58 (a and b) the real (ϵ') and imaginary (ϵ'') parts of dielectric permittivity are plotted as a function of frequency for sample S1 sintered for 2 hours. The high values of permittivity at lower frequencies followed by dispersive region(s) at mid frequencies, for all temperatures, is clear. The dispersion continues at high frequencies also. It means that at high frequencies also, the Li^+ in grain region have enough time to align with external electric field.

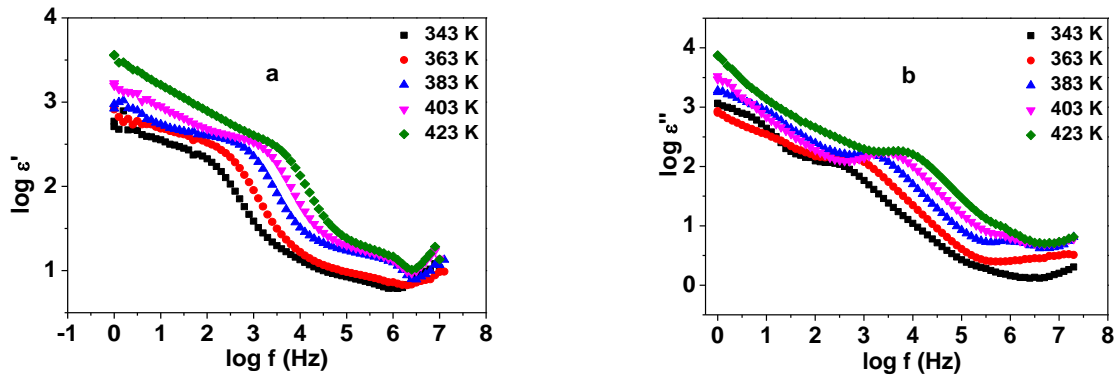


Fig. 5.58 (a) Variation of real part of dielectric permittivity ϵ' with frequency (b) imaginary part of dielectric permittivity ϵ'' with frequency for sample S1-H2 of $\text{Li}_{1.3}\text{Al}_{0.3-x}\text{Y}_x\text{Ti}_{1.7}(\text{PO}_4)_3$ at different temperatures.

The dispersion is due to back and forward hopping sequence [89]. The dispersion shifts to higher frequencies with temperature. There is no significant change in the behavior in the low frequency and dispersive behavior at mid frequencies, at different temperatures and concentration of yttrium. But at higher frequencies, the yttrium rich sample (S6 ($x=0.15$)) in Figs. 5.59 (a and b) has a narrow, flat saturation plateau compared to its yttrium poor counterpart (S1). At higher frequencies, the dispersion (spread) in the saturation plateau is less for real part of dielectric permittivity for all temperatures.

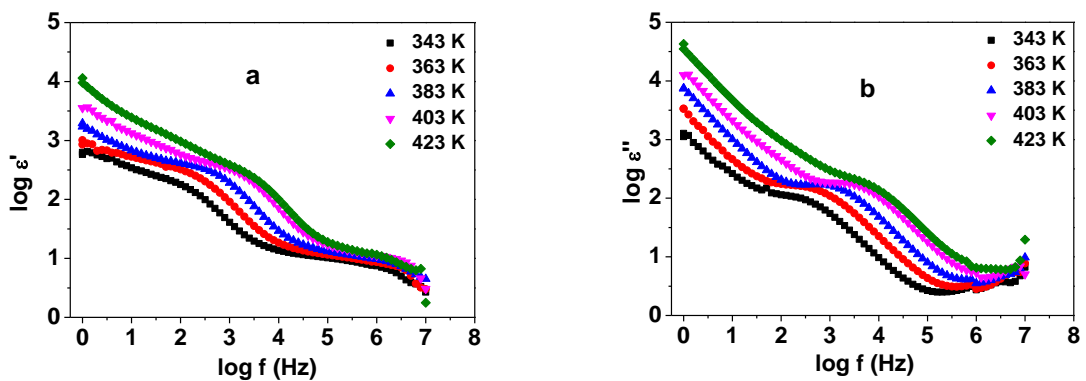


Fig. 5.59 (a) real part ϵ' and (b) imaginary part ϵ'' of dielectric permittivity as function of frequency for $x=0.15$ sample S1-H2 of $\text{Li}_{1.3}\text{Al}_{0.3-x}\text{Y}_x\text{Ti}_{1.7}(\text{PO}_4)_3$ series at different temperatures.

In the below figures of S1 sample exposed to 3 hr sintering, (fig. 5.60) a well developed saturation region at higher frequencies for real part of dielectric permittivity is

observed. The same pattern is followed by imaginary part dielectric permittivity. While in 3 hr sintered S6 sample, (fig. 5.61) the plots are narrow and flat. There is less dispersion at mid frequencies compared to S1. A flat behavior of the plots is seen especially for ϵ'' for S6 (fig. 5.61 (b)).

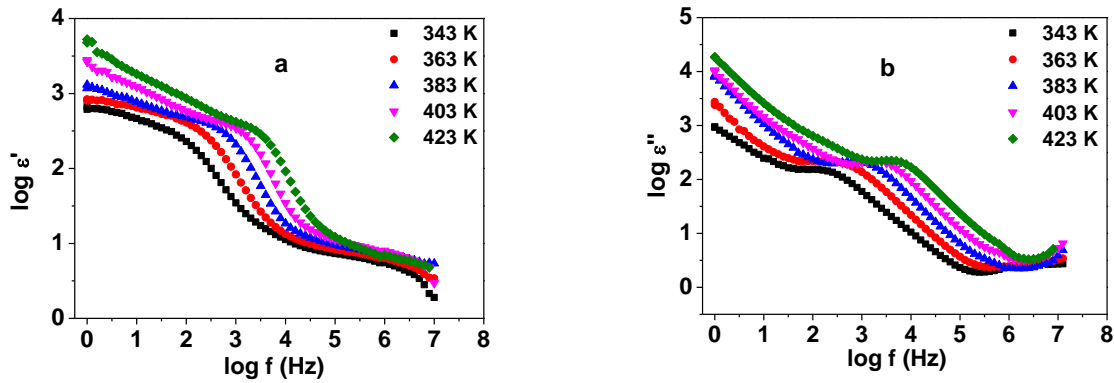


Fig. 5.60 (a) Variation of real part of dielectric permittivity ϵ' and (b) imaginary part of dielectric permittivity ϵ'' with respect to frequency for the sample S1-H3 of $\text{Li}_{1.3}\text{Al}_{0.3-x}\text{Y}_x\text{Ti}_{1.7}(\text{PO}_4)_3$ series at different temperatures.

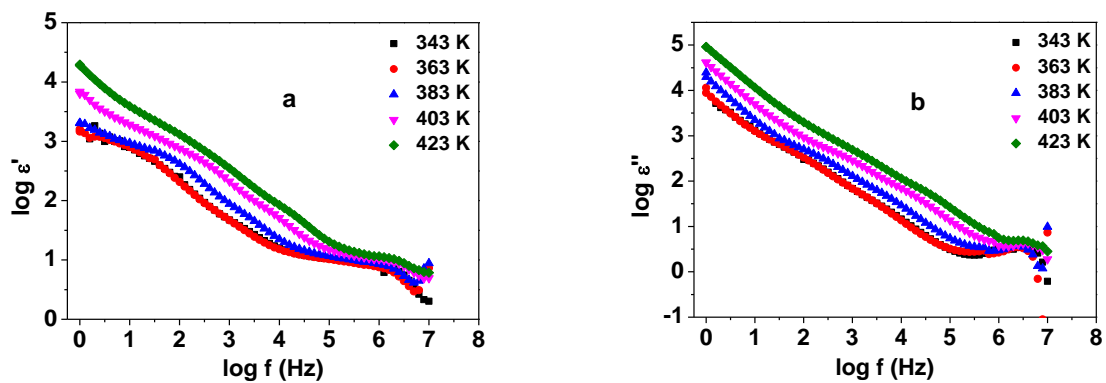


Fig. 5.61 (a) Variation of real part of dielectric permittivity ϵ' (b) Variation of imaginary part of dielectric permittivity ϵ'' with frequency for a sample S6-H3 of $\text{Li}_{1.3}\text{Al}_{0.3-x}\text{Y}_x\text{Ti}_{1.7}(\text{PO}_4)_3$ series at different temperatures.

It can be noticed that the dispersion shifts at higher frequencies in 3 hr sample for S6 compared to S1. This indicates that impurities due to secondary phases of yttrium in S6 are more in grain region, due to which, the Li^+ dipoles have lesser room and cannot easily relax compared to the sample with lesser amount of yttrium.

The $\tan\delta$ graphs for S1 and S6 samples for 2 and 3 hrs sintering duration are plotted below (figs. 5.62 to 5.65). It can be noted that with increasing temperature, the peaks shift

towards higher values of $\tan\delta$ and towards higher frequencies also. This indicates that with increasing temperature, the losses also increase for all samples and that the dipoles have lesser time to relax as frequencies increase. This shifts the peaks towards higher frequency side.

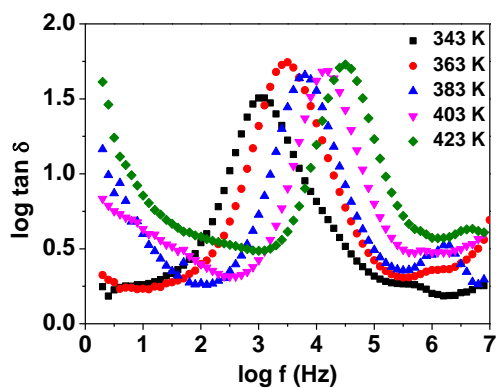


Fig. 5.62 Variation of loss tangent $\tan \delta$ with frequency for S1-H2 sample of $\text{Li}_{1.3}\text{Al}_{0.3-x}\text{Y}_x\text{Ti}_{1.7}(\text{PO}_4)_3$ series at different temperatures.

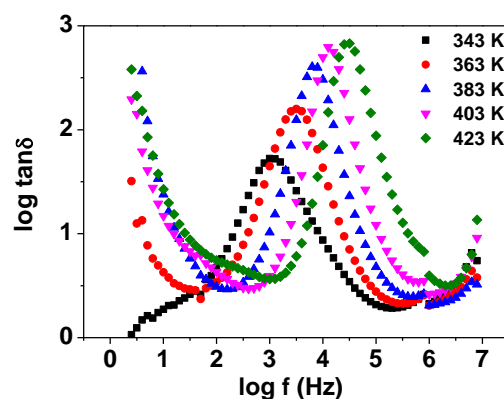


Fig. 5.63 Variation of loss tangent $\tan \delta$ with frequency for S1-H3 sample of $\text{Li}_{1.3}\text{Al}_{0.3-x}\text{Y}_x\text{Ti}_{1.7}(\text{PO}_4)_3$ series at different Temperatures.

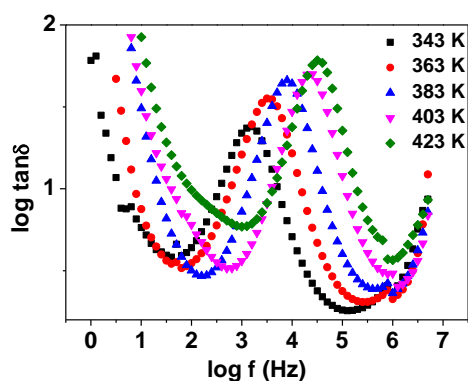


Fig. 5.64 Variation of $\tan \delta$ with frequency of sample S6-H2 of $\text{Li}_{1.3}\text{Al}_{0.3-x}\text{Y}_x\text{Ti}_{1.7}(\text{PO}_4)_3$ series at different temperatures.

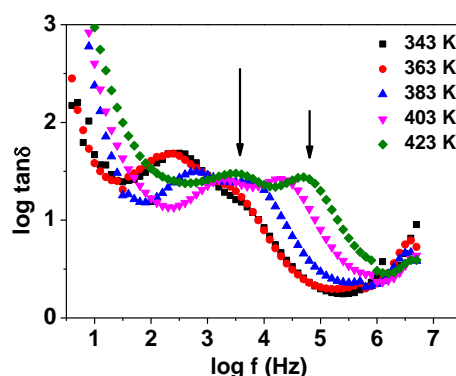


Fig. 5.65 Variation of $\tan \delta$ with frequency of S6-H3 sample of $\text{Li}_{1.3}\text{Al}_{0.3-x}\text{Y}_x\text{Ti}_{1.7}(\text{PO}_4)_3$ series at different temperatures.

Double peaks are seen to form in the plots of $\tan\delta$ of S6 sample (indicated by two arrows). These peaks indicate formation of secondary phases like $\text{LiY}_2(\text{PO}_4)_3$ (LYP) [51, 62] which may also contribute towards Li^+ dielectric relaxation. The dipoles have also another phase (which is mostly amorphous in nature), where they relax [95-97]. The loss tangent peak of S1-1H in fig.5.55 is higher than the loss tangent peaks of S1_2H. It means that with

yttrium in vicinity of Li^+ , the transfer of energy from electric field is efficient in case of sintered sample. The formation and migration of phases like YPO_4 towards grain boundary creates enough space for Li^+ dipoles to oscillate freely in the system [90–93]. Besides, in the S1 samples the amount of yttrium is less. Hence with sintering, the little amount of yttrium is shifted towards grain boundary. Due to this the Li^+ has enough room to execute dipolar oscillations – due to this the losses are less. Hence the loss tangent peaks are lower for 2 h and 3 h samples for all temperatures.

5.3.4 $\text{Li}_{1.3}\text{Al}_{0.3-x}\text{Ga}_x\text{Ti}_{1.7}(\text{PO}_4)_3$ (LAGTP) system.

Dielectric measurements of the gallium doped $\text{Li}_{1.3}\text{Al}_{0.3}\text{Ti}_{1.7}(\text{PO}_4)_3$ (LATP) system, are presented below. Gallium (0.64 Å), can replace Al^{3+} or Ti^{4+} cations in the LATP system [52]. The plots for $\log \varepsilon'$ vs. $\log f$ for samples G1 and G2 are relatively flat. They indicate that the dipoles of Li^+ have maximum value of permittivity gain electric field energy directly and the local impurity phases are less compared to previous series. The maximum permittivity values of the electric field energy is seen for low frequencies, where the Li^+ ions acting also as dipoles, are able to orient according to the electric field direction and absorb the field energy. In mid frequency range, the dispersion occurs but the plots are relatively flat than their yttrium doped counterparts. There is no shift of dispersion frequency towards higher frequencies as well. This means that at different temperatures, the permittivity behavior is different even in the same sample. It is also seen that the relaxation behavior of curves corresponding to increasing temperatures within same sample is different. This is because the gallium doped system is temperature sensitive due to low melting point of gallium in the

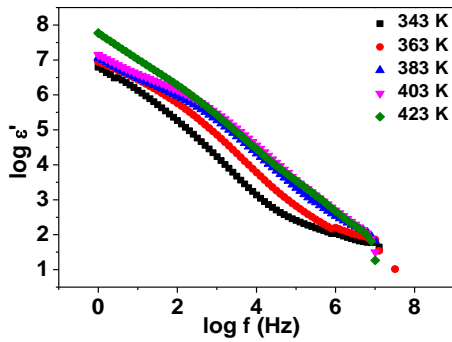


Fig. 5.66 The variation of dielectric permittivity ϵ' with frequency for $\text{Li}_{1.3}\text{Al}_{0.3-x}\text{Ga}_x\text{Ti}_{1.7}(\text{PO}_4)_3$ for ($x=0.01$) sample at different temperatures.

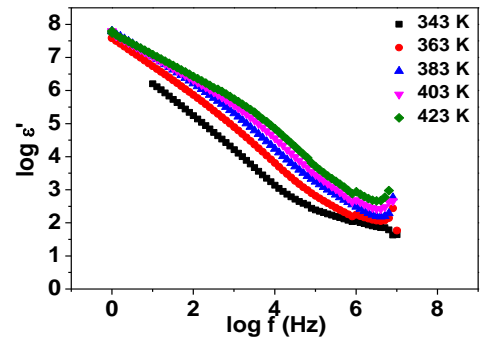


Fig. 5.67 The variation of dielectric permittivity ϵ' with frequency for $\text{Li}_{1.3}\text{Al}_{0.3-x}\text{Ga}_x\text{Ti}_{1.7}(\text{PO}_4)_3$ ($x=0.03$) sample at different temperatures.

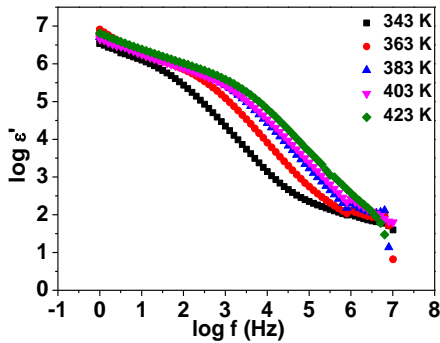


Fig. 5.68 The variation of dielectric permittivity ϵ' with frequency for $\text{Li}_{1.3}\text{Al}_{0.3-x}\text{Ga}_x\text{Ti}_{1.7}(\text{PO}_4)_3$ ($x=0.05$) sample at different temperatures.

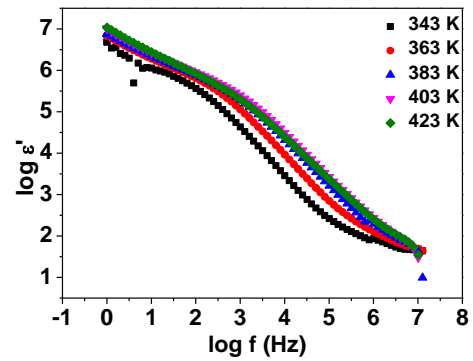


Fig. 5.69 The variation of dielectric permittivity ϵ' with frequency for $\text{Li}_{1.3}\text{Al}_{0.3-x}\text{Ga}_x\text{Ti}_{1.7}(\text{PO}_4)_3$ ($x=0.07$) sample at different temperatures.

system and the local environment within which the Li^+ dipoles relax is constantly changing as the temperature is varied (increased) during the impedance measurement. Hence it sees dynamic structural changes even when the temperature based impedance studies were carried on impedance gain phase analyzer.

For the samples G3 and G4, at higher frequencies, saturation can be noticed. A shift in dispersion is seen for these two samples compared to G1 and G2 which have lesser amount of gallium.

In the below sub section the plots of imaginary parts of dielectric permittivity ϵ'' as a function of frequency for all samples of gallium doped LATP series at different temperatures

are shown. The samples G1 and G2 (fig. 5.70) are relatively flat compared to G3 and G4 samples. Small amount of dispersion towards higher frequencies is seen for G3 and G4 which is indicated by arrows in Fig. 5.71 (a and b).

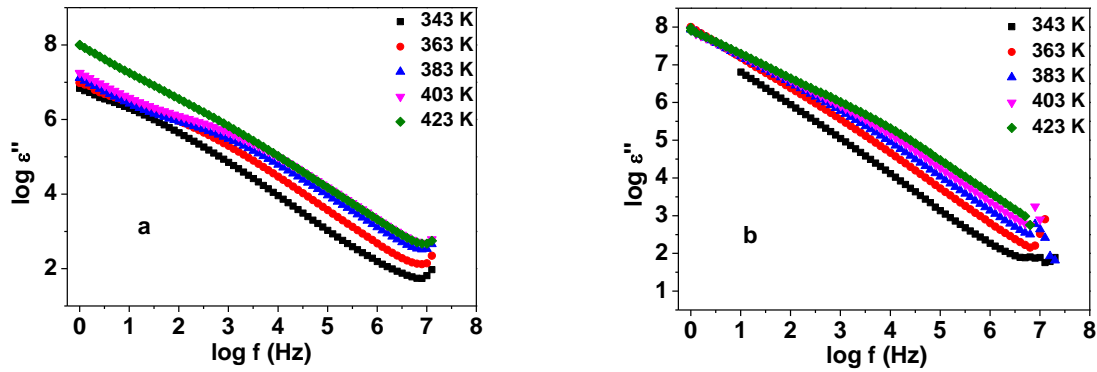


Fig. 5.70 The variation of dielectric permittivity ϵ'' with frequency of $\text{Li}_{1.3}\text{Al}_{0.3-x}\text{Ga}_x\text{Ti}_{1.7}(\text{PO}_4)_3$ sample for (a) $x=0.01$ and (b) $x=0.03$ concentrations.

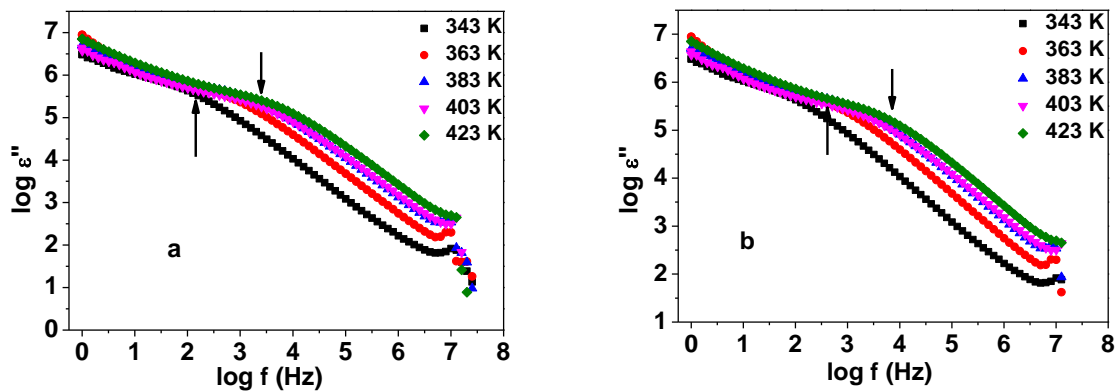


Fig. 5.71 The variation of dielectric permittivity ϵ'' with frequency of $\text{Li}_{1.3}\text{Al}_{0.3-x}\text{Ga}_x\text{Ti}_{1.7}(\text{PO}_4)_3$ sample for (a) $x = 0.05$ and (b) $x = 0.07$ concentrations.

The imaginary dielectric permittivity plots are relatively flat and do not show much shift of the dispersive peaks as temperatures are increased. At lower frequencies, the behavior is similar but as frequencies increase the Li^+ motion becomes more and more localized. But due to higher temperatures, the Li^+ tend to diffuse larger distances within the grain region. At higher frequencies, the Li^+ are forced to be confined to their local sites and execute back and forward hopping motion in their local environment where there are effects of impurities. Due to this there is dielectric relaxation observed at higher temperatures and higher frequencies which is not seen in their yttrium doped counterparts.

In the below sub section the loss tangent peaks (fig.5.72) are presented. The behavior of loss peaks is exactly different from the yttrium doped counterparts in which loss peaks had lower values for lower temperature while, for the gallium doped samples, more loss is observed at lower temperatures. This is because as Li^+ dipoles when gain more thermal energy, tend to break out of lithium containing phases and execute random thermal agitations. This causes them to loss energy seen at low frequencies. Also gallium phases like GaPO_4 , TiO_2 , TiP_2O_7 also tend to segregate at higher temperatures towards grain boundary [61, 98, 99, 100]. But at higher frequencies, the Li^+ do not have enough room and do not tend to spread / give away their energy because their motion is localized. They are forced to orient immediately towards the changed electric polarity and absorb and dissipate the energy. Hence the losses are less when temperature is increased at higher frequencies, compared to yttrium doped counterparts.

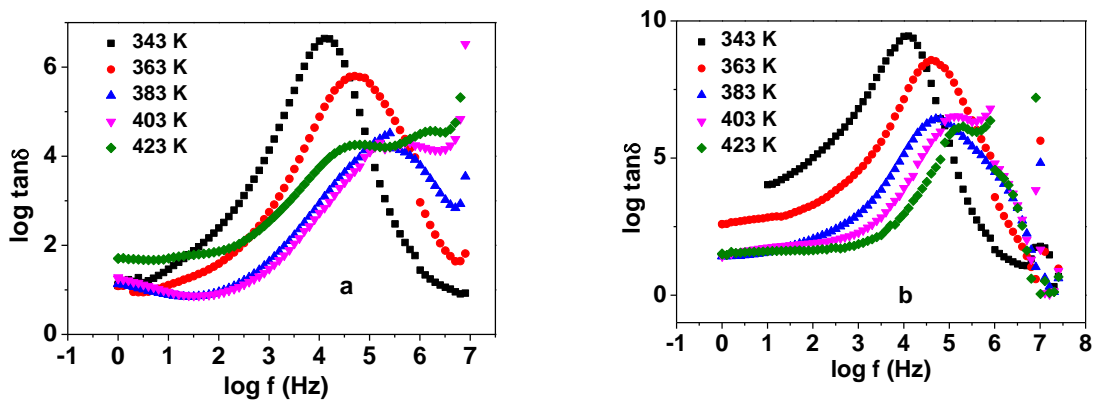


Fig. 5.72 The variation of $\tan \delta$ with frequency for $\text{Li}_{1.3}\text{Al}_{0.3-x}\text{Ga}_x\text{Ti}_{1.7}(\text{PO}_4)_3$ series for: (a) $x = 0.01$ and (b) $x = 0.03$ samples at different temperatures.

Thus gallium doped series samples which are affected easily by temperature variation (on account of low melting point of gallium) during impedance measurements also helps in segregating gallium and other secondary phases towards grain boundary due to which the Li^+ dipole relax easily. The segregated phases and / or impurities like GaPO_4 increase, as the amount in the system increases. Since the local atmosphere in which the Li^+ ions relax is not conducive more losses are noticed in the

samples with higher concentration of gallium (see Figs. 5.72 (a and b) and 5.73 (a and b)).

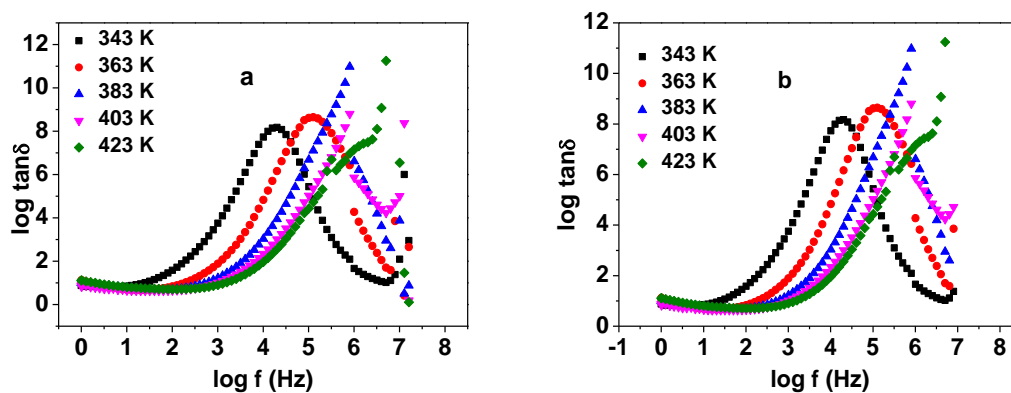


Fig. 5.73 The variation of loss tangent $\tan\delta$ with frequency for $\text{Li}_{1.3}\text{Al}_{0.3-x}\text{Ga}_x\text{Ti}_{1.7}(\text{PO}_4)_3$ series for: (a) $x = 0.05$ and (b) $x = 0.07$ concentrations at different temperatures.

The relatively high losses in gallium rich G4 ($x = 0.07$) in fig. 5.73 (b) is evident. The losses are also more because of the thermal agitations of the Li^+ ions at increasing temperatures which also do not permit a proper relaxation of the Li^+ ions.

5.3.5 $\text{Li}_{1.3}\text{Al}_{0.3-x}\text{Sc}_x\text{Ti}_{1.7}(\text{PO}_4)_3$ (LASTP) system

Scandium – a trivalent cation has been widely studied for its doping in LTP system [46, 101]. We have doped Sc^{3+} in the $\text{Li}_{1.3}\text{Al}_{0.3}\text{Ti}_{1.7}(\text{PO}_4)_3$ (LATP) system, are presented below. The dielectric permittivity (ϵ' and ϵ'') (fig. 5.74 to 5.77) values are high for low frequencies while in mid frequencies, there is a dispersive shift towards higher frequencies as temperature is increased. There is saturation observed at higher frequency values which indicates that Li^+ which oscillates as a dipole does not have enough time to relax and the forward-backward hopping motion of Li^+ is localized [27]. The scandium based phases are formed and segregated towards grain boundary. The behavior of real part of dielectric permittivity (fig. 5.74 and 5.75) of the present scandium doped LATP series is similar to that of yttrium doped LATP series. At low frequencies, the permittivity (real and imaginary parts – both) have higher values for all temperatures. This means the Li^+ traverse larger distance upto electrode before the changed polarity of the electric field cycle forces them to re-orient

and change their direction. Thus at low frequencies, there is accumulation of charges (dipoles) at electrode-electrolyte interface which causes the polarization effects and increased value of dielectric permittivity. Due to this the dielectric permittivity ensuing losses too are more. At higher temperatures, more and more Li^+ are in this de-localized state. But as the frequencies increase, the dispersion and a shift in dispersion is seen. This does not allow the dipoles to travel such large distances as upto electrode-electrolyte interface. The dipoles are forced to change their polarity when they execute motion within grain only. This causes dispersive relaxation in mid frequency range. At higher frequencies, the Li^+ execute back and forward hopping motion which is localized. Hence the dipoles experience a similar environment in which to relax. This result in saturation effect at all temperatures observed at higher frequencies. With increased scandium content we do not observe any remarkable change in permittivity values. But these values of permittivity and subsequent losses are less compared to its yttrium counterparts.

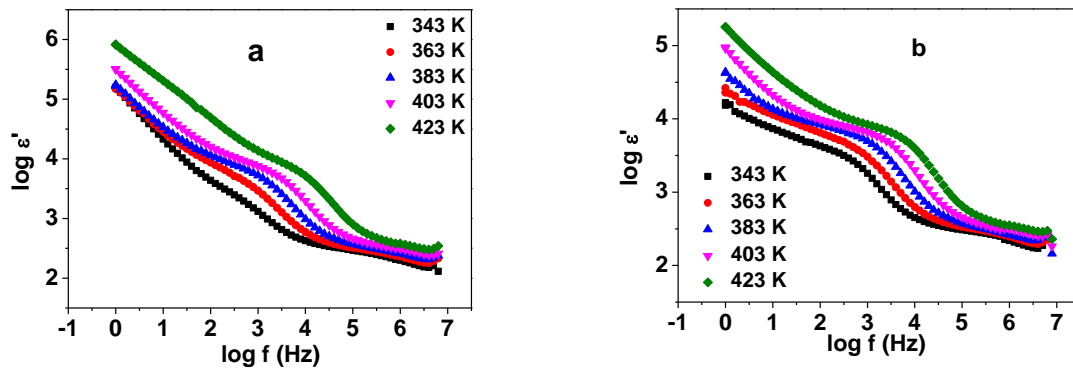


Fig. 5.74 The variation of ϵ' with frequency for $\text{Li}_{1.3}\text{Al}_{0.3-x}\text{Sc}_x\text{Ti}_{1.7}(\text{PO}_4)_3$ series for (a) $x = 0.01$ and (b) $x = 0.03$ samples at different temperatures.

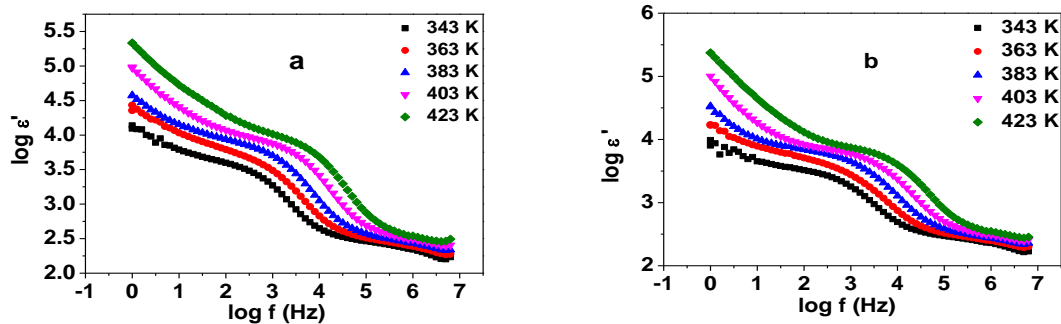


Fig. 5.75 The variation of ε' with frequency and temperature for $\text{Li}_{1.3}\text{Al}_{0.3-x}\text{Sc}_x\text{Ti}_{1.7}(\text{PO}_4)_3$ series for (a) $x = 0.05$ and (b) $x = 0.07$ samples

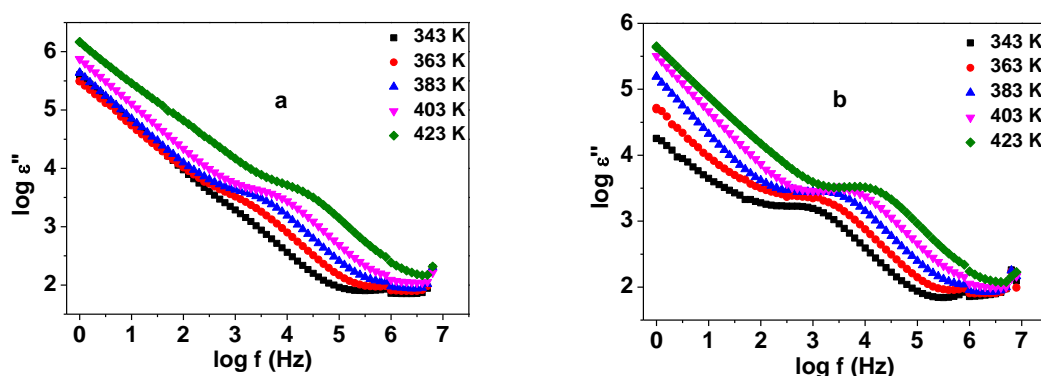


Fig. 5.76 Variation of ε'' with frequency for $\text{Li}_{1.3}\text{Al}_{0.3-x}\text{Sc}_x\text{Ti}_{1.7}(\text{PO}_4)_3$ (a) $x = 0.01$ and (b) $x = 0.03$ samples at different temperatures.

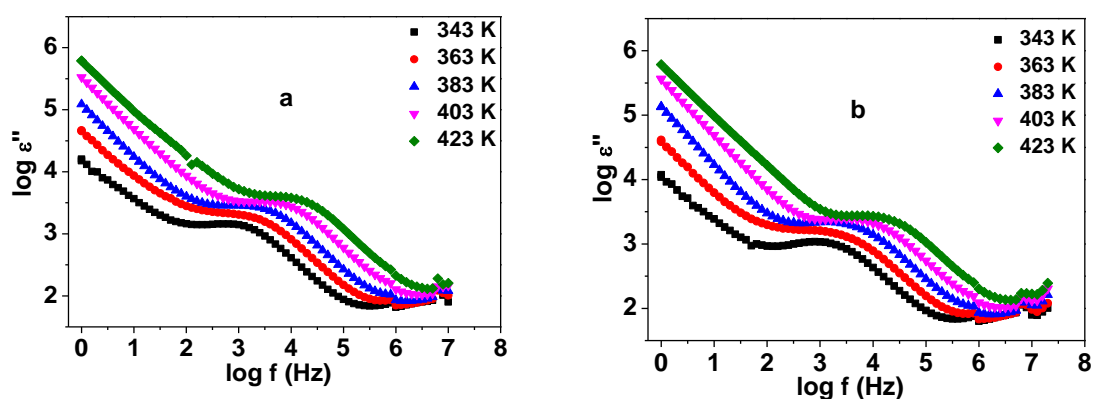


Fig. 5.77 Variation of ε'' with frequency for $\text{Li}_{1.3}\text{Al}_{0.3-x}\text{Sc}_x\text{Ti}_{1.7}(\text{PO}_4)_3$ for (a) $x = 0.05$ and (b) $x = 0.07$ samples at different temperatures.

From the plots of the loss tangent ($\tan\delta$) as a function of frequency, (figs. 5.78 and 5.79) it is clear that for higher temperatures, the losses are more.

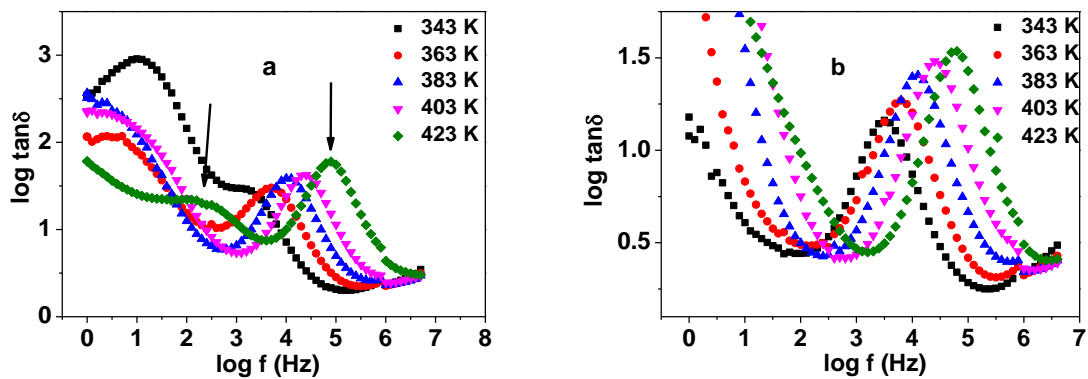


Fig. 5.78 The variation of $\tan \delta$ with frequency for $\text{Li}_{1.3}\text{Al}_{0.3-x}\text{Sc}_x\text{Ti}_{1.7}(\text{PO}_4)_3$ for (a) $x = 0.01$ (b) $x = 0.03$ samples at different temperatures.

It means that as the Li^+ with more thermal energy, tend to have more mobility but as the distance between the Li^+ ions becomes less due to higher mobility, their mutual electropositive repulsion comes into play and they lose the energy to their surrounding in order to relax. The saturation of loss tangent plots for all concentrations is seen at high frequencies. The peaks shift towards higher frequencies as temperature increases. The losses become more as the amount of scandium in the system increases. This is seen in Fig. 5.79 (a and b) below.

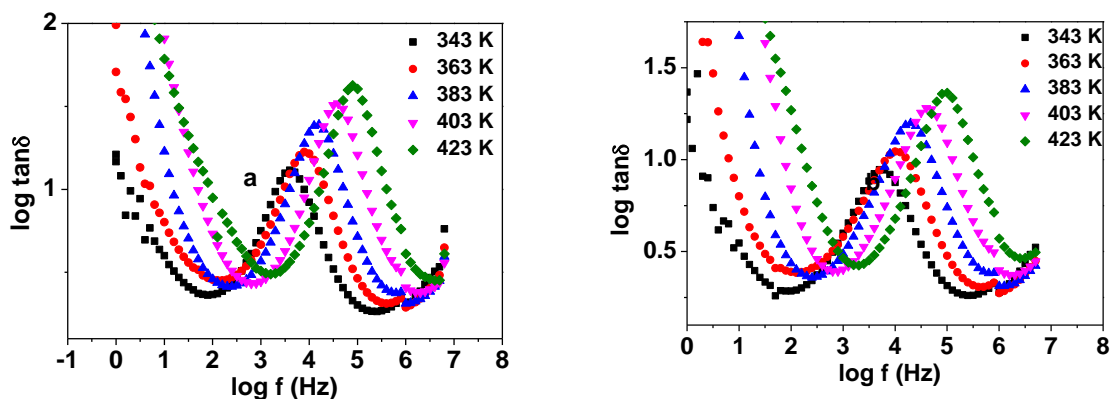


Fig. 5.79 The variation of loss tangent $\tan \delta$ with frequency for $\text{Li}_{1.3}\text{Al}_{0.3-x}\text{Sc}_x\text{Ti}_{1.7}(\text{PO}_4)_3$ for (a) $x = 0.05$ (b) $x = 0.07$ samples at different temperatures.

Two peaks at 423 K are clearly seen in Fig. 5.79 (a). The first loss peak corresponds to a secondary phase in low frequency (grain boundary) region while the second more prominent loss peak corresponds to the main phase in which the Li^+ dipoles. These phases are might be due to rutile aggregates ($\text{TiO}_2 / \text{TiP}_2\text{O}_7$) in the low scandium containing samples.

Summary:

It can be concluded for samples of different concentrations:-

From Fig. 5.80 (a and b), it can be seen that the real part (ϵ') and Fig. 5.81 (a and b) imaginary (ϵ'') part of dielectric permittivity have a steady increasing trend for all concentrations for LAYTP, LAGTP and LASTP systems at constant frequency (2×10^6 Hz). While, at same temperature, the dielectric permittivity values have a dropping trend across concentration for LAGTP, a steady value across the concentration for LASTP and a mixed increasing and decreasing trend in LAYTP series.

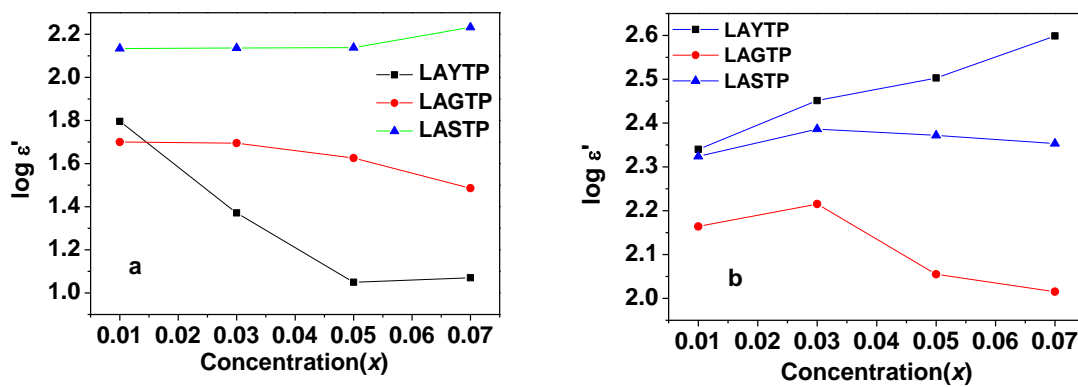


Fig. 5.80 The variation of ϵ' with concentration at 2×10^6 Hz frequency for all samples of the 3 series at: (a) 303 K and (b) 373 K

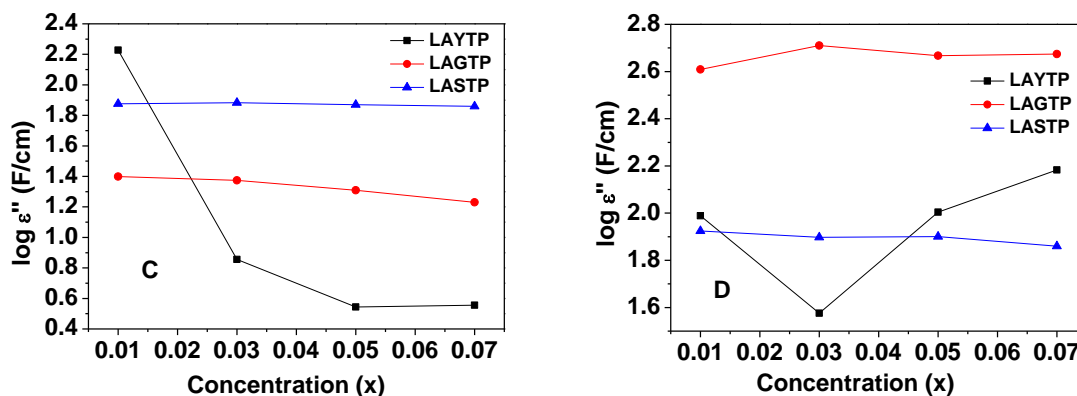


Fig. 5.81 The variation of ϵ'' with concentration at 2×10^6 Hz frequency for all samples of the 3 series at: (a) 303 K and (b) 373 K

The reasons for this are discussed below:

- 1) The values of dielectric permittivity increases across temperatures – this is because, with increase of thermal energy the randomness and disorientation towards the applied electric field increases which contributes towards losses.
- 2) Within same temperature the dielectric values decrease across concentration – because – (i) Gallium substitution of Ti and Al in the LAGTP series, results in segregation of compounds like GaPO₄, AlPO₄, TiO₂ and TiP₂O₇. As concentration of gallium increases, the amount of gallium trying to replace Al and Ti sites increases. Thus, the amounts of secondary phases like GaPO₄ also steadily increase. As the concentration of dopants like Ga³⁺ increases in the system, the dielectric permittivity values decrease because of the presence of these impurities that is, the Li⁺ dipoles do not get adequate sites to relax completely. Hence the dielectric permittivity of the material in presence of these impurities decreases at any given temperature.

5.4 Modulus Studies

The electrical modulus studies are used to study the dielectric response of the material when it is subjected to AC frequencies. The conduction of Li⁺ ions occurs in the solid electrolyte medium due to diffusion of Li⁺ and due to response to applied AC frequencies. The electrical modulus which is expressed by the following formula generally takes into account the AC frequency response.

$$M^* = \frac{1}{\epsilon^*} = j\omega C_0 Z^* = M' + j M'' \quad \dots\dots\dots(5.6)$$

where Z^* is the complex impedance, $\omega = 2\pi f$ is the angular frequency; $C_0 = \epsilon_0 \frac{A}{t}$ is the capacitance in vacuum (absence of any medium between two plates of capacitor); A is the surface area and t is the thickness of the capacitor plates.

Thus modulus is expressed as a function of real and imaginary quantities. This is expressed as below:

$$M^* = \frac{1}{\epsilon - j \epsilon''} \quad \dots\dots\dots(5.7)$$

$$M^* = \frac{\epsilon'}{(\epsilon'^2 + \epsilon''^2)} + j \frac{\epsilon''}{(\epsilon'^2 + \epsilon''^2)} \quad \dots\dots\dots(5.8)$$

$$\text{Therefore } M' = \frac{\epsilon'}{(\epsilon'^2 + \epsilon''^2)} \text{ and } M'' = \frac{\epsilon''}{(\epsilon'^2 + \epsilon''^2)} \quad \dots\dots\dots(5.9)$$

Modulus is also expressed in terms of impedance as follows:

$$M' = 2\pi f \epsilon_0 \left(\frac{A}{t}\right) Z'' = \omega C_0 Z'' \quad \dots\dots\dots(5.10)$$

while

$$M'' = 2\pi f \epsilon_0 \left(\frac{A}{t}\right) Z' = \omega C_0 Z' \quad \dots\dots\dots(5.11)$$

The real part of modulus (M') expresses the inverse behavior of dielectric permittivity. When expressed in terms of impedance notation, it describes the imaginary impedance (Z'') which is the frequency response to the applied frequency. While, the imaginary part of modulus describes, the impedance response of the material exposed to AC frequencies.

The low frequency electrode behavior is suppressed in modulus formalism [102]. While many authors favour modulus formalism to represent the dielectric response [103-107], many others [108-110] think that it is an indirect means and gives incomplete representation of the electrical response of the material exposed to AC frequencies and hence it is not reliable. Since M'' expresses the response of real impedance, we present below the modulus spectra for M'' vs. frequency for different series.

5.4.1 Reference $\text{LiTi}_2(\text{PO}_4)_3$ (LTP) and $\text{Li}_{1.3}\text{Al}_{0.3}\text{Ti}_{1.7}(\text{PO}_4)_3$ (LATP) systems

A reference systems with the chemical formula $\text{LiTi}_2(\text{PO}_4)_3$ (LTP) and $\text{Li}_{1.3}\text{Al}_{0.3}\text{Ti}_{1.7}(\text{PO}_4)_3$ (LATP) were prepared. These system have a primarily a rhombohedral structure. Trivalent cationic species like Sc^{3+} , Ga^{3+} , Y^{3+} were doped to study the effect on the structure of these reference (parent) systems. As mentioned above the M'' represents the response of real part of impedance (Z'). The peak of M'' differs from that of Z' because of the non Debye (ideal) behavior of the oscillator when plotted as a function of frequency. In the Fig. 5.82 (for LTP) and Fig. 5.84(a) (for LATP), the M'' spectra as a function of AC

frequency is presented for 343 K temperature. The peak is well defined and is formed at the characteristic frequency of the Li^+ in the given local environment and microstructure as well as conditions of temperature. It indicates that Li^+ exposed to higher frequencies takes minimum relaxation time in the local environment. This is because, the change of AC frequencies (or polarization) which the Li^+ experiences due to externally applied AC frequency is so fast that the Li^+ can hardly relax into its local environment before it is again exposed to the changed polarization. Thus the relaxation time at this frequency is minimum. The M'' peaks thus give an idea of the local environment in which the Li^+ is exposed to. The temperature plays an important role here. At higher temperatures, the Li^+ also experiences thermal agitations in addition to the change of polarity (due to high frequencies).

The peak is asymmetric with respect to this maximum frequency. This is an indicator of the non Debye behavior of the oscillator (which is Li^+ coupled with its local environment of cation vacancy in this case). The relaxation time as mentioned in the previous chapter is a function of time (t) of the exposure of the electric field (due to AC frequency) and the relaxation time (τ). The relation is (decaying) exponential in nature. It is known as stretched Kohlrausch-Williams-Watts (KWW) function:

$$\varphi(t) = \exp\left[-\left(\frac{t}{\tau}\right)^\beta\right] \quad (\text{where } 0 < \beta < 1) \quad \dots\dots\dots(5.12)$$

The function is called ‘stretched’ function because there is a time lag in the response of the Li^+ to the fast changing AC frequencies. Hence the Li^+ cannot respond immediately to the changed polarization of external field and tends to stretch its relaxation time.

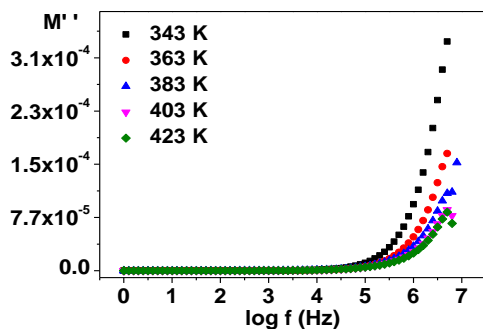


Fig. 5.82 M'' vs freq. for $\text{LiTi}_2(\text{PO}_4)_3$ sample at different temperatures

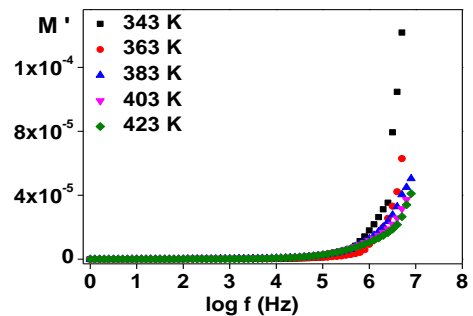


Fig. 5.83 M' vs frequency response for $\text{LiTi}_2(\text{PO}_4)_3$ sample at different temperatures

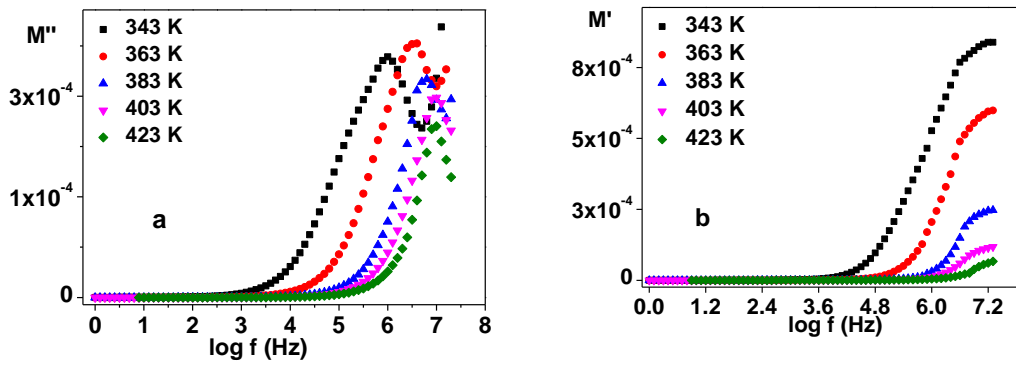


Fig. 5.84(a) M'' vs frequency at different temperatures (b) M' vs frequency response at different temperatures for $\text{Li}_{1.3}\text{Al}_{0.3}\text{Ti}_{1.7}(\text{PO}_4)_3$ sample

The M'' spectra for $\text{Li}_{1.3}\text{Al}_{0.3}\text{Ti}_{1.7}(\text{PO}_4)_3$ (LATP) sample is given in the above figure 5.84(a). At low frequencies, the long tail is indicative of the large capacitive effects (which are suppressed by the modulus formalism) due to electrode-electrolyte interface. Due to long range motion of Li^+ , the charges get accumulated at the interface. The peaks of M'' spectra at higher frequencies become asymmetric although their heights remain same for increasing temperatures. With increasing temperatures, the peaks shift towards higher frequency side. The Li^+ and the local environment in which they are confined experience more thermal agitations at higher temperatures. Also due to high frequencies, the Li^+ are confined in their local environment as they are forced to perform forward and backward hopping. Due to thermal energy, Li^+ easily relaxes and hence takes lesser time in relaxing. Hence, with increasing temperatures, the peaks are supposed to shift towards higher frequency side.

The M'' spectra for all temperatures have almost the same full width at half maxima (FWHM). Due to this it can be said that frequency exponent parameter β is same for all temperatures. β not only indicates the deviation from the ideal Debye behavior but also shows that the Li^+ ions have an almost similar local environment to relax as temperature increases. Thus, the local microstructure of the LATP is not altered when temperature is increased in the experimental range (303 K to 423 K). From M' peaks of LTP and LATP (Figs. 5.83 and 5.84(b)) it is clear that with increasing temperatures the peaks shift towards higher frequency side. The M' and M'' spectra for both LTP and LATP samples show a relaxation peak at

higher frequencies. At higher frequencies however, the Li^+ are confined to their local positions near the potential wells [102].

5.4.2 $\text{Li}_{1.3}\text{Al}_{0.3-x}\text{Y}_x\text{Ti}_{1.7}(\text{PO}_4)_3$ (LAYTP) system

When yttrium is doped in the LTP (reference) system we get the $\text{Li}_{1.3}\text{Al}_{0.3-x}\text{Y}_x\text{Ti}_{1.7}(\text{PO}_4)_3$ (LAYTP) system (where $x = 0.01, 0.03, 0.05, 0.07, 0.10, 0.015$). The yttrium was intended to replace the aluminum at tetrahedral (PO_4) and octahedral (TiO_6) sites. But the Y^{3+} cations replace the Al^{3+} and Ti^{4+} sites as well. The modulus analysis of LAYTP series has been performed in the following to understand the impact of yttrium doping and corresponding changes in M' and M'' spectra. The M'' spectra are shown in the below Figs 5.85, 5.86 and 5.87 for all samples.

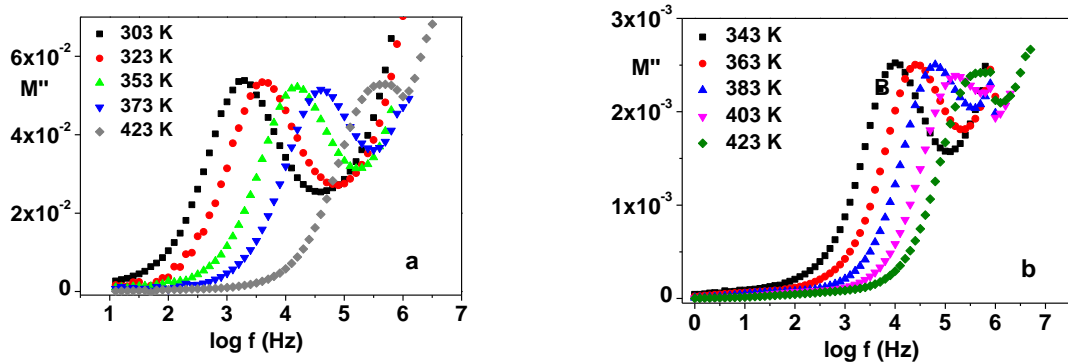


Fig. 5.85 M'' vs frequency response for $\text{Li}_{1.3}\text{Al}_{0.3-x}\text{Y}_x\text{Ti}_{1.7}(\text{PO}_4)_3$ for (a) $x=0.01$ and (b) $x=0.03$ samples at different temperatures.

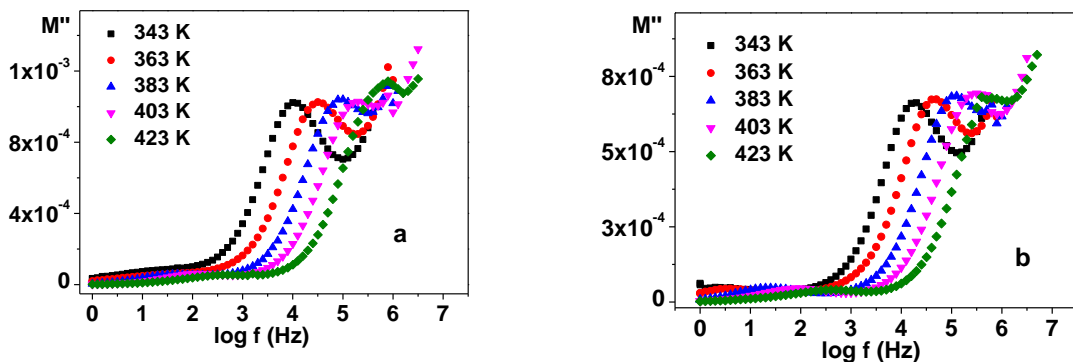


Fig. 5.86 M'' vs frequency response for $\text{Li}_{1.3}\text{Al}_{0.3-x}\text{Y}_x\text{Ti}_{1.7}(\text{PO}_4)_3$ for (a) $x=0.05$ and (b) $x=0.07$ samples at different temperatures

It is clear that the peaks at increasing temperatures tend to shift to higher frequencies. The peaks are asymmetric which is characteristic of non Debye behavior. There is a presence of an extensive spike at the higher frequencies. The uniform peak height and similar peak shape for all temperatures indicate that the Li^+ relaxes in a similar manner. Hence, the local environment seems to be similar within each sample. The shift towards higher frequencies with temperature indicates the enhanced motion of Li^+ which takes shorter time to relax i.e., at higher frequencies.

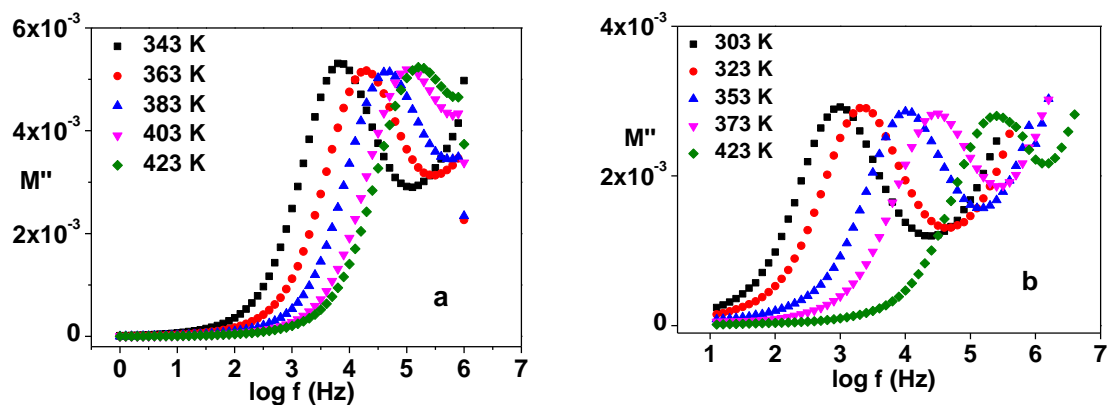


Fig. 5.87 M'' vs frequency response for $\text{Li}_{1.3}\text{Al}_{0.3-x}\text{Y}_x\text{Ti}_{1.7}(\text{PO}_4)_3$ for (a) $x=0.10$ and (b) $x=0.15$ samples at different temperatures.

This suggests that the relaxation behavior of the Li^+ is thermally activated due to hopping charge carriers. The M' spectra show a long tail at low frequencies. This is an indicative of the capacitance associated with electrodes. This capacitance is due to accumulation of Li^+ at the electrode electrolyte interface. The Modulus formalism deletes any artifacts related to electrode capacitive behavior at low frequencies and presents a flat line. It can be noted that as yttrium increases the peak width tends to decrease which indicates a deviation from ideal Debye behavior. Thus yttrium when it tries to replace aluminum at local sites, creates impurities phases like YPO_4 which segregate towards grain boundary and impede the Li^+ across the grain boundary. Such phases are also present within the grain to some extent. Due to this the local environment where the Li^+ relax becomes more rigid. This

makes the relaxation of Li^+ in yttrium containing atmosphere slightly difficult than in the atmosphere even as temperature increases.

The M' versus frequency spectra for all samples of LAYTP series are plotted below (fig. 5.88 to 5.90) it is clear that there relaxation peaks shift towards higher frequency side as temperature increases.

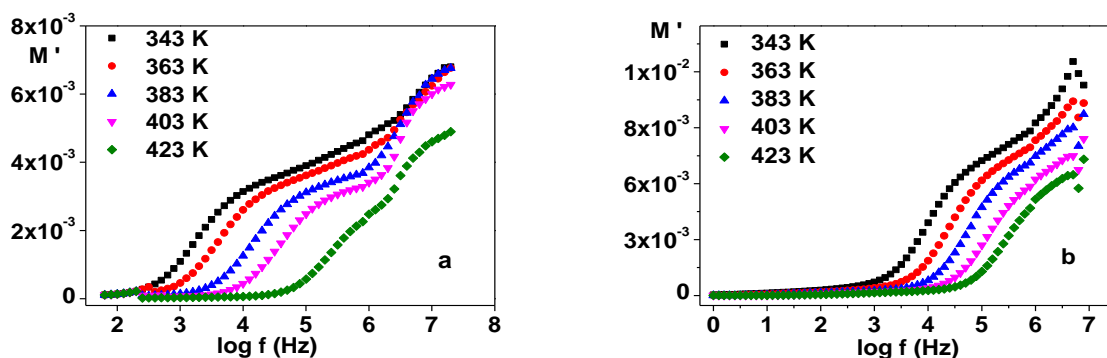


Fig. 5.88 M' vs frequency for $\text{Li}_{1.3}\text{Al}_{0.3-x}\text{Y}_x\text{Ti}_{1.7}(\text{PO}_4)_3$ for (a) $x=0.01$ and (b) $x=0.03$ samples at different temperatures.

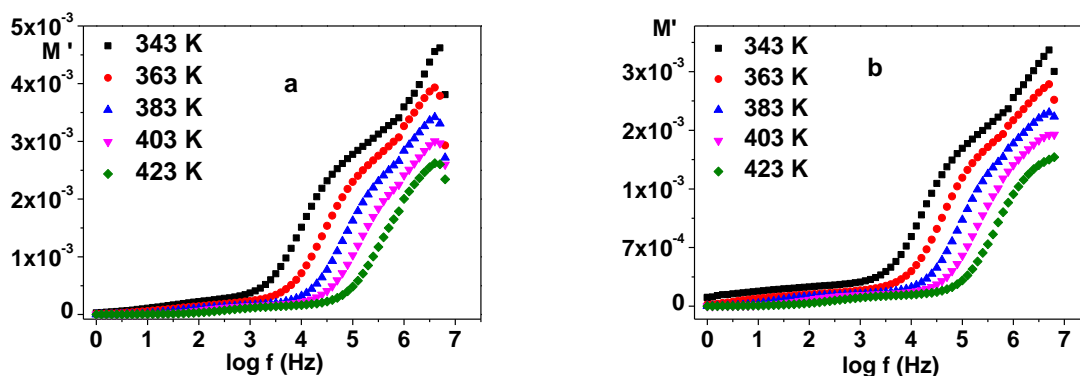


Fig. 5.89 M' vs. frequency for $\text{Li}_{1.3}\text{Al}_{0.3-x}\text{Y}_x\text{Ti}_{1.7}(\text{PO}_4)_3$ for (a) $x=0.05$ and (b) $x=0.07$ samples at different temperatures.

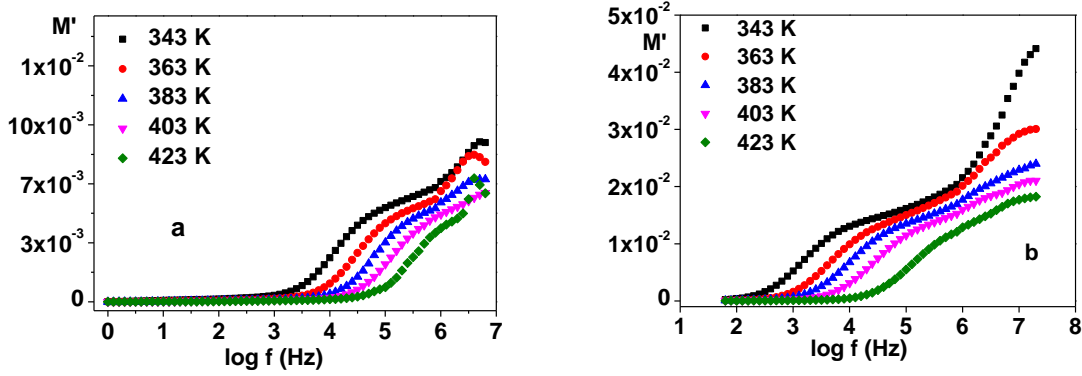


Fig. 5.90 M' vs frequency for $\text{Li}_{1.3}\text{Al}_{0.3-x}\text{Y}_x\text{Ti}_{1.7}(\text{PO}_4)_3$ for (a) $x=0.010$ and (b) $x=0.15$ samples at different temperatures.

The Li^+ relax at higher frequencies as their thermal energy increases. The relaxation peak at higher frequencies is affected with increase in the concentration of yttrium in the system. This indicates that presence of amorphous (impurity) phases like LiAlPO_4 and YPO_4 have an impact on the relaxation mode of Li^+ . The phases act as impurities and do not allow the Li^+ to relax easily. They do not let the electrical configuration near the Li^+ to move as fast which results in slower relaxation compared to the samples with lesser amount of yttrium.

5.4.3 Heat Treated $\text{Li}_{1.3}\text{Al}_{0.3-x}\text{Y}_x\text{Ti}_{1.7}(\text{PO}_4)_3$ (LAYTP) system

In the below section, modulus spectra of heat treated samples of $\text{Li}_{1.3}\text{Al}_{0.3-x}\text{Y}_x\text{Ti}_{1.7}(\text{PO}_4)_3$ (LAYTP) system (where $x = 0.01, 0.15$) is given. Due to heat treatment structural change in the local environment of the Li^+ is expected. The smaller grains aggregate and fuse to form larger grains. Besides, as concluded by other workers [111-112], yttrium at high temperatures tends to segregate towards grain boundary. Hence the grain boundary structure due to presence of increased yttrium phases is likely to be modified due to heat treatment. Due to these factors, the relaxation time and overall conductivity of Li^+ is expected to differ in these two samples which have the minimum and maximum concentration of Yttrium in the $\text{Li}_{1.3}\text{Al}_{0.3-x}\text{Y}_x\text{Ti}_{1.7}(\text{PO}_4)_3$ (LAYTP) system.

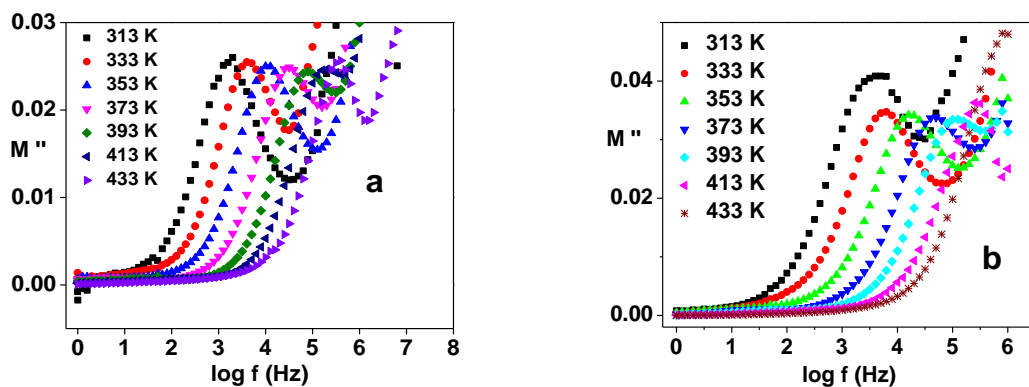


Fig. 5.91 M'' vs frequency for (a) S1-H2 and (b) S6-H2 samples of $\text{Li}_{1.3}\text{Al}_{0.3-x}\text{Y}_x\text{Ti}_{1.7}(\text{PO}_4)_3$ at different temperatures.

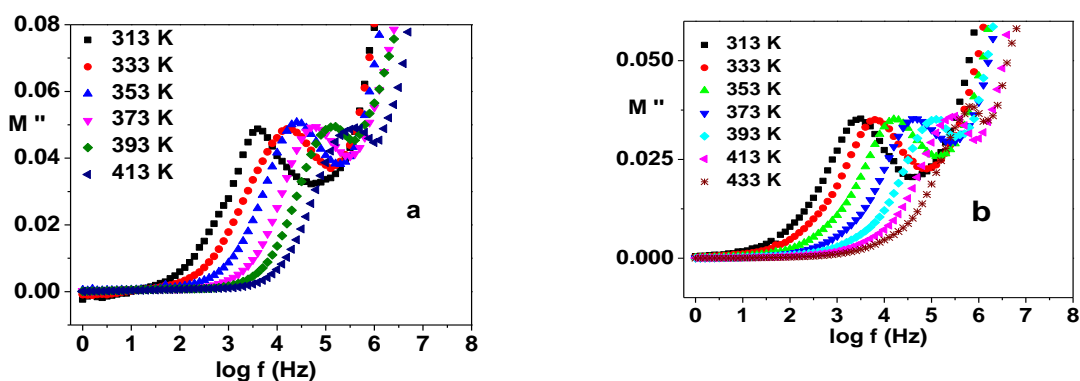


Fig. 5.92 M'' vs frequency for (a) S1-H3 and (b) S6-H3 samples of $\text{Li}_{1.3}\text{Al}_{0.3-x}\text{Y}_x\text{Ti}_{1.7}(\text{PO}_4)_3$ at different temperatures.

It can be seen (from Figs. 5.91 and 5.92) that after heat treatment the value of modulus for samples S6_2h and S6_3h also become comparable to those of S1_2h and S1_3h. This means that the environment for relaxation of Li^+ after heat treatment in yttrium rich samples like S6 ($x = 0.15$) becomes conducive and similar to samples of S1. Thus their mobility is less than the Li^+ in Yttrium poor sample S1. It means S1 has better Li^+ conductivity than S6 (as discussed earlier in conductivity). After heat treatment, the values of the modulus S6_2h and S6_3h increase. Thus from the modulus analysis, the extent of non Debye type of behavior exhibited by Li^+ during the conductivity relaxation and hence an indirect means in probing the local environment in which Li^+ relax.

In the Fig. 5.93, the real part of modulus (M') vs. frequency are shown for all four samples which have received heat treatment. Below are the Fig. 5.99 for 3 hours heat treated

samples for LAYTP series for M' versus frequency spectra. It is clear from the spectra that the M' peaks shift towards higher frequencies as temperature increases. There is a single peak for relaxation observed for all samples. As temperature increases, M' decreases. It is clear that with heat treatment, the M' values increase. That is the capacitance increases.

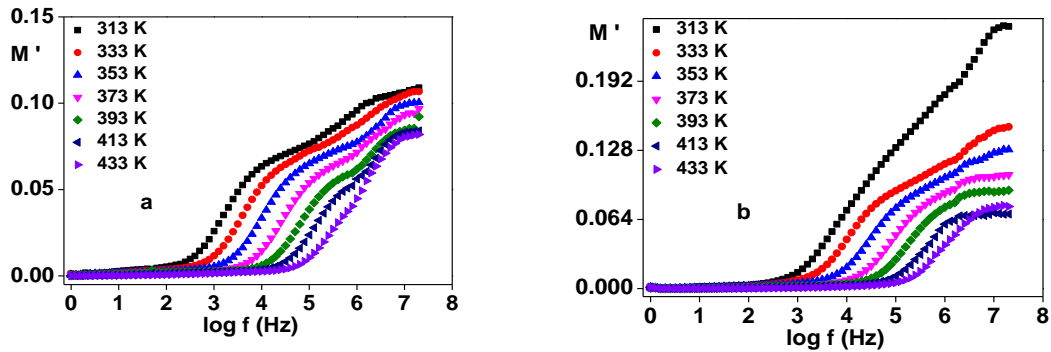


Fig. 5.93 M' vs. frequency of (a) S1-H2 and (b) S6-H2 samples of $\text{Li}_{1.3}\text{Al}_{0.3-x}\text{Y}_x\text{Ti}_{1.7}(\text{PO}_4)_3$ series at different temperatures.

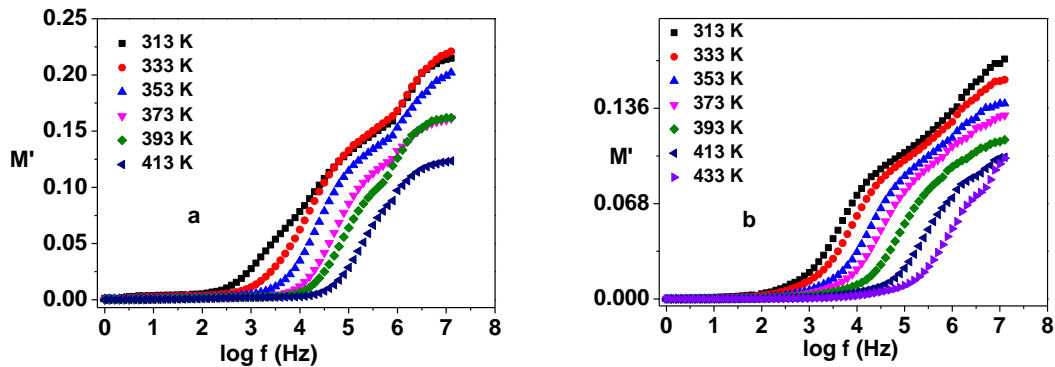


Fig. 5.94 M' vs. frequency of (a) S1-H3 and (b) S6-H3 of $\text{Li}_{1.3}\text{Al}_{0.3-x}\text{Y}_x\text{Ti}_{1.7}(\text{PO}_4)_3$ series at different temperatures.

5.4.4 $\text{Li}_{1.3}\text{Al}_{0.3-x}\text{Ga}_x\text{Ti}_{1.7}(\text{PO}_4)_3$ (LAGTP) system.

The system $\text{Li}_{1.3}\text{Al}_{0.3}\text{Ti}_{1.7}(\text{PO}_4)_3$ (LATP) system was doped with Ga^{3+} , a trivalent cation to obtain the $\text{Li}_{1.3}\text{Al}_{0.3-x}\text{Ga}_x\text{Ti}_{1.7}(\text{PO}_4)_3$ (LAGTP) system ($x = 0.01, 0.03, 0.05, 0.07$) system. The system contains GaPO_4 and $\text{Li}_{1.3}\text{Ga}_{0.3}\text{Ti}_{1.7}(\text{PO}_4)_3$ (LGTP) mixed system.

The plot of M'' versus frequency are plotted as modulus spectra and are shown in Fig. 5.95 for $x = 0.01$ and 0.07 concentration of Gallium. It is clear that the M'' values increase

with temperature. This means, that the structure of the material is affected with the rise in temperature from 303 K to 423 K in which the sample was subjected for electrical measurements. Besides, from the M'' spectra, it is clear that the Li^+ relax in the grain region. The peaks are narrower than an ideal Debye peak indicating that the gallium phases are present in grain and segregated towards grain boundary [47]. Generally, the M'' spectra broaden at high frequency side [116] which indicates non Debye behavior. At higher frequency, the M'' exhibits the highest values mean the largest impedance. These values decrease as temperature rises. Here, the Gallium forms phases which constrict Li^+ motion in the medium. Grant *et al.* [113, 114] have reported that the relaxation is a consequence of cooperative nature amongst the conducting ions (Li^+) in the conduction motion while other workers viz., Hasz [115] believe that relaxation time is connected with the distribution of free energy barriers for ionic jumps.

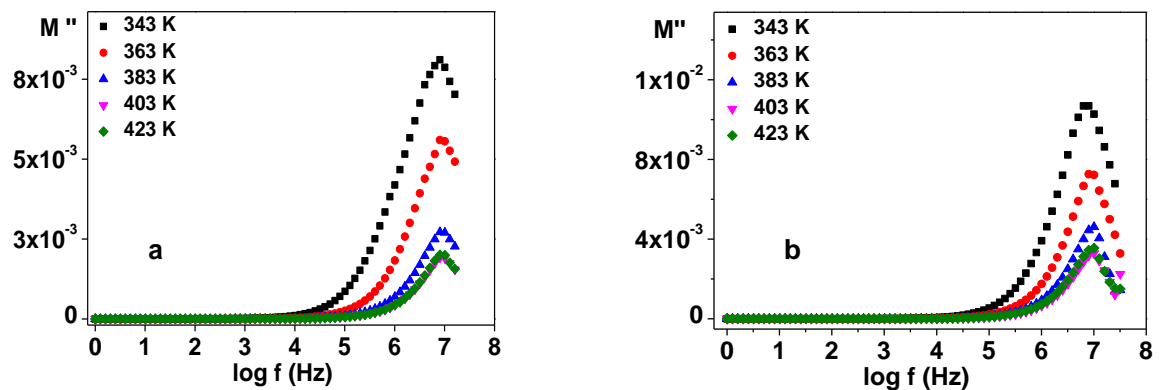


Fig. 5.95 M'' vs frequency plot for (a) $x = 0.01$ and (b) $x = 0.07$ samples of $\text{Li}_{1.3}\text{Al}_{0.3-x}\text{Ga}_x\text{Ti}_{1.7}(\text{PO}_4)_3$ series at different temperatures.

All the same, Gallium doped LATP series forms very good Li^+ conductors. The M' versus Frequency plots for the same two samples of the Gallium series are presented below in fig. 5.96. As temperature increases, the peaks of M' spectra are shifted towards higher frequencies for the samples of Gallium doped series. With increased gallium content, the value of M' increases. That is as impurity phases (mostly near the grain boundary) like GaPO_4 increase in the system, the Li^+ in the system has lesser ease of relaxing even though the

system is less viscous, at higher temperatures; due to presence of such impurity phases the Li^+ in vicinity of grain boundary relaxes with difficulty.

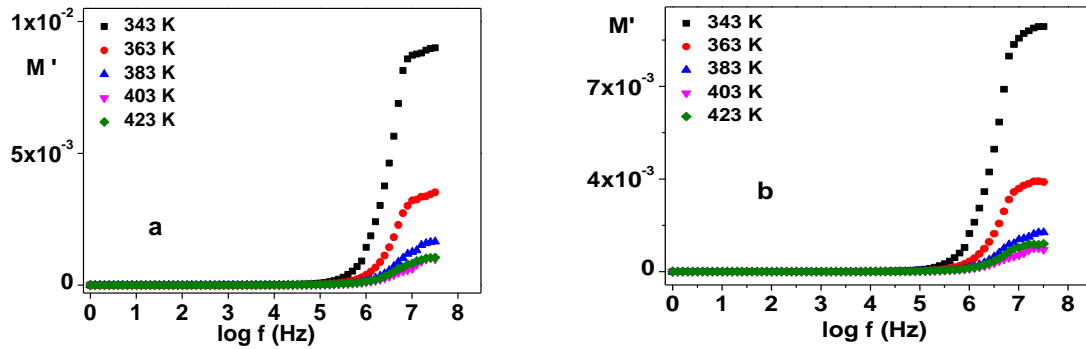


Fig. 5.96 M' vs freq plot for (a) $x = 0.01$ and (b) $x = 0.07$ samples of $\text{Li}_{1.3}\text{Al}_{0.3-x}\text{Ga}_x\text{Ti}_{1.7}(\text{PO}_4)_3$ series at different temperatures.

The values in M' spectra of this Gallium doped series samples, at higher frequencies are more or less constant. At low temperatures (343 K) the M' values are higher than for higher temperatures. This indicates that the Li^+ experiences more impedance when the frequency is increased, and is influenced more when it is not agitating (that is, at low temperatures). But as temperature increases, the effect of frequency on the behavior of the Li^+ with respect to impedance improves because the Li^+ is also agitating due to thermal energy. Hence the effect of applied frequency is lesser as temperature increases.

5.4.5 $\text{Li}_{1.3}\text{Al}_{0.3-x}\text{Sc}_x\text{Ti}_{1.7}(\text{PO}_4)_3$ (LASTP) system

The samples of parent compound $\text{Li}_{1.3}\text{Al}_{0.3}\text{Ti}_{1.7}(\text{PO}_4)_3$ (LATP) were doped with scandium to replace trivalent Al^{3+} in the rhombohedral structure. The modulus studies M'' versus frequency spectra are shown in the Fig. 5.97 for the samples N1 and N4 of different concentration of scandium. The values of M'' does not change much for both concentrations. A noticeable feature of modulus spectra of LASTP series is the high frequency tail that is formed after the initial cusp. The slope of the tail is maximum for low temperature samples. This is because, at very high frequencies, the Li^+ have low mobility and are confined to a localized region. Due to this, the ϵ' values are very small when exposed to high frequencies [117, 118].

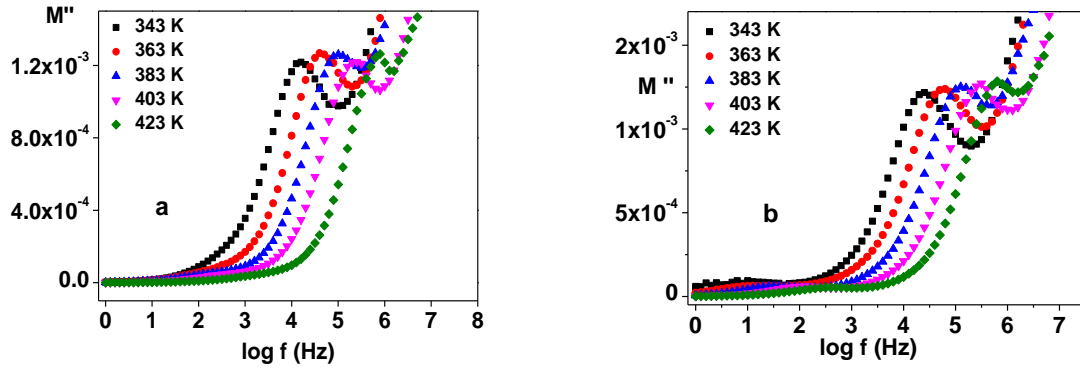


Fig. 5.97 M'' vs frequency plot for (a) $x = 0.01$ and (b) $x = 0.07$ samples of $\text{Li}_{1.3}\text{Al}_{0.3-x}\text{Sc}_x\text{Ti}_{1.7}(\text{PO}_4)_3$ series at different temperatures.

The peak width decreases slightly as temperature increases for each of the samples. But the overall peak width across samples for same temperature, is almost the same. This means with increasing amount of scandium in the system the local environment in which the Li^+ relaxes, is almost the same. Due to this reason, the Li^+ conductivity for all samples N1 to N4 is almost the same. This means that the Li^+ relax in a non Debye manner especially at higher frequencies. The tail also indicates that a grain structure is formed. Some workers [118] believe that in phosphate glass, the coordinated Li^+ motion is independent of temperature. When larger cations are doped in LTP system which has rhombohedral system, the distortion is caused at one of the three phosphate sites. Due to this, the overall structure distorts from the rhombohedral to monoclinic/triclinic. In this distorted lattice, the preference of Li^+ changes from M1 site to M2 site [119]. This distortion is in lattice sites in the grain. Thus, Li^+ experiences a distribution of free energy barriers coordinated between the Li^+ [120] is lesser as the dopant in the system increases.

Some authors [55, 101] believe that in scandium doped NASICON compounds with rhombohedral ($R\bar{3}c$) Sc^{3+} replaces Ti^{4+} . But due to larger size of Sc^{3+} , the lattice cell size increases monotonically. However if the dopant amount increases beyond $x = 0.05$, the symmetry is not retained. Due to larger unit cells, the electro positive repulsive influence increases. This results in stable bonds of Li^+ with oxygen [55, 120] due to which the Li^+ conductivity is less.

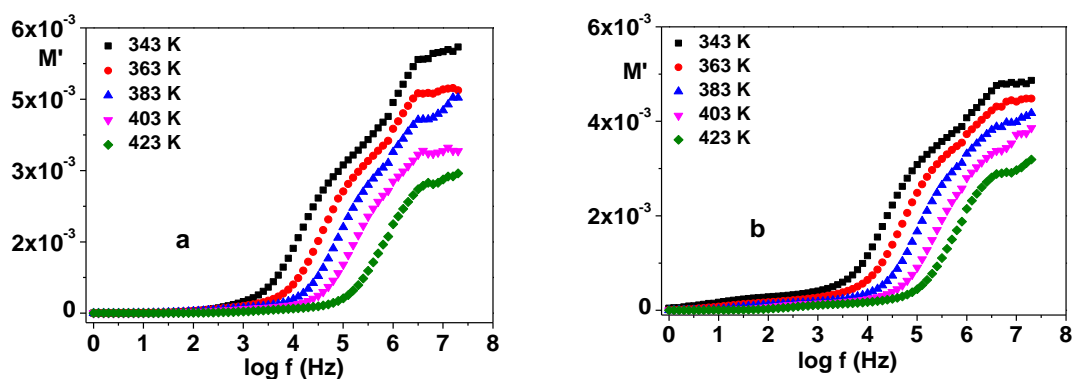


Fig. 5.98 M' vs freq plot for $\text{Li}_{1.3}\text{Al}_{0.3-x}\text{Sc}_x\text{Ti}_{1.7}(\text{PO}_4)_3$ series (a) $x = 0.01$ and (b) $x=0.07$ samples at different temperatures.

The M' vs. frequency spectra are presented in the Fig. 5.98 for N1 to N4 samples. The Li^+ relax in a similar manner at higher frequencies for all concentrations. This behavior is temperature activated and shifts towards higher frequency side with increasing temperature. Thus it can be concluded that with temperature and with concentration of the dopants, the modulus (M'') peaks shift towards higher frequencies. Due to impurity phases in grain and grain boundary, the M'' peaks exhibit deviation from the ideal Debye behavior. This means, the Li^+ are impeded in their relaxation due to such phases. However heat treatment of yttrium rich sample yielded a favorable behavior in the dielectric relaxation in low frequency (grain boundary) regions.

References

- [1] E. R. Losilla, M.A.G.Aranda, M. M. Lara, S. Bruque. Chem. Mater. 9 (1997) 1678
- [2] H. Aono, N. Imanaka, G.Y. Adachi, Acc. Chem. Res. 27 (1994) 265
- [3] H. Aono, E. Sugimoto, Y. Sadoaka, N. Imanaka, G. Adachi. J. Electrochem. Soc. 137 (1990) 1023
- [4] P.M. Maldonado, E.R. Losilla, M.M. Lara, MAG. Aranda, S. Bruque, F.E. Mouahid, M Zahir. Chem Mater. 15 (2003) 1879
- [5] J.M. Winand, A. Rulmont, P Tarte. Solid State Chem. 93 (1991) 341
- [6] A.M. Juarez, J.M. Rojo, J.E. Iglesias, J Sanz. J. Chem Mater. 7 (1995) 1857
- [7] A.M. Juarez, C. Pecharroman, J.M. Rojo, J.E. Iglesias, J Sanz. J. Phys. Chem B. 102 (1998) 372
- [8] J Kuwano, N. Sato, M. Kato. K Tananka. Solid State Ionics, 70-71 (1994) 332

- [9] J.R. MacDonald, Impedance Spectroscopy, New York. Wiley & Sons.
- [10] K. Arbi, S. Mandal, J.M. Rojo, J. Sanz. Chem Mater, 14 (2002) 1091
- [11] K. Arbi, MG. Lazarraga, D.B.H Chehimi, M.A Trabelsi, J.M. Rojo, J Sanz. Chem Mater. 16 (2004) 255
- [12] B.V.R. Chowdhari, G.V Subba Rao, G.Y.H Lee. Solid State Ionics, 136-137 (2000) 1067
- [13] R.O. Fuentes, F.M. Figueiredo, F.M.B Marques, J.I. Franco. Solid State Ionics, 140 (2001) 173
- [14] B Key, D.J Schroeder, B.J. Ingram, J. T Vaughey. Chem Mater. 24 (2012) 287
- [15] P. M Maldonado, MAG Aranda, S Bruque, J Sanz, E.R Losilla. Solid State Ionics, 176 (2005) 1613
- [16] K.M. Nairn, M Forsyth, M Greville, D.R MacFarlane, M. E Smith. Solid State Ionics, 86-88 (1996) 1397
- [17] J Fleig, J Maier. Solid State Ionics, 85 (1996) 9
- [18] R A De Souza J. Maier. Phys Chem Chem. Phys. 5 (2003) 740
- [19] X. Guo. R. Waser. Solid State Ionics, 173 (2004) 63
- [20] Q. Wang, O Varghese, C.A Grimes, E C Dickey. Solid State Ionics, 178 (2007) 187
- [21] C.R. Mariappan, C Yada, F Rosciano, B Roling. J Power Sources, 196 (2011) 6456
- [22] J.L.N Samanate, A.C.M Rodrigues, Solid State Ionics, 181 (2010) 1197
- [23] G.X. Wang, D.H Bradhurst, S.X Dou, H.K Liu. J. Power Sources, 124 (2003) 231
- [24] T. Salkus, E. Kazakevicius, J.R Dygas, Z. Kanape, J. Ronis, M. Dudek, A. Dindune, A.F. Orliukas, Ionics, 16 (2010) 631
- [25] T. Salkus, E. Kazakevicius, A. Kezionis, A. Dindune, Z. Kanape, J. Ronis, J Emery, A Boulant, O Bohnke, A.F. Orliukas, J. Phys. Cond. Matter, 21 (2009) 185502
- [26] A. F. Orliukas, T. Salkus, A. Kezionis, A. Dindune, Z. Kanape, J. Ronis, V. Venckute, V. Kazlauskienė, J. Miskinis, A. Lukauskas. Solid State Ionics, 225 (2012) 620
- [27] K.P Padmasree, D.K.Kanchan, A.R.Kulkarni. Solid State Ionics, 176 (2005) 475
- [28] M.S. Jayswal, D. K Kanchan, P Sharma, M Pant. Solid State Ionics, 186 (2011) 7
- [29] I.Y Pinus, A.V. Khoroshilov, K.S.Gavrichev, V.P.Tarasov, A.B. Yaroslavtsev. Solid State Ionics, 212 (2012) 112
- [30] W. D Kingery. Pure and Applied Chemistry. 56 (1984) 1703
- [31] J Maier. Bur Bunsenges. Phys. Chem. 88 (1984) 1062
- [32] R. A De Souza, J Fleig, J Maier, O Kinezle, Z L Zhang, W Sigle, M Ruhle, J. Am. Ceram. Soc. 86 (2003) 922
- [33] K. P Padmasree, D. K. Kanchan. Mater. Sci. Engg. B 122 (2005) 24
- [34] R Ramaraghavulu, S Buddhudu. Ceramics International, 37 (2011) 3651
- [35] R C Agarwal, S.A Hashmi, G.P Pandey, Ionics, 13 (2007) 295
- [36] K Funke. Solid State Ionics, 28-30 (1988) 100
- [37] K Funke, R. D. Banhatti, C Cramer. Phys. Chem. Chem. Phys., 7 (2005) 157
- [38] A. K Jonscher. Dielectric Relaxation in Solids, Chelsea Dielectric Press. London, 1983

- [39] M Shirpour, B Rahmati, W Sigle, P.A van Aken, R Merkle, J Maier. *J. Phys. Chem C.* 116 (2012) 2453
- [40] P F Yan, T Mori, A Suzuki, Y.Y Wu, G.J. Auchterlonie, J. Zou, J. Drennan. *Solid State Ionics*, 222-223 (2012) 31
- [41] M Shirpour, R Merkle, C.T Lin, J Maier. *Phys. Chem. Chem. Phys.* 14 (2012) 730
- [42] *The CRC Handbook of Solid State Electrochemistry*, Eds. P.J. Gellings, H.J.M Bouwmeester, CRC Press. The Netherlands, 1997
- [43] S. V Rathan, G Govindaraj. *Solid State Ionics*, 181 (2010) 504
- [44] C.R. Mariappan, C Yada, F Rosciano, B Roling. *Electrochem. Commun.*, 14 (2012) 25
- [45] B.E McNealy, J Hertz. *Solid State Ionics*, 256 (2014) 52
- [46] Y Saito, K Ado, T Asai, H Kageyama, O Nakamura. *Solid State Ionics* 58 (1992) 327
- [47] Y Nan, W.E Lee, P F. James. *J. Am. Ceram. Soc.* 75 (1992) 1641
- [48] S. Wong, P.J Newman, A.S Best, K.M Nairn, D.R. MacFarlane, M Forsyth. *J. Mater. Chem.* 8 (1998) 2199
- [49] A.S. Best, M Forsyth, D.R. MacFarlane. *Solid State Ionics* 136-137 (2000) 339
- [50] M. Forsyth, S. Wong, K.M Nairn, A.S. Best, P.J Newman, D.R. MacFarlane. *Solid State Ionics*, 124 (1999) 213
- [51] H. Aono, E. Sugimoto, Y Sadoaka, N. Imanaka, G. Adachi. *Solid State Ionics*, 40-41 (1990) 38
- [52] J. Fu. *J. Mater. Sci.* 33 (1998) 1549
- [53] J. Ross MacDonald. *Solid State Ionics*, 13, (1984) 147
- [54] M. Shirpour, G Gregori, L Houben, R Merkle, J Maier. *Solid State Ionics*, 262 (2014) 860
- [55] M.A. Subramanian, R Subramanian, A Clearfield. *Solid State Ionics*, 18-19 (1986) 562
- [56] L.S. Chun, L.Z. Xiang, *Solid State Ionics* 9-10 (1983) 835
- [57] S. Hambdoune, D Tran Qui. *Solid State Ionics*, 18-19 (1986) 587
- [58] D Tran Qui, S. Hamdoune. *Acta Crystallogr.* C44 (1988) 1360
- [59] R. Sobiastainkas, A. Dindune, Z. Kanepe, J Ronis, A Kezionis, E. Kazakevicius, A Orliukas. *Mat. Sci. Engg. B* 76 (2000) 184
- [60] J. Luo, E.F Hairetdinov, D.P Almond, R Stevens. *Solid State Ionics*, 122 (1999) 205
- [61] H. Yoshida, K. Miura, J. Fujita, T. Inagaki. *J. Am. Ceram. Soc.* 82(1) (1999) 219
- [62] H. Aono, N. Imanaka, G.Y. Adachi, *Acc. Chem. Res.* 27 (1994) 265
- [63] G.Y Adachi, N. Imanaka, H. Aono *Adv. Mater.* 8 (1996) 127
- [64] M.A Paris, A. Martinez-Juarez, J.E. Iglesias, J.M. Rojo, J. Sanz. *J. Chem. Mater.* 9 (1997) 1430
- [65] E. Morin, J. Angelnault, J.C. Courturier, M. Quarton, J. Klinowski. *Eur. J. Solid State Inorg. Chem.* 34 (1997) 947
- [66] J Kuwano, N. Sato, M. Kato. K. Tananka. *Solid State Ionics*, 70-71, (1994) 332
- [67] D. Tran Qui, S. Hamdoune, J.L. Soubeyroux, E.J.Prince, *Solid State Chem.* 72 (1988) 309
- [68] H.M. Rietveld. *J. Appl. Crystallogr.* 2 (1969) 65
- [69] E. R. Losilla, M.A.G. Aranda, M. M. Lara, S. Bruque. *Chem. Mater.* 9 (1997) 1678

- [70] L. W. Finger, D. E. Cox, A.P. Jephcoat. *J. Appl. Crystallogr.* 27 (1994) 892
- [71] F.E. Mouhid, M. Zahir, P.M. Maldonado, S. Bruque, E.R. Losilla, M.A.G Aranda, J. *Chem. Mater.* 11 (2001) 3258
- [72] X. Guo, W. Sigle, J. Maier. *J. Am. Cera. Soc.* 86 (2003) 77
- [73] W.D. Kingery, *J. Am. Cera. Soc.* 57 (1974) 1
- [74] M. Vollmann, R. Waser. *J. Electroceram.* 1 (1997) 51
- [75] X. Guo. R. Waser. *Solid State Ionics*, 173 (2004) 63
- [76] R. Meyer, X. Guo, R. Waser. *Electrochem. and Solid State Letters.* 8 (2005) J1
- [77] A. K Jonscher. *Dielectric Relaxation in Solids*, Chelsea Dielectric Press. London, 1983
- [78] D.K.Kanchan, K.P. Padmasree, H.R.Panchal, A.R.Kulkarni. *J. Ceram. Intl.* 30 (2004) 1655
- [79] B.V.R.Chowdhari, K. Radhakrishnan. *J. Non-Crystat. Solids*, 110 (1989) 101
- [80] E. R. Losilla, M.A.G. Aranda, S. Bruque, M.A.Paris, J.Sanz, A.R.West. *Chem Mater.* 10 (1998) 665
- [81] I.Y Pinus, A.V. Khoroshilov, K.S.Gavrichev, V.P.Tarasov, A.B. Yaroslavtsev. *Solid State Ionics*, 212 (2012) 112
- [82] A. F. Orliukas, T. Salkus, A. Kezionis, V. Venckute, V. Kazlauskienė, J. Miskinis, A. Luakaitis, J. Dudonis. *Solid State Ionics*, 188 (2011) 36
- [83] H. Aono, E. Sugimoto, Y. Sadoaka, N. Imanaka, G. Adachi. *J. Electrochem. Soc.* 137 (1990) 1023
- [84] S. Ibrahim, S.M.M.Yasin, N. M. Nee, R. Ahmad, M.R.Johan. *Solid State Commun.* 152 (2012) 426
- [85] D.K. Kanchan, K.P Padmasree, H.R Panchal, A R Kulkarni, *Ceramics International*, 30 (2004) 1655
- [86] A.K. Jonscher, *Nature*, 267 (1977) 673
- [87] M.C.R. Shastri, K.J Rao. *Solid State Ionics*, 44 (1991) 187
- [88] K.P Padmasree, D. K Kanchan. *Materials Chemistry and Physics* 91 (2005) 551
- [89] M. Abdukhadar, B. Thomas, *Bull. Mater. Sci.* 19 (4) (1996) 631.
- [90] W. D. Kingery. *Pure and Appl. Chem* 56 (1984) 1703
- [91] J.S.Lee, D.Y. Kim. *J. Mater. Res.* 16 (2001) 2739
- [92] F. Iguchi, N. Sata, H. Yugami, *J. Mater. Chem.* 20 (2010) 6265
- [93] T. Oyama, M. Yoshiya, H. Matstubara, K. Matsunaga. *Phys. Rev. B.* 71 (2005) 2341
- [94] S. Kim, J. Maier, *J. Electrochem. Soc.* 149 (2002) J73
- [95] J. Soumen, W.H Zhong, *J. Mater. Sci.* 43 (2008) 4607
- [96] M.G.McLin, C.A Angell, *Solid State Ionics*, 53-56 (1992) 1027
- [97] A.L.Saroj, R.K.Singh, *J. Phys. Chem Solids*, 73 (2012) 162
- [98] H. Jena, K.V.G. kuty, TRN. Kuty. *Mater. Esci. Engg. B*, 113 (2004) 30
- [99] M. Hubert, E. Patracovschi, X Zhang, L. Calvez. *J. Am. Ceram. Soc.* 96 (2013) 1444
- [100] K.K. Reddy, B.R Ravuri Reddy, V.K. Rao *Phase Transitions* 85 (2012) 218
- [101] G.G.Amatucci, A. Safari, F.K.Skokoohi, B.J. Wilkens, *Solid State Ionics* 60 (1993) 357
- [102] K.P. Padmasree, D. K Kanchan, *Mat. Sci. Engg. B* 122 (2005) 24

- [103] C.T. Moynihan. *Solid State Ionics*, 105 (1998) 175
- [104] K.L. Ngai, C Leon. *Solid State Ionics*, 125 (1999) 81
- [105] R. Bergman. *J. Appl. Phys.* 88 (2000) 1356
- [106] K.L. Ngai. *Solid State Ionics* 105 (1998) 231
- [107] C. Leon, A Rivera, A Varez, J Sanz, J Santamaria, K.L Ngai. *Phys. Rev. Lett.* 86 (2001) 1279
- [108] J. R Macdonald. *Appl. Phys. Lett.* 84 (1998) 812
- [109] J. R Macdonald. *Appl. Phys. Lett.* 90 (2001) 153
- [110] J. R Macdonald. *Appl. Phys. Lett.* 118 (2003) 3258
- [111] C. T. Chen, C. E. Danel, S Kim. *J. Mater. Chem.* 21 (2011) 5435
- [112] K. Gomann, G. Bochardt, M. Schulz, A. Gomann, W. Maus-Friedrichs, B.Lesage, O. Kaitasov, S. Hoffman-Effiert, T. Schneller. *Phys. Chem. Chem. Phys.* 7 (2005) 2053
- [113] R. J Grant, M.D Ingram, A.R. West, *Electrochim Acta*, 22 (1977) 729
- [114] R. J Grant, M.D Ingram, L.D.S Turner, C.A Vincent, *J. Phys. Chem.* 82 (1978) 2838
- [115] W.C. Hasz, C.T. Moynihan, P.A. Tick. *J. Non-Cryst. Solids* 172-174 (1994) 1363
- [116] C. R Mariappan, G. Govindaraj, *J. Non-Cryst. Solids* 353 (2006) 2737
- [117] A. Mogus-Milankovic, A. Santic, V. Licina, D.E Day. *J. Non-Cryst. Solid* 351 (2005) 3234
- [118] I.N Chakraborty, R.A. Condrate. *Phys. Chem. Glasses.* 26 (1985) 68
- [119] M.A. Paris, J Sanz. *Phys. Rev. B.* 55 (1997) 14270
- [120] J. Angenault, J.C Couturier, J.P Souron, Siliqi, M Quarton. *J. Mater. Sci. Lett.* 11 (1992) 1705
